COMBINATORIAL LIBRARIES OF POLYMERIC VECTORS FOR siRNA DELIVERY: SYNTHESIS, CHARACTERIZATION AND *IN VITRO* EVALUATION

A Dissertation

Presented to the Faculty of the Graduate School

of Cornell University

in Partial Fulfillment of the Requirements for the Degree of

Doctor of Philosophy

by

Jeisa M. Pelet

May 2011

COMBINATORIAL LIBRARIES OF POLYMERIC VECTORS FOR siRNA DELIVERY: SYNTHESIS, CHARACTERIZATION AND *IN VITRO* EVALUATION

Jeisa M. Pelet, Ph.D.

Cornell University 2011

Gene therapy has emerged as a promising technique to treat many chronic diseases, genetic disorders and even cancer. Furthermore, the recent discovery that RNA interference could be used as an approach to modulate protein expression in mammalian systems sparked a potential revolution in disease treatment. By taking advantage of this endogenous mechanism, gene silencing can be induced by sequence-specific cleavage of a messenger RNA coding for a specific protein, by means of a short interfering RNA (siRNA). Introducing siRNA into cells is limited by numerous challenges, predominantly the lack of effective delivery systems that can safely transport these macromolecules to their site of action while overcoming multiple barriers that hinder the delivery pathway. For siRNA delivery, synthetic vectors, including polymers, have increasingly gained attention primarily due to their easily controllable molecular composition.

In this work, we employed a combinatorial chemistry approach for the rational design of polymers as non-viral delivery systems. We hypothesize that by developing libraries that correlate the structure-function relationship of polymeric vectors, optimal structural parameters will be identified for efficient transport and delivery of siRNA into cells. Toward this goal, we carried out the controlled synthesis of poly(methacrylic acid) (pMAA) and poly(acrylic acid) (pAA) by reversible addition-fragmentation chain transfer (RAFT) polymerization. Based on these two polymer precursors, we evaluated the conjugation of two ligands, D-(+)-galactosamine (Gal) and agmatine (Agm) to generate polymer libraries by varying the binary subtitution of both

moieties. Due to the higher Agm/Gal side chain substitution in pAA as compared to pMAA, pAA conjugates were selected for *in vitro* evaluation. pAA was synthesized with four distinct molecular weights (M_n), specifically 3 kDa (PDI = 1.36), 5 kDa (PDI = 1.32), 10 kDa (PDI = 1.19) and 21 kDa (PDI = 1.19). For each polymer M_n, various combinations of Agm and Gal were substituted, for a total of 22 polymers under evaluation.

From the biophysical and cellular characterization, it was determined that both the Agm/Gal content and the M_n significantly influence the ability of these polymer conjugates to serve as siRNA delivery systems. As distinguished from these analyses, the higher the Agm content, the more compact and stable the polyplexes and the higher transfection efficiency, but also the higher cytotoxicity. As for the effect of molecular weight, the lower the M_n, the more stable the polyplexes and the lower cytotoxicity, but also the lower transfection efficiency. Therefore, a critical balance between Agm/Gal content and polymer M_n must be attained to acheive favorable outcomes - these being high transfection efficiency with low cytotoxicity. The best candidate identified was 5-P3, corresponding to a pAA M_n = 5 kDa, and Agm and Gal contents of 55% and 17%, respectively.

The development of polymer libraries and their *in vitro* evaluation offered a better understanding of the structure-function relationship of polymeric vectors. This approach provided the identification of optimal structural parameters and served as a synthetic foundation upon which safer and more efficient siRNA delivery systems can be developed.

BIOGRAPHICAL SKETCH

Jeisa M. Pelet was born December 12th, 1983 in San Juan, Puerto Rico. She received the Bachelor of Science in Chemical Engineering from the University of Puerto Rico, Mayagüez, in 2005. As an undergraduate student, she conducted research at the University of Puerto Rico, Mayagüez under the guidance of Prof. David Suleiman. In addition, she participated in Research Experience for Undergraduates (REU) Programs at Cornell University, Ithaca NY in summer 2004 (Center for Nanoscale Systems) and summer 2005 (Cornell Center for Materials Research). During this time, she received several awards including American Chemical Society Honor Scholarship, Robert C. Byrd Honor Scholarship, ELA Employees Association Honor Scholarship and HESS Scholarship. She started her MS/PhD studies at the School of Chemical and Biomolecular Engineering at Cornell University under the guidance of Prof. David Putnam in Fall 2006.

To my husband, Alexis.

ACKNOWLEDGMENTS

I owe my deepest gratitude to my advisor, Prof. David Putnam, for his enthusiasm, patience, motivation, immense knowledge and for teaching me the beauty of science and research. His continuous support, guidance and mentoring were invaluable to my development as a scientist and a professional, and I am truly grateful. My sincere gratitude also goes to my committee members, Prof. Michael Shuler and Prof. Geoffrey Coates, for their contributions, valuable insights and discussions about my project. Special thanks to Prof. Christopher Ober for so kindly attending my defense and for his insightful comments.

I would like to express my sincere gratitude to Prof. Shivaun Archer, Prof. Chris Shaffer and Nevjinder Singhota for their support during my participation in the CLIMB GK-12 program. Special thanks to Carolyn for being my partner during the year I participated in the program. Thanks to the support and kindness of the people from the Diversity Programs in Engineering (DPE) and to the Alfred P. Sloan Foundation Graduate Scholarship Programs and National Action Council for Minorities in Engineering. My gratitude is extended to the NBTC and NMR facilities and administrators, especially Anthony Condo and Dr. Ivan Keresztes for their repeated help with the NMR.

I was extremely fortunate to be part of an extraordinary research group. I wish to thank all the past and present Putnam group members and friends: Anne, Sharon, Peter, Dave, Sara, Julius, Jen, Bailey, Lihong, Minghui, Mingchee, Joseph, Lindsey, Nicole and José, for stimulating discussions and for all the fun we had throughout the years. Special thanks to my awesome friends in Ithaca for sharing so many great moments with me winter after winter. Thanks to Karen and Henrique for our weekend escapes to the Anirondacks (among others adventures), Nelson for always keeping me updated with music, Anthony for his visits to the lab

and for always making me laugh, Ritsdeliz for her contagious energy, and Felipe and Annie for the Puertorrican/Mexican dinners. I also thank all my friends outside of Ithaca, especially Pedro for always being there for me.

My deepest gratitude goes to my parents, Eva and Luis, without whom I would not be here today. I thank my mother for her never-ending love, unconditional support and dedication, and for being truly exceptional. I also thank my father, who is watching over me from heaven, for his love and guidance. A heartfelt thanks to my siblings, Yaira and Fernan, for their encouregment and for being a pristine example of hard work and dedication. Thanks to my sister-in-law Melissa, my brother-in-law Jason and beautiful niece and nephew, Paulita and Luisfe, who will always have a special place in my heart. I would also like to express my gratitude to my in-laws, Ivonne and Elias, for welcoming me into their family and their home. Last but not least, I thank my beloved husband, Alexis, who accompanied me on this journey, for his unconditional love and continuous support, for being truly amazing and for giving me the thrust to keep moving forward.

TABLE OF CONTENTS

LIST OF TABLES

LIST OF FIGURES

LIST OF ABBREVIATIONS

A-CPA	4,4’-azobis(4-cyanopentanoic acid)
AA	acrylic acid
Agm	agmatine
BCA	bicinchoninic acid
BSA	bovine serum albumin
CPA-DB	4-cyanopentanoic acid dithiobenzoate
CTA	chain transfer agent
D_2O	deuterium oxide
DMEM	Dulbecco's modified eagle medium
DMTMM	4-(4,6-dimethoxy-1,3,5-triazine-2-yl)-4-methylmorpholinium chloride
DOSY	diffusion-ordered spectroscopy
EtBr	ethidium bromide
EtOH	ethanol
FA	fluoresceinamine
FBS	fetal bovine serum
Gal	D-(+)-galactosamine
GPC	gel permeation chromatography
HBS	HEPES buffered saline
HCl	sodium chloride
HEPES	4-(2-hydroxyethyl)-1-piperazineethanesulfonic acid
I	radical initiator
M_n	number-average molecular weight
M_p	peak-average molecular weight
M_w	weight-average molecular weight
MAA	methacrylic acid
MeOH	methanol
NaOH	sodium hydroxide
NMR	nuclear magnetic resonance
pAA	poly(acrylic acid)
PBS	phosphate buffered saline
PDI	polydispersity index
pMAA	poly(methacrylic acid)

CHAPTER 1

INTRODUCTION

1.1 siRNA delivery

For decades researchers have explored possibilities to treat or even cure chronic diseases, genetic disorders and cancer. Recently, this search has encountered a potentially achievable route through nucleic acid delivery, a revolutionary therapeutic alternative. Particularly, endogenous gene expression can be regulated through the RNA interference (RNAi) machinery within cells. RNAi is an endogenous mechanism in which a short RNA post-transcriptionally interferes with the translation of a particular mRNA with a complementary nucleotide sequence. Silencing genes regulates endogenous cellular pathways and offers protection from invasion of nucleic acids by viral infections[1,2]. RNAi was first identified in plants, and was shortly after recognized in fungi and animals, specifically the roundworm *Caenorhabditis elegans*. In 1998, Fire and colleagues successfully suppressed protein expression in *C. elegans* by the insertion of a double-stranded RNA (dsRNA) that led to the degradation of homologous messenger RNA (mRNA)[3]. Although RNAi is conserved in eukaryotic organisms, initial efforts to apply long dsRNA (> 30 base pairs) to mammalian cells resulted in a potent immune response by interferon release. It was not until 2001 that Elbashir et al. reported suppression of protein expression by 21-nucleotide short interfering RNA (siRNA) in mammalian cells, particularly, human embryonic kidney and HeLa cells[4]. Ever since its discovery, siRNA has become a promising tool to investigate the function of targeted genes and has been contemplated for therapeutic use due to its high specificity and efficiency. However, as a nucleic acid, siRNA suffers from low stability in serum due to nucleases and required assistance for efficient transport and delivery

into cells. In addition, the high anionic density from the phosphate groups in the siRNA backbone and size prevents passive diffusion across cellular membranes. Many of the siRNA delivery vehicles under investigation have been derived from previously studied DNA delivery vehicles and modified accordingly[5]. However, there are many issues that must be taken into consideration for the design of non-viral siRNA delivery systems. For years, researchers have developed different strategies to overcome the challenges encountered in siRNA delivery, many which are described hereafter.

1.2 RNA interference

Several strategies can be executed to induce gene silencing in mammalian systems such as the delivery of synthetic siRNA, a 21-23 base pair nucleotide. Other RNAi effectors include short hairpin RNA (shRNA), or plasmid DNA encoding for shRNA[6]. Regardless of the approach, the molecular mechanism for interference is conserved. After processing the RNAi effectors to achieve siRNA, the siRNA assembles with a multiprotein complex known as the RNA Induced Silencing Complex (RISC). The siRNA is loaded into Argonaute protein (Ago2) within RISC which promotes cleavage of the sense strand generating a single-stranded RNA (antisense or guide strand)[7]. Although still unclear, it is believed that the selection of the sense strand is by thermodynamic asymmetry[8]. The antisense strand guides the activated RISC to search and bind to a complementary mRNA sequence triggering its endonucleolytic cleavage by Ago2, and thus inhibiting protein expression (Figure 1.1). RNAi-based therapies have become extremely attractive due to its high specificity toward a wide range of mRNA targets.

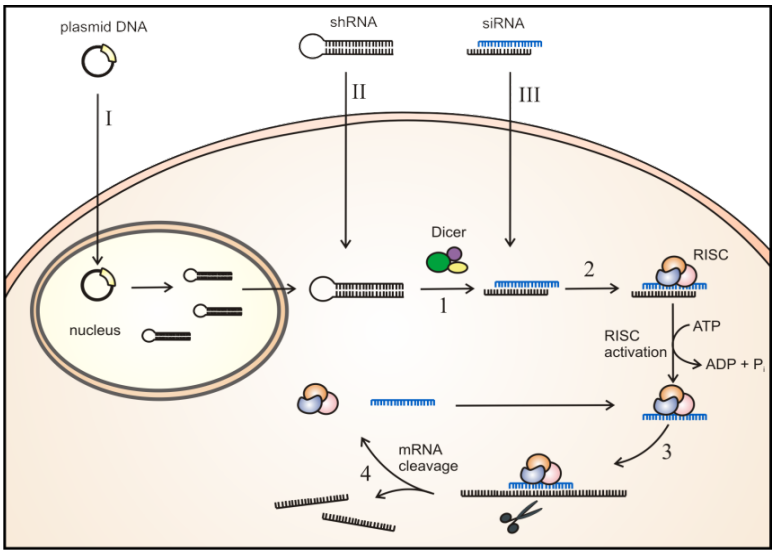

Figure 1.1: RNA interference mechanism in mammalian cells (adapted from Doody, A. et al.[6]): 1. shRNA is processed by Dicer to generate siRNA; 2. siRNA assembles with a multiprotein complex, RISC; 3. RISC unwinds duplex siRNA, cleaves the sense strand, and uses the antisense strand to target mRNAs with complementary sequence; 4. RISC, guided by the antisense sequence siRNA, promotes cleavage and degradation of the mRNA.

1.3 Challenges of siRNA delivery

The design of synthetic delivery vectors is extremely critical given that the system must surpass numerous extracellular and intracellular barriers confronted throughout the delivery pathway (Figure 1.2). Among the extracellular barriers, the known challenges include siRNA packing (binding and encapsulation of siRNA), stability in plasma, nuclease resistance, avoidance of interactions with plasma proteins and uptake from non-target tissues, and increase in circulation time. Once the target cell is reached, the delivery system must be effectively internalized by a specific pathway (i.e. receptor-mediated endocytosis), and promote cytosolic localization (endosomal escape while avoiding lysosomal encapsulation) and complex dissociation in the cytosol to allow the therapeutic effect. More importantly, these vectors must provide minimal cytotoxicity to target and adjacent tissues as well as avoid potential immune responses.

1.3.1 siRNA packing and stability. Naked siRNA can be locally administered to target tissues; however, for systemic delivery, rapid enzymatic degradation in the extracellular medium makes this alternative unfavorable. Various chemical modifications and terminal modifications have been executed to increase siRNA stability and resistance to nucleases, such as cholesterol modifications and 2'-O-methyl modification[9]. The molecular weight and average length of a 21-23 base pair long siRNA is typically ~13 kDa and 6 nm, respectively. Due to its size, renal clearance by glomerular filtration is likely for these molecules, which is highly typical for globular protein of less than 40 kDa or nanoparticles with hydrodynamic diameter of 5-6 nm[10]. These hurdles encourage the use of delivery vectors to facilitate siRNA transport during systemic delivery.

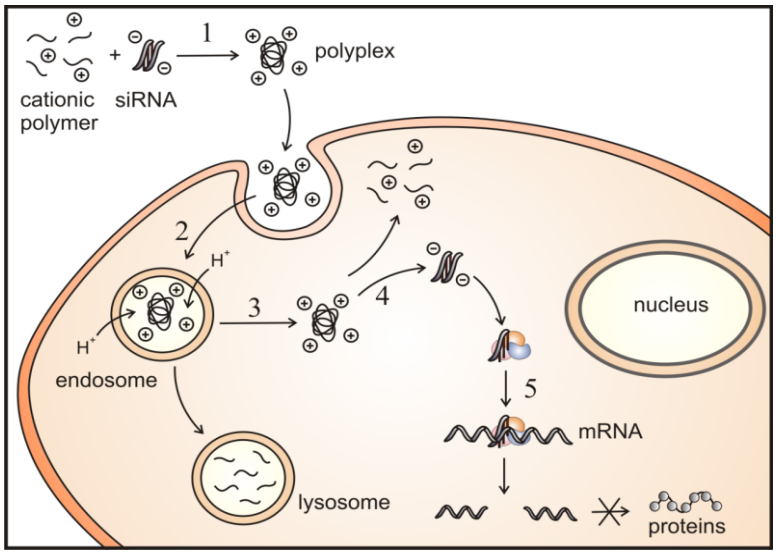

Figure 1.2: siRNA delivery barriers (adapted from Wong, S. et al.[11]): (1) gene packing; (2) internalization; (3) escape from the endosome; (4) complex dissociation; (5) silencing protein expression.

Several strategies have been implemented to encapsulate siRNA into a compact nanoparticle to protect it from nuclease activity. The most common approach is through electrostatic interactions with positively charged biomaterials. Highly cationic biomaterials can produce a negative impact on the stability of the complex given that it can increase non-specific binding to proteins in plasma and to biological surfaces. As a consequence, particle aggregation can be triggered leading to undesired side effects. To avoid non-specific interaction of cationic complexes with proteins and increase systemic circulation, hydrophilic groups such as polyethylene glycol (PEG) are commonly incorporated into the design. PEG can shield particles protecting them from aggregation and increase stability[12,13]. However, the degree of PEGylation can have a significant impact on cellular uptake[14,15]. Alternatively, PEG can be directly conjugated to siRNA through cleavable disulfide bonds, a technique that has previously been shown to offer greater stability and resistance to enzymatic degradation than naked siRNA[16].

1.3.2 Cell targeting and internalization. Systemic delivery of nanoparticles involves traveling through the bloodstream and penetration through the vascular endothelium wall to reach the target tissue. Passive diffusion across the endothelial barrier is limited to nanoparticles with diameters of 5 nm or less. Larger particles are more prone to accumulate in the liver, spleen and leaky tumors. In the case of hepatocytes, fenestration of the liver endothelium is 100-150 nm.

There are several alternatives to target specific tissues. Targeting ligands that are recognized by specific cell surface receptors can stimulate cellular internalization through clathrin-dependent or receptor-mediated endocytosis. Particles with diameters of 200 nm or less are able to be internalized by cells through this pathway[17]. Numerous functional groups including sugars[16,18,19], antibodies[20], peptides[21,22] and folates[23,24] are commonly incorporated into the synthetic delivery vectors depending on the target tissue. For instance, galactose can interact

with asialoglycoprotein receptors in hepatocytes cell membrane[13]. Galactose can also be used for targeting lung tissues through beta-galactoside-binding lectins in the cell surface[25]. Similarly, mannose can be employed to target mannose receptors found in macrophages[26]. Folate receptors, although found in healthy cells, are over-expressed in many cancer cells and can therefore be used for targeting. Other targeting ligands, including peptides and nucleic acid-based aptamers, have been directly conjugated to siRNA[27,28]. Moreover, innate cell-targeting mechanisms of viruses including cell penetrating peptides (CPP), such as Tat (transactivator of transcription) and integrin-binding RGD peptide, which allow rapid internalization into cells have been used[29,30].

1.3.3 Cytosolic localization. For siRNA delivery, cytosolic localization is vital. Following cellular internalization by receptor-mediated endocytosis, the delivery system will enter the endocytic pathway. In this process, the endocytic vesicles will fuse with early endosomes, after which receptors can be recycled back to the plasma membrane. Early endosomes will mature into late endosomes which will eventually fuse with lysosomes, the degradation organelle of the cell. Lysosomes have lower pH (~5.0-5.5) values as compared to endosomes (~6.0). It is imperative that the delivery system escapes from this pathway before reaching the lysosomal compartment to avoid degradation. For this purpose, pH-responsive biomaterials that are able to destabilize the endosomal membrane by changes in pH within the compartments are very attractive[15]. Other alternatives to induce endosomal escape is by the incorporation of endosomolytic reagents (i.e. chloroquine) that can destabilize the endosomal membrane or fusogenic peptides (i.e. HA2) that undergo conformational changes upon acidification of the endosome[31].

1.4 Polymeric delivery systems

1.4.1 Polycations. Cationic polymers are promising delivery vectors due to their ability to electrostatically interact with negatively charged phosphate groups along the siRNA backbone allowing complexation of the siRNA into nanometer-sized particles. These interactions can protect the siRNA from enzymatic degradation and provide stability in the extracellular medium, as well as assist cellular uptake. Cationic polymers including linear and dendrimeric poly-L-lysine[15,20,31], protamine[22] and polyethyleneimine (PEI) have been evaluated for siRNA delivery. Among these, the most widely investigated polycation for nucleic acid delivery *in vitro* and *in vivo* is PEI, first introduced by Boussif and collaborators[32]. PEI is considered one of the most effective delivery vectors due to its relatively high transfection efficiency and consistency in different types of cells. In addition to forming a strong electrostatic interaction with negatively charged nucleic acids, the high density of amino groups in PEI are believed to offer buffering capacity below physiological pH. It is hypothesized that this property triggers an increase in the osmotic pressure within the endosomal compartment inducing its rupture and allowing cargo escape into the cytosol (i.e the proton sponge effect). The biophysical and structural characteristics of various PEIs with different architectures and molecular weights have been studied for siRNA delivery[33]. However, despite its high transfection efficiency, PEI suffers from high cytotoxicity. The cytotoxicity increases with increasing molecular weight and increasing branching[34]. Various chemical modifications to PEI have been performed to address this disadvantage including structural modifications with lipids (i.e. stearic acid)[20], PEG[12,35,36], chitosan[37] and poly(γ-benzyl-L-glutamate)[38]. PEI has been used successfully for siRNA delivery in several tissues *in vivo,* such as lungs, nervous system and tumors[13,16,20,39-41].

1.4.2 Polysaccharides. Polysaccharides are an attractive alternative as nucleic acid delivery

vehicles due to their biocompatibility, biodegradability and reduced cytotoxicity. Among these natural polymers, chitosan has been investigated for siRNA delivery[42]. Reviews solely on chitosan-based delivery vectors are available[43]. Other popular delivery systems are cyclodextrin-based vectors. Cyclodextrins are cyclic oligosaccharides composed of 6 to 8 D-(+)-glucose units. A successful cyclodextrin-based polycation was developed by Davis and collaborators[44]. This delivery system, composed of cyclodextrin, PEG and transferrin, is able to encapsulate siRNA into small stable nanoparticles (~50 nm). In cynomolgus monkeys, it showed high delivery efficiency with relatively mild immune responses at high doses (27 mg siRNA/kg) and is currently undergoing human clinical trials as the first targeted polymer-based delivery system.

1.4.3 Dendrimers. Dendrimers are highly branched, spherical structures with a core-shell arrangement attractive due to their ability for internal siRNA packing. This internal packing is possible by incorporating positive charges to the interior structure while maintaining the surface charge neutral, for instance in polyamidoamines (PAMAM)[45]. Other types of packing possible with dendrimers include surface adsorption and direct chemical conjugation. Although dendrimers require a step-by-step synthesis approach, a high level of control over their molecular structure can be achieved. Dendrimers may cause cytotoxicity due to apoptosis induction by mitochondria membrane permeabilization[46]. The cytotoxicity is directly related to the molecular structure and surface charge[47]. To avoid cytotoxicity and enhance biocompatibility, surface modifications, such as the incorporation of PEG, has been carried out[48,49]. Other than PAMAM, poly(propylene imine) (PPI) has also been evaluated for siRNA delivery with promising outcomes for tumors *in vivo*[49].

1.4.4 siRNA-polymer conjugates. siRNA can be chemically conjugated to small molecules, lipids, oligopeptides (i.e. CPPs) or polymers (i.e. PEG) to enhance stability and cellular uptake[50].

The covalent attachment between the siRNA and the molecule or carrier is primarily through disulfide linkages, which are cleaved upon internalization into cells. A particularly interesting delivery vehicle was developed by Rozema et al. named 'siRNA Dynamic PolyConjugates' for targeted delivery to hepatocytes[51]. They incorporated various components, each with a specific purpose for enhanced intracellular delivery. The system backbone is an amphipathic poly(vinyl ether) composed of butyl and amino vinyl ethers. To this, PEG and N-acetylgalactosamine ligand, were reversibly attached through an acid-labile maleamate linkage, which can be cleaved within the endosome exposing the amines from the polymer backbone. Finally, the siRNA was attached through a disulfide linkage. This system was able to knockdown two different genes, apolipoprotein B and peroxisome proliferator-activator receptor alpha, *in vivo* up to 80-90% with no measurable cytotoxicity.

1.4.5 Biodegradable polymers. Biodegradable copolymers have the advantage of integrating multiple desirable properties into one carrier. For instance, poly(lactic-*co*-glycolic acid) (PLGA) is a biocompatible, biodegradable copolymer exploited for many pharmaceutical applications including drug/gene delivery. For siRNA delivery, PLGA microspheres have been applied for sustained siRNA release *in vivo*[52]. Additionally, surface modifications with cationic polymers such as chitosan or PEI have been carried out to improve cellular uptake[53,54]. Other biodegradable copolymers that integrate various functionalities have been developed. For instance, Convertine et al. produced a copolymer which incorporates a siRNA condensing block of dimethylaminoethyl methacrylate (DMAEMA) and a terpolymer endosomal-releasing block of DMAEMA, propylacrylic acid and butyl methacylate[55].

1.4.6 Combinatorial Libraries. Combinatorial chemistry approach is a appealing technique to investigate the structure-function relationship of synthetic vectors with nucleic acid delivery and

to develop new therapeutics[56]. So far, combinatorial libraries have primarily focused on the development of DNA delivery vectors[57-61]. However, design criteria borrowed from DNA-based vectors may not be optimal for siRNA delivery systems. Thus, different approaches for siRNA-based vectors need to be developed. The most favorable structural characteristics of polymeric vectors for siRNA delivery can be efficiently investigated through this approach. Mapping the structure-function parameter space through polymer libraries can help to understand the mechanisms of siRNA delivery leading to safer and more efficient delivery systems.

1.5 Other relevant non-viral delivery systems

Other than cationic polymers, the leading non-viral vectors for siRNA delivery are cationic lipids. Lipid-based delivery systems, such as liposomes, micelles and solid lipid nanoparticles (SLP), are attractive due to their biocompatibility and reduced cytotoxicity. However, poor complex stability ultimately affects their cellular uptake and delivery efficiency. Of particular interest, stable nucleic acid lipid particles (SNALPs) were recently developed and have been shown to be efficient for siRNA delivery *in vivo*, particularly for the liver[62]. SNALPs are composed of ionizable cationic lipids coated with PEG. Studies with cynomolgus monkeys showed that a single siRNA injection of this system produced a reduction in apolipoprotein B expression with a maximal silencing of 90%[63]. Lipoloids, which are lipid-like materials, are also considered promising siRNA delivery vectors, showing high efficacy *in vivo*, specifically for the liver, at low doses (0.01 mg/kg)[64]. The development of these lipoloids was achieved through combinatorial synthesis and screening of various types of materials which enabled the identification of optimal formulations for enhanced siRNA delivery[65].

1.6 Clinical trials

The discovery of RNAi sparked a revolution in the search for potential new disease treatment alternatives. Ever since, the advancement in the development of RNAi-based therapies, particularly with siRNA, has been significantly increasing. The first clinical trial was launched in 2004, for the treatment of age-related macular degeneration (Bevasiranib) by local siRNA delivery. Afterwards, other siRNA-based therapies followed in clinical trials. Although most of the siRNA therapeutics reaching this state are naked siRNA, delivery vectors including lipid-based and cyclodextrin-based systems are also being evaluated. siRNA-based treatments currently undergoing clinical trials are listed in Table 1.1.

Table 1.1: Current clinical trials for siRNA-based treatments.[a]

Company	Product	Vector
Opko Health, Inc.	Bevasiranib (macular degeneration – phase III)	naked
Sirna Therapeutics (Allergan)	Sirna027 (Choroidal Neovascularization – phase II)	chemically-modified siRNA
Alnylam Pharmaceuticals	ALN-RSV01 (respiratory viral infection – phase II)	lipid-based
Nucleonics	NUC B1000 (hepatitis – phase I)	lipid-based
Quark Pharmaceuticals	15NP (kidney injury – phase II)	naked
Pfizer/Quark Pharmaceuticals	REDD14NP (macular degeneration – phase I)	naked
Calando Pharmaceuticals	CALAA01 (Solid Tumors – phase I)	cyclodextrin-polycations
Pachyonychia Congenita Project	TD101 (pachyonychia congenita - phase I)	naked
Silence Therapeutics AG	Atu027 (solid tumors - phase I)	lipid-based
Tekmira Pharmaceuticals Corporation	PRO-040201 (Hypercholesterolemia - phase I)	liposome

[a]Information available through clinicaltrials.gov

REFERENCES

1 Dykxhoorn, D. M. & Lieberman, J. The silent revolution: RNA interference as basic biology, research tool, and therapeutic. *Annu. Rev. of Med.* **56**, 401-423 (2005).

2 Dillon, C. P. *et al.* "RNAi as an experimental and therapeutic tool to study and regulate physiological and disease processes". *Annu. Rev. Physiol.* **67**, 147-173 (2005).

3 Fire, A. *et al.* Potent and specific genetic interference by double-stranded RNA in Caenorhabditis elegans. *Nature* **391**, 806-811 (1998).

4 Elbashir, S. M. *et al.* "Duplexes of 21-nucleotide RNAs mediate RNA interference in cultured mammalian cells". *Nature* **411**, 494-498 (2001).

5 Gary, D. J., Puri, N. & Won, Y.-Y. Polymer-based siRNA delivery: Perspectives on the fundamental and phenomenological distinctions from polymer-based DNA delivery. *J. Control. Release* **121**, 64-73 (2007).

6 Doody, A. & Putnam, D. RNA-interference effectors and their delivery. *Crit. Rev. Ther Drug Carrier Syst.* **23**, 134-160 (2006).

7 Matranga, C., Tomari, Y., Shin, C., Bartel, D. P. & Zamore, P. D. Passenger-strand cleavage facilitates assembly of siRNA into Ago2-containing RNAi enzyme complexes. *Cell* **123**, 607-620 (2005).

8 Rand, T. A., Petersen, S., Du, F. & Wang, X. Argonaute2 cleaves the anti-guide strand of siRNA during RISC activation. *Cell* **123**, 621-629 (2005).

9 Ikeda, Y. & Taira, K. Ligand-targeted delivery of therapeutic siRNA. *Pharm. Res.* **23**, 1631-1640 (2006).

10 Choi, H. S. *et al.* Renal clearance of quantum dots. *Nat. Biotechnol.* **25**, 1165-1170 (2007).

11 Wong, S. Y., Pelet, J. M. & Putnam, D. Polymer systems for gene delivery - Past, present and future. *Prog. Polym. Sci.* **32**, 799-837 (2007).

12 Merkel, O. M. *et al.* Stability of siRNA polyplexes from poly(ethylenimine) and poly(ethylenimine)-g-poly(ethylene glycol) under in vivo conditions: Effects on pharmakokinetics and biodistribution measured by Fluorescence Fluctuation Spectroscopy and Single Photon Emission Computed Tomography (SPECT) imaging. *J. Control. Release* **138**, 148-159 (2009).

13 Rudolph, C. *et al.* Thyroid hormone (T3)-modification of polyethyleneglycol (PEG)-polyethyleneimine (PEI) graft copolymers for improved gene delivery to hepatocytes. *Biomaterials* **28**, 1900-1911 (2007).

14 Mishra, S., Webster, P. & Davis, M. E. PEGylation significantly affects cellular uptake and intracellular trafficking of non-viral gene delivery particles. *Eur. J. Cell Biol.* **83**, 97-111 (2004).

15 Meyer, M. *et al.* Synthesis and biological evaluation of a bioresponsive and endosomolytic siRNA−polymer conjugate. *Mol. Pharm.* **6**, 752-762 (2009).

16 Günther, M. *et al.* Polyethylenimines for RNAi-mediated gene targeting in vivo and siRNA delivery to the lung. *Eur. J. Pharm. Biopharm.* **In Press, Uncorrected Proof**.

17 Rejman, J., Oberle, V., Zuhorn, I. S. & Hoekstra, D. Size-dependent internalization of particles via the pathways of clathrin- and caveolae-mediated endoxytosis. *Biochem. J.* **377**, 159-169 (2004).

18 Matsumoto, S. *et al.* Environment-responsive block copolymer micelles with a disulfide cross-linked core for enhanced siRNA delivery. *Biomacromolecules* **10**, 119-127 (2009).

19 Nakamura, Y., Kogure, K., Futaki, S. & Harashima, H. Octaarginine-modified multifunctional envelope-type nano device for siRNA. *J. Control. Release* **119**, 360-367 (2007).

20 Alshamsan, A. *et al.* The induction of tumor apoptosis in B16 melanoma following STAT3 siRNA delivery with a lipid-substituted polyethylenimine. *Biomaterials* **31**, 1420-1428 (2010).

21 Choi, S. W., Lee, S. H., Mok, H. & Park, T. G. Multifunctional siRNA delivery system: Polyelectrolyte complex micelles of six-arm PEG conjugate of siRNA and cell penetrating peptide with crosslinked fusogenic peptide. *Biotechnol. Prog.* **26**, 57-63 (2010).

22 Choi, Y.-S. *et al.* The systemic delivery of siRNAs by a cell penetrating peptide, low molecular weight protamine. *Biomaterials* **31**, 1429-1443 (2010).

23 York, A. W., Huang, F. Q. & McCormick, C. L. Rational design of targeted cancer therapeutics through the multiconjugation of folate and cleavable siRNA to RAFT-synthesized (HPMA-s-APMA) copolymers. *Biomacromolecules* **11**, 505-514 (2010).

24 Kim, S. H., Mok, H., Jeong, J. H., Kim, S. W. & Park, T. G. Comparative evaluation of target-specific GFP gene silencing efficiencies for antisense ODN, synthetic siRNA, and siRNA plasmid complexed with PEI-PEG-FOL conjugate. *Bioconjugate Chem.* **17**, 241-244 (2006).

25 Chen, J. *et al.* Galactose-poly(ethylene glycol)-polyethylenimine for improved lung gene transfer. *Biochem. Biophys. Res. Comm.* **375**, 378-383 (2008).

26 Irache, J. M., Salman, H. H., Gamazo, C. & Espuelas, S. Mannose-targeted systems for the delivery of therapeutics. *Expert Opin. Drug. Del.* **5**, 703-724 (2008).

27 Chu, T. C., Twu, K. Y., Ellington, A. D. & Levy, M. Aptamer mediated siRNA delivery. *Nucl. Acids Res.* **34**, e73- (2006).

28 McNamara, J. O. *et al.* Cell type-specific delivery of siRNAs with aptamer-siRNA chimeras. *Nat. Biotech.* **24**, 1005-1015 (2006).

29 Moschos, S. A., Williams, A. E. & Lidsay, M. A. Cell-penetrating-peptide-mediated siRNA lung delivery. *Biochem. Soc. Trans.* **35**, 807-810 (2007).

30 Xiong, X. B., Uludağ, H. & Lavasanifar, A. Virus-mimetic polymeric micelles for targeted siRNA delivery. *Biomaterials* **31**, 5886-5893 (2010).

31 Inoue, Y. *et al.* Efficient delivery of siRNA using dendritic poly(L-lysine) for loss-of-function analysis. *J. Control. Release* **126**, 59-66 (2008).

32 Boussif, O. *et al.* A versatile vector for gene and oligonucleotide transfer into cells in culture and in vivo: Polyethylenimine. *Proc. Natl. Acad. Sci.* **92**, 7297-7301 (1995).

33 Grayson, A. C. R., Doody, A. M. & Putnam, D. Biophysical and structural characteristics of polyethylenimine-mediated siRNA delivery in vitro. *Pharm. Res.* **23**, 1868-1876 (2006).

34 Hunter, A. C. Molecular hurdles in polyfectin design and mechanistic background to polycation induced cytotoxicity. *Adv. Drug Del. Rev.* **58**, 1523-1531 (2006).

35 Liu, C. *et al.* Novel biodegradable lipid nano complex for siRNA delivery significantly improving the chemosensitivity of human colon cancer stem cells to paclitaxel. *J. Control. Release* **140**, 277-283 (2009).

36 Nimesh, S. & Chandra, R. Polyethylenimine nanoparticles as an efficient in vitro siRNA delivery system. *Eur. J. Pharm. Biopharm.* **73**, 43-49 (2009).

37 Jere, D. *et al.* Chitosan-graft-polyethylenimine for Akt1 siRNA delivery to lung cancer cells. *Int. J. Pharm.* **378**, 194-200 (2009).

38 Chen, J. *et al.* A highly efficient siRNA carrier of PBLG modified hyperbranched PEI. *Macromol. Biosci.* **9**, 1247-1253 (2009).

39 Ge, Q. *et al.* Inhibition of influenza virus production in virus-infected mice by RNA interference. *Proc. Natl. Acad. Sci.* **101**, 8676-8681 (2004).

40 Tan, P. H., Yang, L. C., Shih, H. C., Lan, K. C. & Cheng, J. T. Gene knockdown with intrathecal siRNA of NMDA receptor NR2B subunit reduces formalin-induced nociception in the rat. *Gene Ther.* **12**, 59-66 (2005).

41 Urban-Klein, B., Werth, S., Abuharbeid, S., Czubayko, F. & Aigner, A. RNAi-mediated gene-targeting through systemic application of polyethylamine (PEI)-complexed siRNA in vivo. *Gene Ther.* **12**, 461-466 (2005).

42 Katas, H. & Alpar, H. O. Development and characterisation of chitosan nanoparticles for siRNA delivery. *J. Control. Release* **115**, 216-225 (2006).

43 Mao, S., Sun, W. & Kissel, T. Chitosan-based formulations for delivery of DNA and siRNA. *Adv. Drug Del. Rev.* **62**, 12-27 (2009).

44 Davis, M. The first targeted delivery of siRNA in humans via a self-assembling, cyclodextrin polymer-based nanoparticle: From concept to clinic. *Mol. Pharm.* **6**, 659-668 (2009).

45 Patil, M. L. *et al.* Internally cationic polyamidoamine PAMAM-OH dendrimers for siRNA delivery: Effect of the degree of quaternization and cancer targeting. *Biomacromolecules* **10**, 258-266 (2009).

46 Lee, J.-H. *et al.* Nanosized polyamidoamine (PAMAM) dendrimer-induced apoptosis mediated by mitochondrial dysfunction. *Toxicol. Lett.* **190**, 202-207 (2009).

47 Svenson, S. Dendrimers as versatile platform in drug delivery applications. *Eur. J. Pharm. Biopharm.* **71**, 445-462 (2009).

48 Elsabahy, M. *et al.* Delivery of nucleic acids through the controlled disassembly of multifunctional nanocomplexes. *Adv. Funct. Mater.* **19**, 3862-3867 (2009).

49 Taratula, O. *et al.* Surface-engineered targeted PPI dendrimer for efficient intracellular and intratumoral siRNA delivery. *J. Control. Release* **140**, 284-293 (2009).

50 Jeong, J. H., Mok, H., Oh, Y.-K. & Park, T. G. siRNA conjugate delivery systems. *Bioconjugate Chem.* **20**, 5-14 (2009).

51 Rozema, D. B. *et al.* Dynamic PolyConjugates for targeted in vivo delivery of siRNA to hepatocytes. *Proc. Natl. Acad. Sci.* **104**, 12982-12987 (2007).

52 Khan, A. *et al.* Sustained polymeric delivery of gene silencing antisense ODNs, siRNA, DNAzymes and ribozymes: in vitro and in vivo studies. *J. Drug Target.* **12**, 393-404 (2004).

53 Tahara, K., Yamamoto, H., Hirashima, N. & Kawashima, Y. Chitosan-modified poly(D,L-lactide-co-glycolide) nanospheres for improving siRNA delivery and gene-silencing effects. *Eur. J. Pharm. Biopharm.* **74**, 421-426 (2010).

54 Patil, Y. & Panyam, J. Polymeric nanoparticles for siRNA delivery and gene silencing. *Int. J. Pharm.* **367**, 195-203 (2009).

55 Convertine, A. J., Benoit, D. S. W., Duvall, C. L., Hoffman, A. S. & Stayton, P. S. Development of a novel endosomolytic diblock copolymer for siRNA delivery. *J. Control. Release* **133**, 221-229 (2009).

56 Brocchini, S. Combinatorial chemistry and biomedical polymer development. *Adv. Drug Delivery Rev.* **53**, 123-130 (2001).

57 Lynn, D. M., Anderson, D. G., Putnam, D. & Langer, R. Accelerated discovery of synthetic transfection vectors: Parallel synthesis and screening of a degradable polymer library. *J. Am. Chem. Soc.* **123**, 8155-8156 (2001).

58 Wong, S. Y., Sood, N. & Putnam, D. Combinatorial evaluation of cations, pH-sensitive and hydrophobic moieties for polymeric vector design. *Mol.Ther.* **17**, 480-490 (2009).

59 Anderson, D. G., Lynn, D. M. & Langer, R. Semi-automated synthesis and screening of a large library of degradable cationic polymers for gene delivery. *Angew. Chem., Int. Ed.* **42**, 3153-3158 (2003).

60 Anderson, D. G., Akinc, A., Hossain, N. & Langer, R. Structure/property studies of polymeric gene delivery using a library of poly(β-amino esters). *Mol. Ther.* **11**, 426-434 (2005).

61 Green, J. J., Langer, R. & Anderson, D. G. A combinatorial polymer library approach yields insight into nonviral gene delivery. *Acc. Chem. Res.* **41**, 749-759 (2007).

62 Semple, S. C. *et al.* Rational design of cationic lipids for siRNA delivery. *Nat. Biotechnol.* **28**, 172-U118 (2010).

63 Zimmermann, T. S. *et al.* RNAi-mediated gene silencing in non-human primates. *Nature* **441**, 111-114 (2006).

64 Love, K. T. *et al.* Lipid-like materials for low-dose, in vivo gene silencing. *Proc. Natl. Acad. Sci. U. S. A.* **107**, 1864-1869 (2010).

65 Mahon, K. P. *et al.* Combinatorial approach to determine functional group effects on lipidoid-mediated siRNA delivery. *Bioconjugate Chem.* **21**, 1448-1454 (2010).

CHAPTER 2[1]

RAFT POLYMERIZATION OF METHACRYLIC ACID AND ACRYLIC ACID

2.1 Introduction

Poly(methacrylic acid) (pMAA) and poly(acrylic acid) (pAA) are versatile polymers that can be employed in many processes. One of the most attractive characteristics of these amphiphilic macromolecules is their unique responsiveness to pH and ionic strength. These properties can be applied to many applications, including particle and micelle formation[1-3] and hydrogel fabrication[4,5].

One of the major challenges in polymer synthesis is the control of molecular weight with narrow polydispersity indices (PDI), defined as the ratio of the weight average molecular weight (M_w) to the number average molecular weight (M_n). Several techniques have been employed to synthesize methacrylic acid (MAA) and acrylic acid (AA) homopolymers and MAA- or AA-containing block copolymers, including free radical polymerization (FRP)[6] and atom transfer radical polymerization (ATRP)[7]. FRP tends to produce uncontrolled polymerizations giving rise to high PDI values. In the case of ATRP, direct polymerization of the acidic form is challenging[8] and thus the salt form or other derivatives, such as sodium methacrylate[9], *n*-butyl methacrylate[10] and *tert*-butyl acrylate[11] are typically used.

Reversible addition-fragmentation chain transfer (RAFT) polymerization, developed by Rizzardo and collaborators[12], has risen to become a resourceful technique that can potentially address the limitations that other radical polymerizations encounter in MAA and AA polymerizations. RAFT is a controlled/living free-radical polymerization method that uses both

[1]Reproduced in part with permission from Pelet, J.M., Putnam, D., *Macromolecules* **2009**, 42, 1494-1499.

a radical initiator (I) and a chain transfer agent (CTA). The RAFT mechanism, shown in Figure 2.1, involves a series of addition-fragmentation steps followed by chain equilibration between propagating radicals and dormant species, during which all polymer chains grow at equal rates. RAFT possesses many synthetic advantages, including applicability to a wide range of monomers, flexibility of reaction conditions (including water as the solvent) and the ability to produce complex architectures[13]. The selection of the monomer-initiator pair and the polymerization conditions are critical factors that directly influence the outcome[14,15]. RAFT polymerization of MAA and AA has been previously shown for block copolymers, such as poly(MAA-*block*-methyl methacrylate)[13,16], poly(MAA-*block*-benzyl methacrylate)[13], poly(N-isopropylacrylamide)-*block*-pAA[17] and poly(N-isopropylmethacrylamide)-*block*-pAA[11]. Additionally, RAFT homopolymerization of MAA has been reported by Yang, et al.[18] They performed the synthesis and characterization, as well as a kinetics analysis, of MAA and N-(isopropylacrylamide) homopolymers and poly(N-isopropylacrylamide)-*block*-pMAA block copolymers using the commercially available CTA, carboxylmethyl dithiobenzoate. For MAA homopolymers, they reported a kinetic analysis based on a single set of reaction conditions (methanol, T = 60 ºC, $[MAA]_0$ = 1.90 mol L^{-1} and $[MAA]_0$:$[I]_0$:$[CTA]_0$ = 100:0.25:1) that generated MAA homopolymers with M_n up to 13,300 and PDI = 1.3. However, carboxylmethyl dithiobenzoate degraded during the polymerization, which limits the polymerization control affecting particularly the PDI. On the other hand, RAFT homopolymerization of AA has been reported previously using different CTAs and in a variety of solvents including ethanol, 2-propanol, dioxane, methanol, water and dimethylformamide[12,19-21]. Based upon these initial reports, we sought to identify a synthetic method to create relatively high M_n MAA and AA homopolymers with narrow PDI.

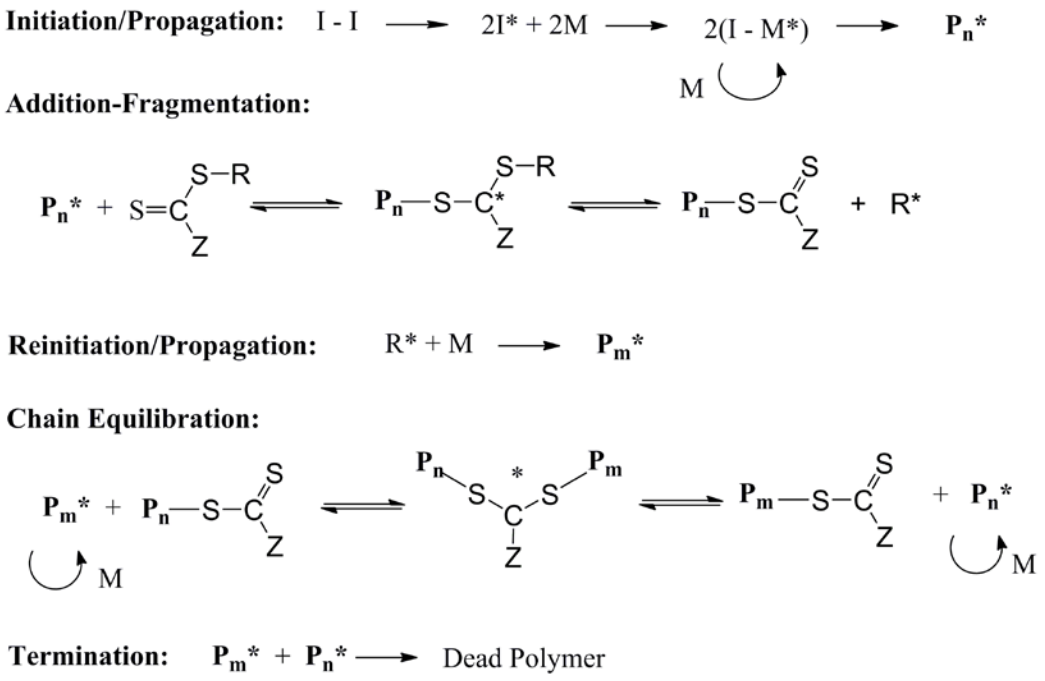

Figure 2.1: The RAFT mechanism. P_n and P_m are polymer chains; P_n* and P_m* are propagating radicals; M is monomer; I is radical initiator; R and Z vary depending on the RAFT CTA.

Herein we report the synthesis and characterization of pMAA and pAA by RAFT polymerization using 4-cyanopentanoic acid dithiobenzoate[22] (CPA-DB) as the CTA under a range of synthesis conditions. The system employs 4,4'-azobis(4-cyanopentanoic acid) (A-CPA) as a radical initiator, which in conjunction with CPA-DB, is an efficient RAFT initiator pair for several polymers including methacrylates[12,23] and methacrylamides[24,25]. In our analysis, we evaluated the effect of $[MAA]_0$:$[CTA]_0$ and$[CTA]_0$:$[I]_0$ ratios as well as two different solvents, methanol and water/1,4-dioxane, initial monomer concentration and pH on MAA homopolymerization in order to obtain well controlled polymerization that achieves relatively high M_n pMAA with narrow PDI. Based on the results obtained for pMAA, pAA we synthesized in a similar fashion by RAFT polymerization in methanol. We report the relationship of M_n with conversion as well as a kinetic analysis of both polymerization under various conditions. In addition, we highlight the conditions that achieve a range of M_n with narrow PDI up to a M_n of 113,900 with PDI~1.13 and M_n of 55,200 with PDI~1.23 for MAA and AA homopolymerization, respectively.

2.2 Materials and methods

2.2.1 Materials. Methacrylic acid (99%), acrylic acid (99%), 4,4'-azobis(4-cyanopentanoic acid) (98.0%, Fluka) and 1,4-dioxane, anhydrous (99.8%) were purchased from Sigma-Aldrich and used as received. Poly(methacrylic acid), sodium salt standards were purchased from Polysciences, Inc. (Warrington, PA) and Polymer Standard Services (Mainz, Germany). Elemental analysis was performed by Quantitative Technologies Inc. (Whitehouse, NJ). Melting points were obtained using a Fisher-Johns melting point apparatus. 4-cyanopentanoic acid dithiobenzoate (CPA-DB) was synthesized as previously described by Mitsukami, et al.[26]

(Characterization: ^{1}H NMR (300MHz, $CDCl_3$, ppm): δ 1.95 (s, 3H), δ 2.40-2.78 (m, 4H), δ 7.40 (m, 2H), δ 7.58 (t, 1H), δ 7.91 (d, 2H). Elemental analysis: Calculated ($C_{13}H_{13}NO_2S_2$): C, 55.89%; H, 4.69%; N, 5.01%. Found: C, 56.15%; H 4.72%; N 4.86%. Melting point: 97.0ºC). Unless otherwise stated, all other chemicals were purchased from Fisher Scientific at the highest purity available.

2.2.2 RAFT polymerization. Prior to every experiment, all liquid reagents were purged under argon or nitrogen for at least 10 min. Individual stock solutions of the radical initiator (A-CPA) and CTA (CPA-DB) were prepared with the respective solvent to ensure accurate reactant ratios for a set of reactions at a given condition. For the water/1,4-dioxane solvent (4:1 v/v) system, a water/HCl stock solution (pH = 4) was prepared.

A representative example for MAA polymerization in methanol is as follows: in a 1mL glass ampule equipped with a magnetic stir bar, MAA (0.170 mL, 2 mmol) and CPA-DB (3.72 mg, 13.3 μmol; in 0.5 mL of MeOH) were transferred using a fixed volume pipettor. After 5 min of purging under argon or nitrogen, A-CPA (0.93 mg, 3.3 μmol; in 0.170 mL of MeOH) was added to the ampule. The solution was purged under argon or nitrogen for 2 additional min. The ampule was flame-sealed and inserted in a 60 °C oil bath under continuous stirring. The reaction was stopped at 24 h by inserting the ampule in an ice bath and exposing the solution to air. The polymer was recovered by precipitation in a generous amount of stirring diethyl ether (~50 mL), filtered and dried under vacuum overnight. M_n and PDI calculated by GPC for this particular sample were 12,900 Da and 1.19, respectively and the percent conversion estimated by gravimetric analysis was 91%. ^{1}H NMR (D_2O, ppm): δ 1.07 (br s,3H), δ 1.98 (br s, 2H).

A representative example for MAA polymerization in water/1,4-dioxane is as follows: to a 1 mL glass ampule with a magnetic stir bar containing MAA (0.170 mL, 2 mmol), water/HCl

(0.536 mL) at pH = 4 and CPA-DB (3.72 mg, 13.3 μmol; in 0.074 mL of 1,4-dioxane) were transferred using a fixed volume pipettor. The solution was purged with argon or nitrogen for 5 min followed by the addition of A-CPA (0.93 mg, 3.3 μmol; in 0.060 mL of 1,4-dioxane). The ultimate pH of the solution was 2.8. Following the addition of all reactants, the ampule was purged under argon or nitrogen for 2 additional min, flame-sealed and inserted in a 60 °C oil bath for 4 h under continuous stirring. The product was purified with dialysis using Spectra/Por regenerated cellulose dialysis tubing (3.5 kDa MWCO) against deionized-water for 3 days and lyophilized for 24 h. For the case of small molecular mass polymers (M_n < 7,000 Da), purification was performed using Spectra/Por regenerated cellulose dialysis tubing (1 kDa MWCO). M_n and PDI calculated by GPC for this particular sample were 24,100 Da and 1.18, respectively and the percent conversion estimated by gravimetric analysis was 90%.

A representative example for AA polymerization in methanol is as follows: in a 1 mL glass ampule equipped with a magnetic stir bar, AA (0.150 mL, 2.19 mmol) and CPA-DB (4.09 mg, 14.6 μmol; in 0.4 mL of MeOH) were transferred using a fixed volume pipettor. After 5 min of purging under argon or nitrogen, A-CPA (1.02 mg, 3.65 μmol; in 0.180 mL of MeOH) was added to the ampule. The solution was purged under argon or nitrogen for 2 additional min. The ampule was flame-sealed and inserted in a 60 °C oil bath under continuous stirring. The reaction was stopped at 24 h by inserting the ampule in an ice bath and exposing the solution to air. The polymer was purified and recovered by placing the solution under vacuum for 10 min to evaporate ~50% of the MeOH, diluting with deionized-water, dialyzing using Spectra/Por regenerated cellulose dialysis tubing (3.5 kDa or 1 kDa MWCO) for 3 days against water and lyophilizing for 24 h. M_n and PDI calculated by GPC for this particular sample were 7,400 Da and 1.21, respectively and the percent conversion estimated by gravimetric analysis was 34%.

^{1}H NMR (D_2O, ppm): 1.8 (br t, 2H), δ 2.4 (br s,1H).

2.2.3 Characterization of pMAA and pAA. M_n and PDI for pMAA and pAA were obtained using a Waters Gel Permeation Chromatography (GPC) system equipped with two Ultrahydrogel^{TM} columns (Waters) in series (500 Å and 250 Å), 1515 isocratic HPLC pump and 2414 refractive index detector. Temperature throughout the system was controlled at 30 °C. The mobile phase employed was phosphate buffer saline (pH = 7.4) at a rate of 0.8 mL min^{-1} calibrated with six individual poly(methacrylic acid), sodium salt standards with peak molecular weights ranging from 1,670 to 110,000 Daltons and PDI from 1.02 to 1.11. ^{1}H NMR was performed using a Mercury 300MHz spectrometer with deuterium oxide (D_2O) as the solvent and 3-(trimethylsilyl)-1-propanesulfonic acid, sodium salt (DSS) as an internal reference. Resonances were referenced to DSS at 0 ppm and HOD at 4.81 ppm.

2.3 Results and discussion

2.3.1 Effect of $[monomer]_0$:$[I]_0$:$[CTA]_0$ ratios on MAA and AA polymerizations. Both pMAA and pAA were synthesized via RAFT polymerization using A-CPA as the radical initiator and CPA-DB as the chain transfer agent (Figure 2.2). For pMAA, two different $[MAA]_0$:$[CTA]_0$ ratios (150:1 and 250:1) as well as two $[I]_0$:$[CTA]_0$ ratios (0.25:1 and 0.1:1) were evaluated and compared. The selection of reactant ratios is of vital importance for the polymerization control and directly impacts the final molecular weight.

Figure 2.3 shows the relationship of M_n with conversion for pMAA under the selected reactant ratios in methanol at 60 °C. Experimental M_n as determined by GPC were compared with theoretical M_n calculated using equation 2.1[27], where $[m]_0$ and $[RAFT]_0$ are the initial monomer and CTA concentrations respectively, x is the fractional monomer conversion, M_o is

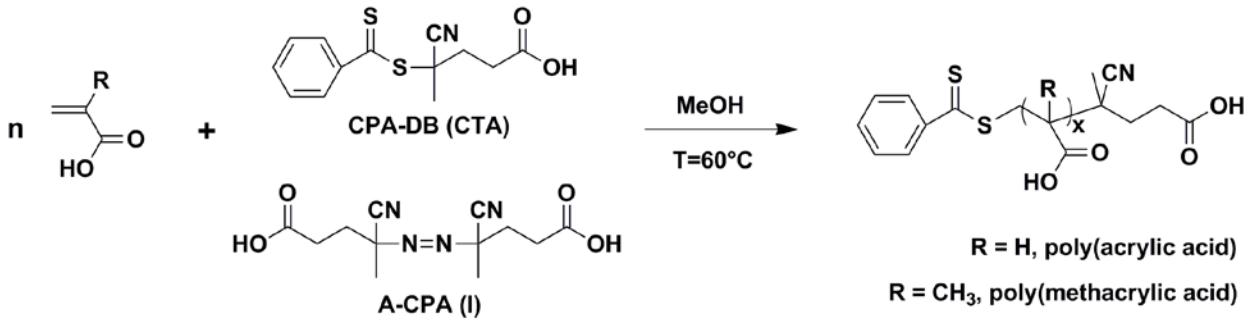

Figure 2.2: Synthesis schematic of pAA or pMAA by RAFT polymerization

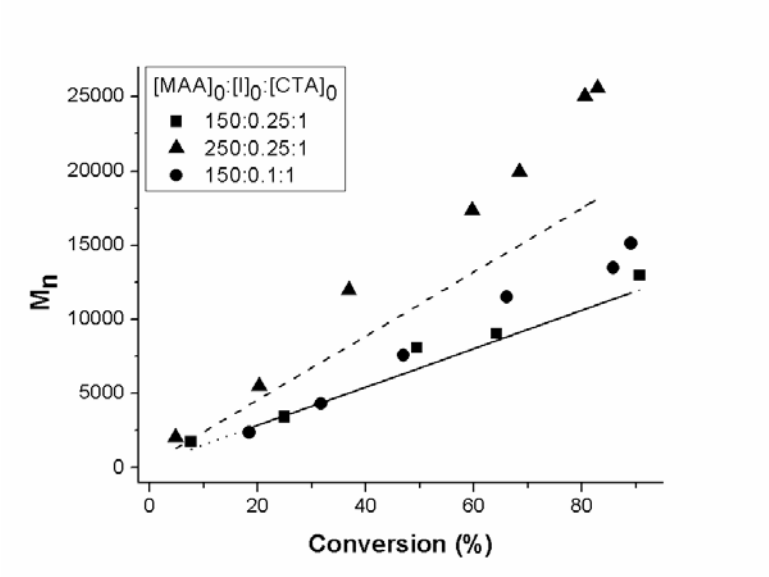

Figure 2.3: Relationship of M_n (GPC) and M_n (theory) with monomer conversion of MAA RAFT polymerization using A-CPA as the radical initiator and CPA-DB as the chain transfer agent. Three initial reactant ratios ($[MAA]_0:[I]_0:[CTA]_0$) were selected: 150:0.25:1 (■), 250:0.25:1 (▲) and 150:0.1:1 (●). The polymerization was conducted in methanol at 60 °C with $[MAA]_0$ = 2.4 mol L^{-1}. M_n (theory) was calculated using equation 2.1 for the three $[MAA]_0:[I]_0:[CTA]_0$: 150:0.25:1 (·····), 250:0.25:1 (----) and 150:0.1:1 (—). Data points were generated from an average of two repetitions that had an error of less than 18%.

the molar mass of the monomer and M_{RAFT} is the molar mass of the CTA.

$$\overline{M}_{n,th} = \frac{[m]_0 \cdot M_0 \cdot x}{[RAFT]_0} + M_{RAFT} \qquad (2.1)$$

For all three conditions, M_n linearly increases with conversion, characteristic of controlled/living polymerizations. The higher $[MAA]_0$:$[CTA]_0$ ratio yields higher M_n due to more free monomer available relative to the CTA initially present. Maintaining $[MAA]_0$:$[CTA]_0$ constant and lowering the $[I]_0$:$[CTA]_0$ ratio (from 0.25:1 to 0.1:1) has a small increasing effect on the M_n throughout the reaction. This behavior has also been distinguished in methacrylamide-based homopolymers employing the same CTA/I RAFT system[24].

It is usually desired to minimize the radical initiator species concentration (particularly $[I]_0 << [CTA]_0$) to favor polymer chain growth exclusively from the CTA species, which can give greater polymerization control and generate lower PDI[14]. However, reducing the radical initiator concentration 2.5-fold did not have a significant impact on the PDI, which only at high conversions (> 88%) were under 1.20. At low conversion, PDI has relatively high values and it gradually decreases as M_n increases (Figure 2.4A). In particular, for $[MAA]_0$:$[I]_0$:$[CTA]_0$ = 150:0.25:1 in methanol, PDI decreased from 1.52 at 8% conversion to 1.19 at 91% conversion. Similar continuously decreasing behavior was observed for all other conditions analyzed. For $[MAA]_0$:$[I]_0$:$[CTA]_0$ = 250:0.25:1, a PDI of 1.17 was achieved at 80% conversion and for $[MAA]_0$:$[I]_0$:$[CTA]_0$ = 150:0.1:1, a PDI of 1.20 was achieved at 88% conversion. It is important to note that changes in the solution color were not observed even at long reaction times, suggesting that the CTA remained undegraded throughout the reaction.

Experimental M_n for the lower reactant ratios ($[MAA]_0$:$[CTA]_0$ = 150:1) were very consistent with theoretical M_n calculated based on actual monomer conversion data demostrating a controlled polymerization behavior. Higher reactant ratios ($[MAA]_0$:$[CTA]_0$ = 250:1)

experienced slightly higher experimental M_n than theoretical M_n (~1.3 times higher) relative to lower reactant ratios. Still, high reactant ratios maintained good agreement with theoretical values. For the current system, the effectiveness of the chosen chain transfer agent with a good free-radical leaving group was demonstrated by the controlled polymerizations achieved that generated polymers with narrow PDI and M_n consistent with theoretical values.

Given the controlled polymerization of MAA in methanol, AA was polymerized in a similar fashion with $[AA]_0:[I]_0:[CTA]_0$ = 150:0.25:1 and $[AA]_0$ = 3.0 mol L^{-1}. Figure 2.4B shows the relationship of M_n and PDI with conversion at these conditions. Although relatively higher experimental M_n were obtained compared to theoretical values, a linear trend of M_n with conversion was achieved, characteristic of controlled/living polymerizations. Similarly to MAA, PDI gradually decreases as M_n increases. Particularly, PDI decreased from 1.36 at 4% conversion to 1.24 at 79% conversion.

2.3.2 Effect of solvent selection on MAA and AA polymerizations. Solvent selection has a dramatic effect on the M_n profiles as well as on the polymerization kinetics. A variety of solvents, including different organics (i.e. benzene, dimethylformamide, ethyl acetate and methanol) in addition to water-based solvent systems have been employed in many RAFT polymerization[13,15,18,28]. The potential applicability of water-based solvents to RAFT polymerizations offers many advantages mainly due to their stability, low cost and ease of use. In particular, pMAA has higher solubility in alcohols and water than in most organics and its previous synthesis was performed in methanol[18]. Therefore, we investigated the effect of solvent on the polymerization progression by comparing an alcohol (methanol) with an aqueous system (water/1,4-dioxane) while maintaining all other parameters constant (i.e. temperature, reactant ratios and concentration). Because CPA-DB is not readily soluble in water at room temperature,

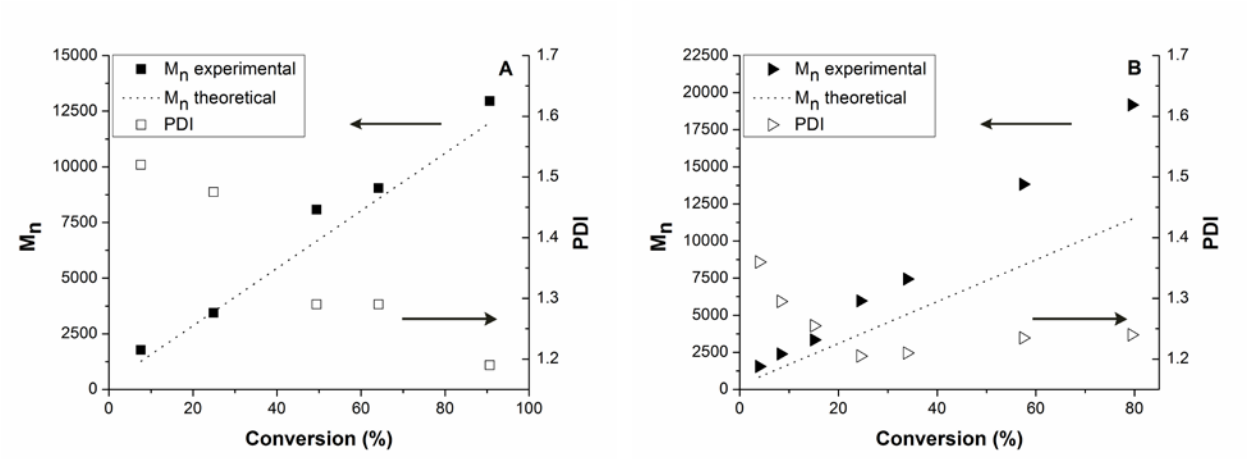

Figure 2.4: Relationship of M_n (GPC), M_n (theory) and PDI with conversion of MAA (A) and AA (B) RAFT polymerizations using A-CPA as the radical initiator and CPA-DB as the chain transfer agent. M_n (theory) was calculated using equation 2.1. The polymerization was conducted at $[monomer]_0:[I]_0:[CTA]_0 = 150:0.25:1$ in methanol at 60 °C with $[MAA]_0 = 2.4$ mol L^{-1} and $[AA]_0 = 3.0$ mol L^{-1}. Data points were generated from an average of two repetitions that had an error of less than 13%.

the addition of a water-miscible organic solvent, in this case 1,4-dioxane, was used to further enhance solubility. The co-solvent issue could have been avoided by selecting a CTA with higher water solubility (i.e. trithiocarbonate).

As seen in Figure 2.5 for the water/1,4-dioxane solvent system, M_n increases linearly with conversion obtaining much higher values (~2 times higher) than both the theoretical M_n calculated using equation 2.1 and the methanol system under the same reaction conditions. A remarkable increase in viscosity after 4 h (90% conversion) which increased until 30 h (93% conversion) in addition to a change in color after 30 h was observed. Interestingly, like methanol, the water-based solvent system achieved low PDI values at high conversion (PDI < 1.20 at conversions > 85%). The apparent rapid increase in M_n could be attributed to many factors such as a faster reaction rate due to higher propagation rate coefficient in this particular solvent system. However, the deviation from theoretical M_n and change in solution color indicates poorer stability of the reactants in aqueous solutions than in methanol, suggesting that the latter is a better solvent choice to achieve greater polymerization control.

One of the undesirable effects associated with water-based systems is the potential hydrolysis of the dithioester group of the CTA, which is temperature and pH dependent[28,29]. CTA hydrolysis leads to its inactivation, generating fewer reactive species than originally introduced into the system leading to higher M_n than the initialy calculated. Therefore, the pH of the solution was maintained at ~3, since for this particular CTA, low pH values have shown to reduce the hydrolysis rate of the dithioester group[29,30].

To further investigate the behavior of MAA RAFT polymerization in water-based solvent, several experiments were performed in different pH solutions. Table 2.1 shows the data for aqueous MAA RAFT polymerization conducted at different pH ranging from 2.8 to 12.8. At

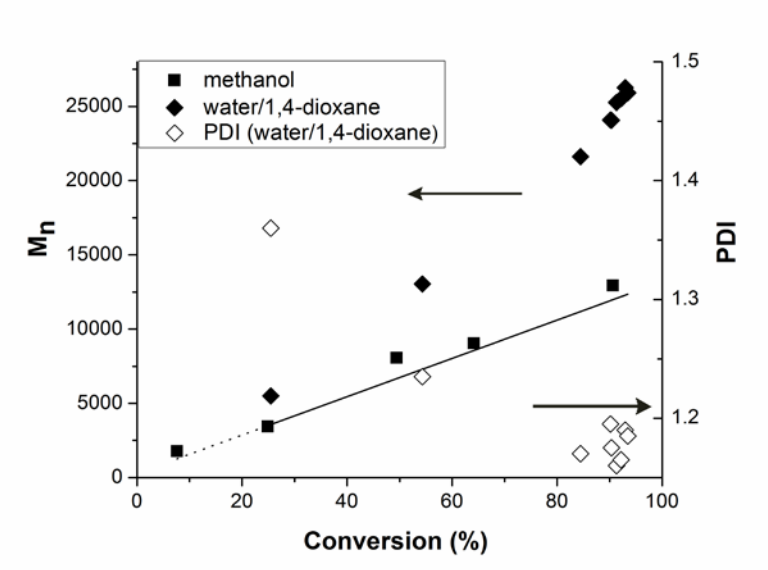

Figure 2.5: Relationship of M_n (GPC), M_n (theory) and PDI with monomer conversion of MAA RAFT polymerization using A-CPA as the radical initiator and CPA-DB as the chain transfer agent in two different solvent: methanol (■) and water/1,4-dioxane (4:1 v/v) (♦). Dotted line (⋯) represents M_n (theory) of MAA RAFT polymerization in methanol and solid line (—) represents M_n (theory) of MAA RAFT polymerization in water/1,4-dioxane, both calculated using equation 2.1. The polymerizations were conducted at $[MAA]_0:[I]_0:[CTA]_0$ = 150:0.25:1 at 60 °C with $[MAA]_0$ = 2.4 mol L^{-1}. Data points were generated from an average of two repetitions that had an error of less than 16%.

constant reaction time (t = 4 h), the monomer conversion gradually decreases as the solution pH increases. The same behavior applies to M_n with the exception of pH = 12.8, where the bimodal molecular weight distribution shifted M_n to a higher value (Figure 2.6). PDI progressively increases as the solution becomes more basic achieving PDI~2 at pH of 12.8. Under this condition (pH 12.8), the loss of polymerization control was clearly observed due to the large disagreement with theoretical M_n, high PDI, pronounced solution decoloration and formation of a bimodal molecular weight distribution, consistent with findings of Albertin et al.[31] using the same CTA agent in basic pH solutions. This behavior has been attributed to degradation of the CPA-DB due to hydrolytic instability in basic pH solutions.

For pAA, polymerizations in three additional solvents, ethanol, 2-propanol and water/1,4-dioxane (4:1 v/v), were conducted at analogous conditions to polymerizations conducted in methanol for 48 h. Data for these polymerizations are included in Table 2.2. Polymerizations conducted in alcohols yielded similar M_n and monomer conversions. Polymerization conducted in water/1,4-dioxane yielded higher experimental M_n (2.2-fold) and higher monomer conversions (1.4-fold); however, PDI remain comparable to the PDI obained for reactions in methanol. This behavior in water-based solvent systems is in accordance with the previous results obtained for MAA RAFT polymerizations in water/1,4-dioxane.

2.3.3 Kinetic analyses of MAA and AA polymerization. MAA and AA homopolymerizations are characteristic of pseudo-first order kinetics that takes place after an initial apparent induction period which is a stage of slow reaction rate dependent on many factors including the monomer/CTA selection. The induction times for MAA polymerizations were estimated to be short (< 1.5 h) for all cases. In the case of AA polymerizations, the induction time was relatively longer (~5.7 h). As seen in Figure 2.7A for MAA, the polymerization develops linearly with

Table 2.1: Experimental and theoretical M_n, PDI and monomer conversion data for aqueous MAA RAFT polymerizations conducted at different pH.[a]

Entry	pH	M_n (GPC)[b]	PDI[b]	Conversion[c] (%)	M_n (theory)[d]
1	2.8[e]	24,100	1.18	90	11,900
2	4.8[f]	10,700	1.39	54	7,300
3	6.7[f]	5,000	1.41	25	3,500
4	12.8[f]	8,600	1.95	12	1,800

[a]MAA RAFT polymerizations were conducted in water/1,4-dioxane (4:1 v/v) at 60 °C for 4 h using A-CPA as radical initiator and CPA-DB as chain transfer agent with $[MAA]_0:[I]_0:[CTA]_0 = 150:0.25:1$ and $[MAA]_0 = 2.4$ mol L^{-1}. Data was generated from an average of two repetitions that had an error of less than 5%. [b]As determined by gel permeation chromatography calibrated with poly(methacrylic acid) standards with PBS (pH=7.4) as mobile phase. [c]As determined by gravimetric analysis. [d]As determined using equation 2.1. [e]pH of solution was adjusted by HCl additions. [f]pH of solution was adjusted by NaOH additions.

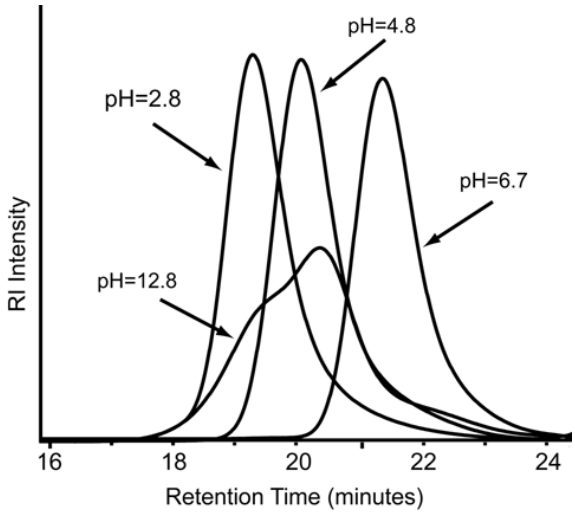

Figure 2.6: Molecular weight distributions for MAA RAFT polymerizations using A-CPA as the radical initiator and CPA-DB as the chain transfer agent, conducted at 60 °C with $[MAA]_0:[I]_0:[CTA]_0 = 150:0.25:1$ and $[MAA]_0 = 2.4$ mol L^{-1}. Polymerizations were carried out in water/1,4-dioxane (4:1 v/v) at different pH.

Table 2.2: Experimental and theoretical M_n, PDI and monomer conversion data for aqueous AA RAFT polymerizations conducted in different solvents.[a]

Entry	Solvent	M_n (GPC)[b]	PDI[b]	Conversion[c] (%)	M_n (theory)[d]
1	methanol	13,800	1.23	57	8,400
2	ethanol	13,700	1.22	63	9,200
3	2-propanol	11,200	1.32	57	8,400
4	water/1,4-dioxane	30,000	1.21	82	11,800

[a]AA RAFT polymerizations were conducted at 60 °C for 48 h using A-CPA as radical initiator and CPA-DB as chain transfer agent with $[AA]_0:[I]_0:[CTA]_0 = 150:0.25:1$ and $[AA]_0 = 3.0$ mol L^{-1}. Data was generated from an average of two repetitions that had an error of less than 6%. [b]As determined by gel permeation chromatography calibrated with poly(methacrylic acid) standards with PBS (pH = 7.4) as mobile phase. [c]As determined by gravimetric analysis. [d]As determined using equation 2.1.

time until nearly complete monomer consumption where the rate of polymerization is minimal and cannot be accurately measured. Increasing $[MAA]_0$:$[CTA]_0$ causes a decrease in the polymerization rate; however, PDI is not affected and the ultimate M_n obtained is higher. Moreover, reducing the concentration of radical initator decreases the polymerization rate due to the lack of radical initiator species that could potentially initiate polymer chains. In agreement with Figure 2.5, the solvent has a dramatic effect on polymerization rate. For the aqueous system the polymerization progresses extremely rapid at very short times and slows after about 6 h, a behavior that might have been affected by the type of solvent and increase in viscosity. AA polymerization evolves much slower than MAA polymerization in methanol (Figure 2.7B). This slow polymerization rate will influence the reaction time required to achieve complete monomer conversion and can also ultimately affect the PDI.

Several factors, including initial monomer concentration and temperature, have been found to directly impact the propagation rate coefficients in free-radical polymerizations of MAA[32-35]. For this reason, we investigated the effect of initial monomer concentration on MAA RAFT polymerizations in both solvents.

Table 2.3 includes the data for MAA homopolymerizations at three initial MAA concentrations, 1.0 mol L^{-1}, 2.4 mol L^{-1} and 5.0 mol L^{-1} in two solvents, methanol and water/1,4-dioxane, at 60 °C. For both systems (aqueous and methanol), it is apparent that at the same reaction time, higher $[MAA]_0$ yields higher monomer conversion which may indicate that the polymerization becomes faster as $[MAA]_0$ increases. For the aqueous systems at high monomer conversions, all three conditions demonstrated similar high deviation from theoretical M_n values calculated using equation 2.1. However, higher $[MAA]_0$ generated polymers with narower PDI. For the methanol system, all three conditions achieve narrow PDI at high monomer conversion.

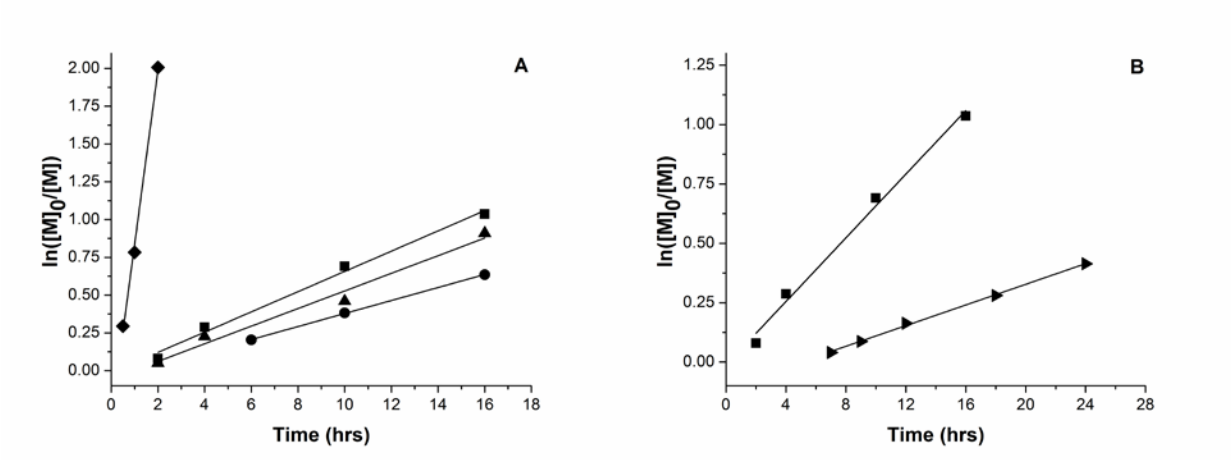

Figure 2.7: Relationship of $\ln([M]_0/[M])$ with time. (A) MAA RAFT polymerization at three initial reactant ratios and two different solvents. Ratio (MAA:I:CTA), solvent → ■ 150:0.25:1, methanol; ▲ 250:0.25:1, methanol; ● 150:0.1:1, methanol; ♦ 150:0.25:1, water/dioxane (4:1 v/v). The polymerizations were conducted at 60 °C with $[MAA]_0$ = 2.4 mol L^{-1}. Solid lines (—) represent linear regressions calculated based on short times only where chain growth is linear with time (16 h for methanol and 2 h for water/1,4-dioxane). R^2 values for linear regressions > 0.97 for all cases. (B) AA RAFT polymerization. Ratio (AA:I:CTA), solvent → ► 150:0.25:1, methanol. The polymerizations were conducted at 60 °C with $[AA]_0$ = 3.0 mol L^{-1}. Solid lines (—) represent linear regressions. R^2 values for linear regressions > 0.99. Data for MAA RAFT polymerization at analogous conditions ($[MAA]_0$:$[I]_0$:$[CTA]_0$ = 150:0.25:1, methanol) was included for comparison (■).

Table 2.3: Experimental and theoretical M_n, PDI and monomer conversion data of MAA RAFT polymerization conducted at different initial MAA concentration in two solvents, methanol and water/1,4-dioxane (4:1 v/v).[a]

Entry	Solvent	$[MAA]_0$ (mol L^{-1})	Time (hrs)	M_n (GPC)[b]	PDI[b]	Conversion (%)[c]	M_n (theory)[d]
1	water/1,4-dioxane	1.0	0.5	4,200	1.34	21	3,000
2	water/1,4-dioxane	1.0	2	17,600	1.38	82	10,900
3	water/1,4-dioxane	2.4	0.5	5,500	1.36	25	3,500
4	water/1,4-dioxane	2.4	2	21,600	1.17	84	11,100
5	water/1,4-dioxane	5.0	0.5	3,400	1.65	31	4,300
6	water/1,4-dioxane	5.0	2	22,200	1.18	91	12,000
7	methanol	1.0	4	2,000	1.32	5	900
8	methanol	1.0	24	10,800	1.17	60	8,000
9	methanol	2.4	4	3,400	1.48	25	3,500
10	methanol	2.4	24	12,900	1.19	91	12,000
11	methanol	5.0	4	6,900	1.28	40	5,400
12	methanol	5.0	24	19,600	1.11	89	11,800

[a]MAA RAFT polymerizations were conducted in methanol or water/1,4-dioxane (4:1 v/v) at 60 °C using A-CPA as radical initiator and CPA-DB as chain transfer agent with $[MAA]_0:[I]_0:[CTA]_0 = 150:0.25:1$. Data was generated from an average of two repetitions that had an error of less than 17%. [b]As determined by gel permeation chromatography calibrated with poly(methacrylic acid) standards with PBS (pH = 7.4) as mobile phase. [c]As determined by gravimetric analysis. [d]As determined using equation 2.1.

Still, higher $[MAA]_0$ seems to have a greater deviation from theoretical values suggesting that lower $[MAA]_0$ in methanol acheives better polymerization control.

2.3.4 Effect of increasing $[monomer]_0$:$[CTA]_0$ ratio on molecular weight. Table 2.4 includes experimental M_n determined by GPC, theoretical M_n calculated using equation 2.1, monomer conversions and PDI values for the range of investigated $[MAA]_0$:$[CTA]_0$ ratios of RAFT polymerizations performed in methanol at an initial monomer concentration of 2.4 mol L^{-1} and constant reaction time of 48 h. By adjusting the $[MAA]_0$:$[CTA]_0$ ratio, a variety of M_n were obtained ranging from 4,600 up to 113,900. In agreement with the controlled behavior of RAFT polymerizations, when M_n is normalized with conversion and plotted against $[MAA]_0$:$[CTA]_0$ ratios, a linear trend (Figure 2.8A) is observed as expected, consistent with theoretical M_n values. Excluding very low $[MAA]_0$:$[I]_0$:$[CTA]_0$ ratios (50:0.25:1 and 100:0.25:1), all PDI obtained by GPC were below 1.20.

For the RAFT polymerizations of AA, Table 2.5 includes experimental M_n determined by GPC, theoretical M_n calculated using equation 2.1, monomer conversions and PDI values for the range of investigated $[AA]_0$:$[CTA]_0$ ratios of RAFT polymerizations performed in methanol at an initial monomer concentration of 3.0 mol L^{-1} and constant reaction time of 48 h. Similar to MAA polymerizations, by adjusting the $[AA]_0$:$[CTA]_0$ ratio, a variety of M_n were obtained, ranging from 2,900 up to 55,100. Due to the lower polymerization rate, at a fixed reaction time of 48 h, the monomer conversion were much lower (37% - 67%) than for MAA polymerizations. This is accompanied by slightly higher PDI obtained for AA polymerizations. Nevertheless, a linear trend results for M_n normalized with conversion plotted against $[AA]_0$:$[CTA]_0$ ratios (Figure 2.8B), characteristic of controlled polymerizations.

Though a specific M_n can be obtained by allowing the polymerization to progress until a

Table 2.4: Experimental and theoretical M_n, PDI and monomer conversion data of MAA RAFT polymerization conducted in methanol at different initial reactant ratios ($[MAA]_0$:$[CTA]_0$).[a]

Entry	$[MAA]_0$:$[CTA]_0$	M_n (GPC)[b]	PDI[b]	Conversion (%)[c]	M_n (theory)[d]
1	50	4,600	1.36	97	4,500
2	100	8,100	1.24	96	8,500
3	150	16,700	1.18	89	11,800
4	225	21,900	1.15	86	16,900
5	375	35,600	1.15	88	28,700
6	500	42,200	1.15	86	35,300
7	750	56,200	1.15	80	51,900
8	1250	82,300	1.16	77	83,100
9	2500	113,900	1.13	49	105,700

[a]MAA RAFT polymerizations were conducted in methanol at 60° C for 48 h using A-CPA as radical initiator and CPA-DB as chain transfer agent with $[I]_0$:$[CTA]_0$ = 0.25:1 and $[MAA]_0$ = 2.4 mol L^{-1}. Data was generated from an average of three repetitions that had an error of less than 7%. [b]As determined by gel permeation chromatography calibrated with poly(methacrylic acid) standards with PBS (pH = 7.4) as mobile phase. [c]As determined by gravimetric analysis. [d]As determined using equation 2.1.

Table 2.5: Experimental and theoretical M_n, PDI and monomer conversion data of AA RAFT polymerization conducted in methanol at different initial reactant ratios ($[AA]_0$:$[CTA]_0$).[a]

Entry	$[AA]_0$:$[CTA]_0$	M_n (GPC)[b]	PDI[b]	Conversion (%)[c]	M_n (theory)[d]
1	50	2 900	1.36	37	2 000
2	80	5 700	1.31	53	4 200
4	110	7 300	1.24	42	4 600
5	150	13 000	1.22	53	7 700
6	275	20 900	1.19	53	13 900
7	350	33 200	1.21	65	21 700
8	620	55 100	1.23	67	39 300

[a]AA RAFT polymerizations were conducted in methanol at 60 °C for 48 h using A-CPA as radical initiator and CPA-DB as chain transfer agent with $[I]_0$:$[CTA]_0$ = 0.25:1 and $[AA]_0$ = 3.0 mol L^{-1}. Data was generated from an average of three repetitions that had an error of less than 7%. [b]As determined by gel permeation chromatography calibrated with poly(methacrylic acid) standards with PBS (pH = 7.4) as mobile phase. [c]As determined by gravimetric analysis. [d]As determined using equation 2.1.

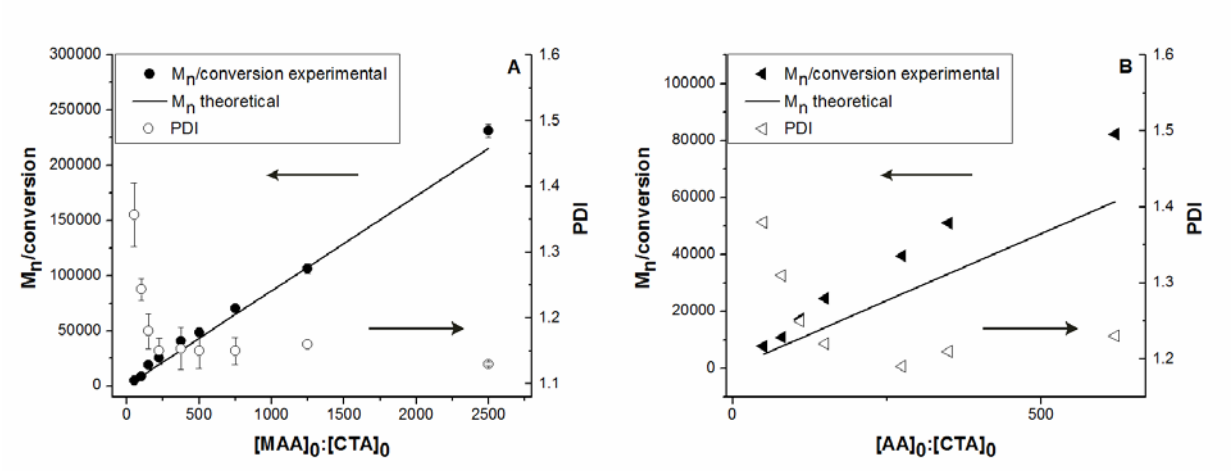

Figure 2.8: Relationship of M_n/conversion (GPC), M_n (theory) and PDI with initial reactant ratio ($[monomer]_0$:$[CTA]_0$) using A-CPA as the radical initiator and CPA-DB as the chain transfer agent. The polymerizations were conducted at 60 °C for 48 h. (A) MAA RAFT polymerization. For each reaction, the solvent volumes were adjusted to maintain the MAA concentration at 2.4 mol L^{-1} (0.21 g/mL). Data points were generated from an average of three repetitions that had an error of less than 7%. Error bars represents standard errors. (B) AA RAFT polymerization. For each reaction, the solvent volumes were adjusted to maintain the AA concentration at 3.0 mol L^{-1} (0.28 g/mL). Data points were generated from an average of two repetitions that had an error of less than 5%.

specific monomer conversion (or a definite time), varying the $[monomer]_0$:$[CTA]_0$ ratio and allowing the polymerization to continue to near completion seems to be a more effective approach given that it can yield polymers with narrower PDI. In this case, we fixed the reaction time to have a controlled variable. However, higher $[monomer]_0$:$[CTA]_0$ required longer times to reach completion which is why a normalized M_n was included in the plot for molecular weights vs. reactant ratios shown in Figure 2.8(A-B). For high reactant ratios in MAA polymerizations (2500:0.25:1), M_n was as high as 113,900 at only 49% conversion with a narrow PDI of 1.13. For AA polymerizations, M_n up to 55,100 with 67% conversion and PDI of 1.23 were achieved. Narrow PDIs for low M_n polymers using this system are difficult to achieve but could be obtained by employing a CTA with much higher transfer constant. Experimental M_n obtained were slightly higher than the theoretical values calculated from conversion data since the theoretical values assume absolute polymerization control and non-degradation of the CTA which, although to a minimal extent, is inevitable even in alcohol systems.

2.4 Conclusions

RAFT polymerization was employed to synthesize pMAA and pAA with controlled molecular weights and narrow PDIs. Both polymers can potentially serve as precursors to polymer conjugates; therefore, they were further evaluated for single and binary conjugations of two ligands, D-(+)-galactosamine and agmatine. However, only pAA was selected as a precursor to polymer conjugates to be evaluated for siRNA delivery due to a higher degree of conjugation for both ligands as compared to pMAA. For the polymer libraries evaluated, pAA with four distinct M_n, 2,900 (PDI = 1.36), 4,800 (PDI = 1.32), 10,400 (PDI = 1.19) and 20,900 (PDI = 1.19), were synthesized as herein described.

REFERENCES

1 Kumar, A., Lahiri, S. S., Punyani, S. & Singh, H. Synthesis and characterization of pH sensitive poly(PEGDMA-MAA) copolymeric microparticles for oral insulin delivery. *J. Appl. Polym. Sci.* **107**, 863-871 (2008).

2 Burkhardt, M. *et al.* Polyisobutylene-block-poly(methacrylic acid) diblock copolymers: self-assembly in aqueous media. *Langmuir* **23**, 12864-12874 (2007).

3 Bromberg, L. Polymeric micelles in oral chemotherapy. *J. Control. Release* **128**, 99-112 (2008).

4 He, H., Li, L. & Lee, L. J. Photopolymerization and structure formation of methacrylic acid based hydrogels in water/ethanol mixture. *Polymer* **47**, 1612-1619 (2006).

5 Kim, I. S. & Oh, I. J. Drug release from the enzyme-degradable and pH-sensitive hydrogel composed of glycidyl methacrylate dextran and poly(acrylic acid). *Arch. Pharm. Res.* **28**, 983-987 (2005).

6 Kaneko, Y., Iwakiri, N., Sato, S. & Kadokawa, J.-i. Stereospecific free-radical polymerization of methacrylic acid calcium salt for facile preparation of isotactic-rich polymers. *Macromolecules* **41**, 489-492 (2008).

7 Yuan, J., Shi, Y., Fu, Z. & Yang, W. Synthesis of amphiphilic poly(methyl methacrylate)-block-poly(methacrylic acid) diblock copolymers by atom transfer radical polymerization. *Polym. Int.* **55**, 360-364 (2006).

8 Matyjaszewski, K. & Xia, J. Atom transfer radical polymerization. *Chem. Rev.* **101**, 2921-2990 (2001).

9 Ashford, E. J., Naldi, V., O'Dell, R., Billingham, N. C. & Armes, S. P. First example of the atom transfer radical polymerisation of an acidic monomer: direct synthesis of methacrylic acid copolymers in aqueous media. *Chem. Commun.* **14**, 1285-1286 (1999).

10 Lee, S. B., Russell, A. J. & Matyjaszewski, K. ATRP synthesis of amphiphilic random, gradient, and block copolymers of 2-(dimethylamino)ethyl methacrylate and n-butyl methacrylate in aqueous media. *Biomacromolecules* **4**, 1386-1393 (2003).

11 Rathfon, J. M. & Tew, G. N. Synthesis of thermoresponsive poly (N-isopropylmethacrylamide) and poly(acrylic acid) block copolymers via post-functionalization of poly(N-methacryloxysuccinimide). *Polymer* **49**, 1761-1769 (2008).

12 Chiefari, J. *et al.* Living free-radical polymerization by reversible addition-fragmentation chain transfer: The RAFT process. *Macromolecules* **31**, 5559-5562 (1998).

13 Chong, B. Y. K., Le, T. P. T., Moad, G., Rizzardo, E. & Thang, S. H. A more versatile route to block copolymera and other polymers of complex architecture by living radical polymerization: The RAFT process. *Macromolecules* **32**, 2071-2074 (1999).

14 Moad, G. *et al.* Living free radical polymerization with reversible addition - fragmentation chain transfer (the life of RAFT). *Polym. Int.* **49**, 993-1001 (2000).

15 Moad, G., Chong, Y. K., Postma, A., Rizzardo, E. & Thang, S. H. Advances in RAFT polymerization: the synthesis of polymers with defined end-groups. *Polymer* **46**, 8458-8468 (2005).

16 Sprong, E., Wet-Roos, D. D., Tonge, M. P. & Sanderson, R. D. Characterization and rheology properties of model alkali-soluble rheology modifiers synthesized by reversible addition-fragmentation chain-transfer polymerization. *J. Polym. Sci., Polym. Chem. Ed.* **41**, 223-235 (2003).

17 Kulkarni, S. *et al.* Controlling the aggregation of conjugates of streptavidin with smart block copolymers prepared via the RAFT copolymerization technique. *Biomacromolecules* **7**, 2736-2741 (2006).

18 Yang, C. & Cheng, Y.-L. RAFT synthesis of poly(N-isopropylacrylamide) and poly(methacrylic acid) homopolymers and block copolymers: kinetics and characterization. *J. Appl. Polym. Sci.* **102**, 1191-1201 (2006).

19 Ji, J., Jia, L., Yan, L. & Bangal, P. R. Efficient synthesis of poly(acrylic acid) in aqueous solution via a RAFT process. *J. Macrom. Sci., Part A* **47**, 445 - 451 (2010).

20 Loiseau, J. *et al.* Synthesis and characterization of poly(acrylic acid) produced by RAFT polymerization. Application as a very efficient dispersant of CaCO3, kaolin, and TiO2. *Macromolecules* **36**, 3066-3077 (2003).

21 Ladavière, C., Dörr, N. & Claverie, J. P. Controlled radical polymerization of acrylic acid in protic media. *Macromolecules* **34**, 5370-5372 (2001).

22 Thang, S. H., Chong, Y. K., Mayadunne, R. T. A., Moad, G. & Rizzardo, E. A novel synthesis of functional dithioesters, dithiocarbamate, xanthates and trithiocarbonates. *Tetrahedron Lett.* **40**, 2435-2438 (1999).

23 Xiong, Q., Ni, P., Zhang, F. & Yu, Z. Synthesis and characterization of 2-(dimethylamino)ethyl methacrylate homopolymers via aqueous RAFT polymerization and their application in miniemulsion polymerization. *Polym. Bull.* **53**, 1-8 (2004).

24 Scales, C. W., Vasilieva, Y. A., Convertine, A. J., Lowe, A. B. & McCormick, C. L. Direct, controlled synthesis of the nonimmunogenic, hydrophilic polymer, poly(N-(2-hydroxypropyl)methacrylamide) via RAFT in aqueous media. *Biomacromolecules* **6**, 1846-1850 (2005).

25 Li, Y., Lokitz, B. S. & McCormick, C. L. Thermally responsive vesicles and their structural "locking" through polyelectrolyte complex formation. *Angew. Chem. Int. Edit.* **45**, 5792-5795 (2006).

26 Mitsukami, Y., Donovan, M. S., Lowe, A. B. & McCormick, C. L. Water-soluble polymers. 81. direct synthesis of hydrophilic styrenic-based homopolymers and block copolomers in aqueous solutions via RAFT. *Macromolecules* **34**, 2248-2256 (2001).

27 Brouwer, H. d., Schellekens, M. A. J., Klumperman, B., Monteiro, M. J. & German, A. L. Controlled radical copolymerization of styrene and maleic anhydride and the synthesis of novel polyolefin-based block copolymers by reversible addition-fragmentation chain-transfer (RAFT) polymerization. *J. Polym. Sci., Polym. Chem. Ed.* **38**, 3596-3603 (2000).

28 Baussard, J.-F., Habib-Jiwan, J.-L., Laschewsky, A., Mertoglu, M. & Storsberg, J. New chain transfer agents for reversible addition-fragmentation chain transfer (RAFT) polymerisation in aqueous solution. *Polymer* **45**, 3615-3626 (2004).

29 Thomas, D. B., Convertine, A. J., Hester, R. D., Lowe, A. B. & McCormick, C. L. Hydrolytic susceptibility of dithioester chain transfer agents and implications in aqueous RAFT polymerizations *Macromolecules* **37**, 1735-1741 (2004).

30 McCormick, C. L. & Lowe, A. B. Aqueous RAFT polymerization: recent developments in synthesis of functional water-soluble (co)polymers with controlled structures. *Acc. Chem. Res.* **37**, 312-325 (2004).

31 Albertin, L., Stenzel, M. H., Barner-Kowollik, C. & David, T. P. Effect of an added base on (4-cyanopentanoic acid)-4-dithiobenzoate mediated RAFT polymerization in water. *Polymer* **47**, 1011-1019 (2005).

32 Beuermann, S., D. A. Paquet, J., McMinn, J. H. & Hutchinson, R. A. Propagation Kinetics of Methacrylic Acid Studied by Pulse-Laser Polymerization. *Macromolecules* **30**, 194-197 (1997).

33 Kuchta, F.-D., Herk, A. M. v. & German, A. L. Propagation Kinetics of Acrylic and Methacrylic Acid in Water and Organic Solvents Studied by Pulse-Laser Polymerization. *Macromolecules* **33**, 3641-3649 (2000).

34 Beuermann, S., Buback, M., Hesse, P. & Lacik, I. Free-radical propagation rate coefficient of nonionized methacrylic acid in aqueous solution from low monomer concentration to bulk polymerization. *Macromolecules* **39**, 184-193 (2006).

35 Beuermann, S. *et al.* Termination kinetics of the free-radical polymerization of nonionized methacrylic acid in aqueous solution. *Macromolecules* **41**, 3513-3520 (2008).

CHAPTER 3[1]

AN IN-DEPTH ANALYSIS OF POLYMER ANALOGOUS CONJUGATION USING DMTMM

3.1 Introduction

Combinatorial libraries have become increasingly prominent in the field of functional biomaterials. For instance, combinatorial libraries of polymers[1] have been widely explored for biomedical applications including gene delivery[2-8] and medical device development[9-11]. Of particular importance to the advancement of the field is the development of new synthetic strategies to create increasingly larger and more diverse libraries. In particular, polymeric libraries provide insight to the structure-function relationships of biomaterials to identify favorable structural parameters and allow further optimization of their design.

One approach for creating diverse polymer libraries is polymer-analogous conjugation of functional groups to polymer scaffolds. For example, coupling between the carboxyl groups of a polymer and the amino groups or hydroxyl groups of different ligands can lead to polymer libraries with a range of pre-engineered functionalities. Over the past few years, numerous condensing agents have been developed and extensively used to form amides and esters[12,13]. Carbodiimides, such as dicyclohexylcarbodiimide (DCC) and N-(3-dimethylaminopropyl)-N'-ethylcarbodiimide (EDC), are particularly popular condensing agents. While these condensing agents are widely used, their synthetic byproducts can be difficult to remove. Additionally, many of these reagents require the use of organic solvents and anhydrous conditions to avoid competitive hydrolysis by water, and are expensive. Condensation of both

[1]Reproduced in part with permission from Pelet, J.M., Putnam, D., *Bioconjugate Chem.* **2011**, DOI: 10.1021/bc100125r.

poly(methacrylic acid) (pMAA) and poly(acrylic acid) (pAA) with amine-containing antibodies has been previously reported with carbodiimides and N-hydroxysuccinimide (NHS)[14]. [1,3,5]-triazine based condensing agents have been exploited due to their great versatility[15,16]. Recently, 4-(4,6-dimethoxy-1,3,5-triazin-2-yl)-4-methylmorpholinium chloride (DMTMM) was developed and shown to facilitate an efficient one-step condensation of both small molecules and polymers[17-19]. Other favorable attributes of DMTMM are easy removal of excess reagent and byproducts from the reaction, compatibility with many solvents including water, alcohols and diethyl ether, ethyl acetate and tetrahydrofuran[16], high reaction yields, and it is relatively inexpensive. DMTMM can adapt to a wide pH range, and in some cases no rigorous pH control is necessary[20,21]. DMTMM has been employed for the modification of a number of polymers including polysaccharides[21,22], poly-γ-D-glutamic acid[23], and as a coupling agent for peptidomimetics[24]. Furthermore, DMTMM has been previously reported for direct conjugation of amine-containing ligands, including hydrophobic and hydrophilic groups, to pAA[20]. Although these groups were substituted to the side chains with high efficiency, successful conjugation is dependent on a manifold of parameters including the ligand properties, particularly when cationic species are involved. To our knowledge, the optimization for effective conjugation of such moieties to polymer precursors using DMTMM has yet to be reported. The characterization of post-polymerization modifications of polymers with structurally heterogeneous functional groups will be of significant benefit for the development of new materials.

Herein we report the conditions for optimal polymer-analogous conjugation of two diverse model ligands, D-(+)-galactosamine (Gal) and agmatine (Agm), to the side chain carboxyl groups of both pMAA and pAA. The choice of these two amine-containing ligands is based on their unique structural characteristics, particularly their different size and net charge,

which can influence the conjugation efficacy by steric hindrance or electrostatic effects. We report optimal conditions under which these model ligands conjugate to pMAA and pAA using DMTMM and create limited polymer libraries containing several single and binary substitution ratios of both ligands to each individual polymer. The goal of this work is to form the synthetic foundation upon which large, diverse polymer libraries can be generated to investigate the structure-function relationships of polymeric materials.

3.2 Materials and Methods

3.2.1 Materials. 4-(4,6-Dimethoxy-1,3,5-triazin-2-yl)-4-methylmorpholinium chloride hydrate (+99%) and D-(+)-galactosamine hydrochloride (99%) were purchased from Acros Organics. Agmatine sulfate was purchased from Fluka (≥ 99%) or Sigma-Aldrich (≥ 97%), and was recrystallized from water/ethanol (1.4:1 v/v). N-hydroxysuccinimide (98%) and N-(3-dimethylaminopropyl)-N'-ethylcarbodiimide hydrochloride were purchased from Sigma-Aldrich. All other reagents were purchased from Fisher Scientific at the highest purity available. pMAA with average-number molecular weight (M_n) of 8,100 and polydispersity index (PDI) of 1.24 was synthesized by reversible addition-fragmentation chain transfer (RAFT) polymerization as previously reported by our group[25]. pAA was synthesized analogous to pMAA by RAFT polymerization with the exception of $[AA]_0$ = 3.0 mol L^{-1} and the purification process. Instead of precipitation in diethyl ether as for pMAA, pAA was purified by drying under vacuum for 10 min to remove ~50% of the methanol and diluting with deionized-water, followed by dialysis using Spectra/Por regenerated cellulose dialysis tubing (3.5 kDa MWCO) against deionized-water for 3 days. Samples were subsequently lyophilized for 24 h. Initial reactant ratios were varied to obtain polymers with different M_n; $[AA]_0$:$[I]_0$:$[CTA]_0$ = 110:0.25:1 corresponded to M_n

= 10,400 (PDI = 1.20), $[AA]_0$:$[I]_0$:$[CTA]_0$ = 350:0.25:1 corresponded to M_n = 33,200 (PDI = 1.21), and $[AA]_0$:$[I]_0$:$[CTA]_0$ = 620:0.25:1 corresponded to M_n = 55,100 (PDI = 1.23). M_n values for pAA were calculated based on pMAA standards.

3.2.2 Gal and Agm conjugation to pMAA or pAA using DMTMM. A representative example for 40% targeted Gal conjugation to pMAA which corresponds to $[COOH]_0$:$[DMTMM]_0$:$[Gal]_0$ = 1:0.4:0.8 (Table 3.1, entry 1) is as follows: In a 10 mL pear-shaped flask equipped with a magnetic stir bar, pMAA (24 mg, 0.28 mmol repeating units) and Gal (47 mg, 0.22 mmol) were dissolved with 6 mL of 0.1 M borate buffer, pH = 8.5. After 10 min under stirring, a DMTMM solution (30 mg, 0.11 mmol; in 2 mL of 0.1 M borate buffer, pH = 8.5) was transferred dropwise, and the pH was adjusted to 6.7 with additions of 1 N hydrochloric acid (HCl). The reaction flask was capped with a rubber septum and continuously stirred (600 rpm) for 24 h at room temperature. The product was purified by dialysis using Spectra/Por regenerated cellulose dialysis tubing (3.5 kDa MWCO) against 0.001 M borate buffer (pH = 8.5) for 2 days and deionized-water for 2 additional days and lyophilized for 24 h. The ligand content relative to the total repeating units (or side chains) in each polymer was determined by ^{1}H NMR and is referred to as a percentage value. For example, pMAA-12%Gal means 12% of the total side chains in pMAA are grafted with a pendant Gal. Agm conjugations to pMAA, Gal conjugations to pAA and Agm conjugations to pAA followed the same procedure as previously described with the pH adjusted to 9.1, 7.0 and 8.0, respectively, by additions of 1 N HCl or 1 N sodium hydroxide (NaOH). For Agm conjugations to pMAA and pAA, the product was purified by dialysis using Spectra/Por regenerated cellulose dialysis tubing (3.5 kDa MWCO) against 0.001 M HCl (pH~3) for 2 days and deionized-water for 2 additional days and lyophilized for 24 h.

3.2.3 Gal and Agm conjugation to pMAA using EDC/NHS. The conjugation of amine-containing ligands to pMAA using EDC/NHS was modified from previously established protocols[13]. A representative example for 100% targeted Gal conjugation to pMAA which corresponds to $[COOH]_0$:$[EDC]_0$:$[NHS]_0$:$[Gal]_0$ = 1:1:2.5:5 (Table 3.1, entry 11) is as follows: In a 25 mL pear-shaped flask equipped with a magnetic stir bar, pMAA (20 mg, 0.23 mmol repeating units) was dissolved with 6 mL of 0.05 M MES, 0.5 M NaCl buffer, pH 6.5. After complete dissolution, EDC (44mg, 0.23 mmol; in 2 mL of 0.05 M MES, 0.5 M NaCl buffer, pH 6.5) and NHS (67mg, 0.58 mmol; in 2 mL of 0.05 M MES, 0.5 M NaCl buffer, pH 6.5) solutions were sequentially added to the reaction, and the pH was adjusted to 6.5 with additions of 1 N NaOH. The reaction flask was capped with a rubber septum and continuously stirred (600 rpm) for 1 h at room temperature after which a Gal solution (248 mg, 1.15 mmol; in 2mL of 0.1 M phosphate buffer, pH 7.5 was transferred dropwise. The pH was readjusted to 7.5 with additions of 1 N NaOH, and the reaction was allowed to continuously stir overnight (600 rpm) at room temperature. The product was purified by dialysis using Spectra/Por regenerated cellulose dialysis tubing (3.5 kDa MWCO) against 0.001 M phosphate buffer (pH = 7.5) for 2 days and deionized-water for 2 additional days and lyophilized for 24 h. The ligand content relative to the total repeating units (or side chains) in each polymer was determined by ^{1}H NMR and is referred to as a percentage value. Agm conjugations to pMAA were carried out under the same reaction conditions. The product was purified by dialysis using Spectra/Por regenerated cellulose dialysis tubing (3.5 kDa MWCO) against 0.001 M HCl (pH~3) for 2 days and deionized-water for 2 additional days and lyophilized for 24 h.

3.2.4 Sequential conjugation of Gal or Agm to pMAA-*graft*-Gal, pAA-*graft*-Gal or pAA-*graft*-Agm using DMTMM. A representative example for 50% targeted Agm conjugation to

available carboxyl groups in pMAA-12%Gal which corresponds to $[COOH]_0$:$[DMTMM]_0$:$[Agm]_0$ = 1:0.5:1 (Table 3.5, entry 1) is as follows: In a 10 mL pear-shaped flask equipped with a magnetic stir bar, pMAA-12%Gal (24 mg, 0.20 mmol COOH) and Agm (46 mg, 0.20 mmol) were dissolved with 6 mL of 0.1 M borate buffer, pH = 8.5. After 10 min under stirring, a DMTMM solution (28 mg, 0.10 mmol; in 2 mL of 0.1 M borate buffer, pH = 8.5) was transferred dropwise, and the pH was adjusted to 9.1 with additions of 1 N NaOH. The reaction flask was capped with a rubber septum and continuously stirred (600 rpm) for 24 h at room temperature. The product was purified by dialysis using Spectra/Por regenerated cellulose dialysis tubing (3.5 kDa MWCO) against 0.001 M HCl (pH~3) for 2 days and deionized-water for 2 additional days and lyophilized for 24 h. The ligand content relative to the total repeating units (or side chains) in each polymer was determined by ^{1}H NMR and is referred to as a percentage value. Agm conjugations to pAA-*graft*-Gal and Gal conjugations to pAA-*graft*-Agm followed the same procedure as previously described with the pH adjusted to 8.0 and 7.0, respectively, by additions of 1 N HCl or 1 N NaOH. For Gal conjugations to pAA-*graft*-Agm, the product was purified by dialysis using Spectra/Por regenerated cellulose dialysis tubing (3.5 kDa MWCO) against 0.001 M borate buffer (pH = 8.5) for 2 days and deionized-water for 2 additional days and lyophilized for 24 h.

3.2.5 Simultaneous conjugation of Gal and Agm to pAA using DMTMM. A representative example for 25% targeted Gal and 75% targeted Agm conjugations to pAA which corresponds to $[COOH]_0$:$[DMTMM]_0$:$[Gal]_0$:$[Agm]_0$ = 1:1:0.25:0.75 (Table 3.6, entry 1) is as follows: In a 10 mL pear-shaped flask equipped with a magnetic stir bar, pAA (24 mg, 0.33 mmol repeating units, Gal (18 mg, 0.083 mmol) and Agm (57 mg, 0.25 mmol) were dissolved with 6 mL of 0.1 M borate buffer, pH = 8.5. After 10 min under stirring, a DMTMM solution (91 mg, 0.33 mmol;

in 2 mL of 0.1 M borate buffer, pH = 8.5) was transferred dropwise, and the pH was adjusted to 7.0 with additions of 1 N HCl. The reaction flask was capped with a rubber septum and continuously stirred (600 rpm) for 24 h at room temperature. The product was purified by dialysis using Spectra/Por regenerated cellulose dialysis tubing (3.5 kDa MWCO) against 0.001 M HCl (pH~3) for 2 days and deionized-water for 2 additional days and lyophilized for 24 h. The ligands content relative to the total repeating units (or side chains) in each polymer was determined by ^{1}H NMR and is referred to as a percentage value.

3.2.6 NMR spectroscopy. ^{1}H NMR spectra of polymer conjugates were obtained using an Inova 400MHz spectrometer. 2-D DOSY NMR spectra of polymer conjugates were obtained using an Inova 600MHz spectrometer. Deuterium oxide (D_2O) was used as the solvent. To the samples that were not readily soluble in D_2O, small additions of deuterium chloride or sodium deuteroxide (30% wt. in D_2O) were added. Resonances were referenced to HOD at 4.81 ppm.

3.3 Results and discussions

The effective design of polymeric libraries with a range of functionalities requires careful characterization of the conjugation process, which is greatly influenced by the polymer precursor and selected ligands. In this study, we evaluate two polymer backbones, pMAA and pAA. Both polymers are readily soluble in water and can easily undergo chemical modifications. The high content of carboxyl groups from the side chains allows diverse combinations of multiple pendant groups grafted to the polymer backbone via amide bonds. However, these related but structurally different polymers showed significant differences in conjugation efficiencies of our two model ligands, Gal and Agm, which sparked our interest to investigate the trends distinguished for such conjugations under various conditions.

3.3.1 NMR analyses for Gal and Agm conjugation to pMAA or pAA. The side chains of both pMAA and pAA were modified by the substitution of Gal and Agm using DMTMM as the condensing agent (Figure 3.1). DMTMM activates the carboxyl groups in the polymer by forming a 2-acyloxy-4,6-dimethoxy-1,3,5-triazine intermediate followed by the nucleophilic attack of the amino group resulting in an amide linkage between the polymer side chains and the ligand of interest[19].

The degree of side chain substitution was determined from the peak intensity ratio of the polymer backbone to the side chain groups by ^{1}H NMR (Inova 400MHz) spectroscopy with D_2O as the solvent, and is referred to as a percentage value. Figure 3.2(A-C) shows the ^{1}H NMR spectra for pMAA-20%Gal, pMAA-37%Agm and pMAA-18%Gal-24%Agm, respectively. The chemical shift for the protons in the α-methyl group (-CH_3) in the polymer backbone of pMAA are distinguished at 0.6-1.4 ppm (peak a) while the protons of the methylene group (-CH_2) are at 1.4-2.3 ppm (peak b). Gal has distinctive chemical shifts at 3.5-4.7 ppm corresponding to 6H along the ring structure at C-2 to C-6 positions and at 5.2 ppm corresponding to 1H at C-1 position (peaks d). Similarly, Agm proton chemical shifts are located at 1.6 ppm for 4H (peak f) and at 3.2 ppm for 4H (peak e). Figure 3.2(D-F) illustrates the ^{1}H NMR spectra for pAA-56%Gal, pAA-30%Agm and pAA-56%Gal-33%Agm, respectively. In the case of pAA and pAA conjugates, the pAA backbone protons have chemical shifts of 1.2-2.0 ppm (peak b) and 2.0-2.8 ppm (peak c) for the methylene (-CH_2) and methyne group (-CH), respectively. Grafted Gal and Agm to pAA have chemical shifts analogous to the pMAA conjugates. However, for pAA, an unexpected peak was observed at 3.7 ppm. Further analysis revealed that this peak was from methanol esterification of the carboxylic acid during RAFT polymerization. The peak was accounted for the quantitation of Gal substitution in pAA.

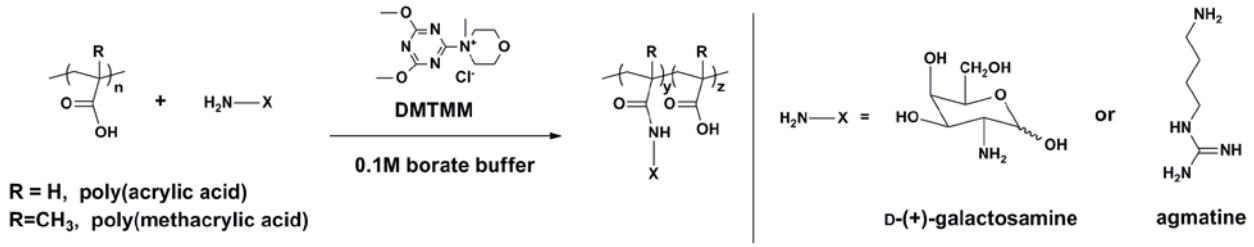

Figure 3.1: Synthesis schematic for condensation reaction of pMAA or pAA and amine-containing ligand (Gal and Agm) using DMTMM as the condensing agent.

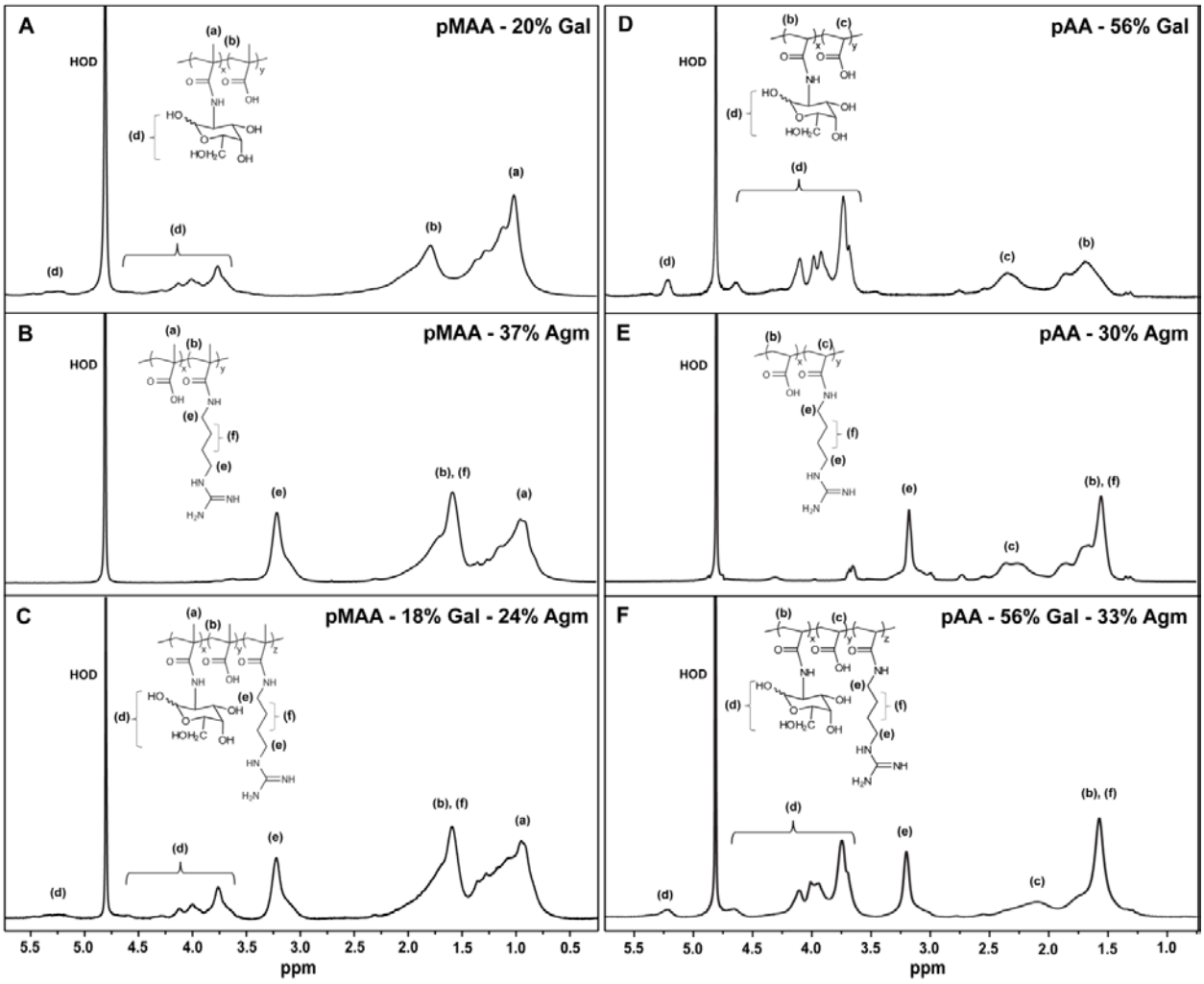

Figure 3.2: ^{1}H NMR spectra (400 MHz, D_2O) of (A) pMAA-20%Gal, (B) pMAA-37%Agm, (C) pMAA-18%Gal-24%Agm, (D) pAA-56%Gal, (E) pAA-30%Agm, and (F) pAA-56%Gal-33%Agm. Peaks: (a) and (b) pMAA backbone; (b) and (c) pAA backbone; (d) Gal; (e) and (f) Agm. pMAA M_n = 8,100 (PDI = 1.24); pAA M_n = 10,400 (PDI = 1.20).

Because of the cationic nature of Agm, the removal of excess Agm from the reaction was performed through dialysis against an acidic environment (pH~3). To corroborate the absence of unconjugated ligand in the final product, diffusion-ordered spectroscopy (DOSY) was carried out for both pMAA and pAA conjugates. DOSY is a pulsed field gradient NMR experiment in which species in a mixture are distinguished by their translational diffusion coefficients. Figure 3.3 shows a representative example of the 2-D DOSY NMR spectrum in D_2O for pAA-56%Gal-33%Agm that demonstrates that both ligands are covalently attached to the polymer side chains and that no residual ligands or byproducts remained in solution after dialysis. In the spectrum generated, the diffusion coefficients have arbitrary units; however, it is important to note that all species in the polymer have the same translational diffusion and that this diffusion is much slower than water (HOD peak), a much smaller molecule. Similar results were obtained for pMAA conjugates.

3.3.2 Effect of pH on Gal and Agm conjugation to pMAA. The extent to which both Gal and Agm conjugate to pMAA is influenced by the pH of the selected buffer. It was previously established that prior to the addition of DMTMM to the reaction, both the carboxylic acid and the amine should be pre-mixed to form an ammonium carboxylate salt[19]. Formation of this salt can also be enhanced by maintaining the pH of the aqueous solution between the acid dissociation constants (pK_a) of both the acid and the amine of interest. The pK_a for the amino group in Gal is 8.49 and 8.02 for the α- and β- configuration, respectively[26], while for the amino group in Agm is 9.07[27]. The pK_a for weak polyacids varies depending on the solution conditions and polymer structure. A titration curve of pMAA with NaOH revealed a functional pK_a of 6.3. Based on this information, the pH range that is likely most favorable for Gal conjugation to pMAA is from 6.3 to 8 and for Agm conjugation to pMAA is from 6.3 to 9. In addition, at these

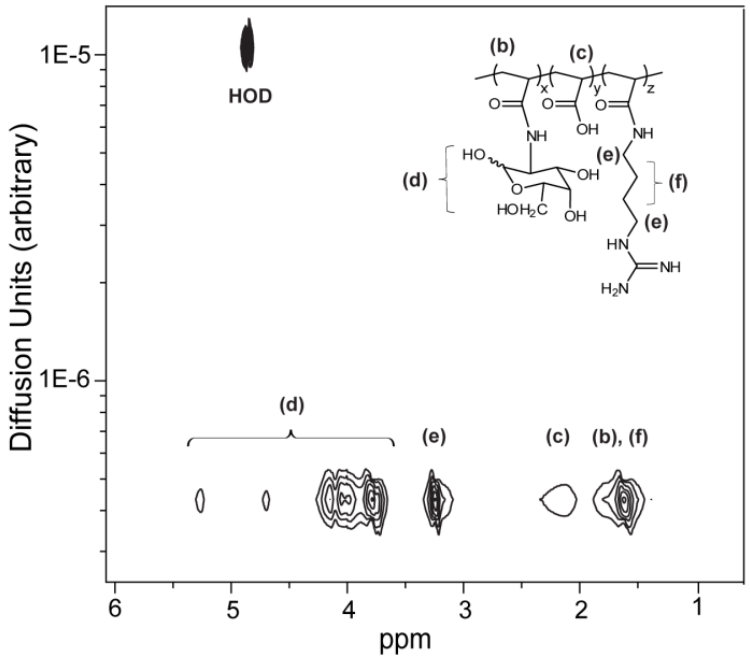

Figure 3.3: 2-D DOSY NMR spectrum (600 MHz, D_2O) of pAA-56%Gal-33%Agm. Chemical shifts and relative diffusion coefficients are shown along the horizontal and vertical axes, respectively. pAA M_n = 10,400 (PDI = 1.20).

pH values the polymer chain is in an extended conformation due to the charge repulsion from the carboxylate groups along the polymer backbone. Figure 3.4A shows the relationship of conjugation efficiency for both Gal and Agm as a function of pH. The conjugation efficiency was calculated from the molar ratio of actual ligand content in the polymer to targeted substitution. pMAA-Agm conjugates experienced solubility issues mostly in acidic environments, and the pH range at which these conjugates were soluble directly depended on the degree of Agm substitution. Moreover, reactions conducted at pH 8 formed conjugates that precipitated out of solution and were not able to be properly analyzed (represented by dashed line in Figure 3.4A). From this analysis, it was determined that the optimal pH in 0.1 M borate buffer for the highest conjugation efficiency of Gal and Agm to pMAA was 6.7 and 9.1, achieving a maximum conjugation efficiency of 20% and 37%, respectively.

3.3.3 Effect of pH on Gal and Agm conjugation to pAA. pAA's behavior in aqueous media is remarkably different from pMAA. A titration curve for pAA generated with NaOH reflected a functional pK_a of 5.9 which gives a slightly larger pH range for effective conjugation as compared to pMAA. The optimal pH in 0.1 M borate buffer was found to be 7.0 and 8.0, corresponding to conjugation efficiencies of 52% and 57% for Gal and Agm conjugation to pAA, respectively (Figure 3.4B). Interestingly, although the pAA structure is comparable to pMAA, the conjugation efficiencies for pAA were significantly higher (2.6- and 1.5-fold for Gal and Agm, respectively) at their optimal pH values. The lack of an α-methyl group in the pAA backbone may have permitted higher conjugation efficiencies relative to pMAA.

During Agm and Gal conjugations to both pMAA and pAA, the solution pH was noticed to decrease to ~ 6.5-8.5 as the reaction proceeded. At these pH values, amine groups will have a lower reactivity toward the ester intermediate. However, increasing the pH to 8 or 9 after 5 h of

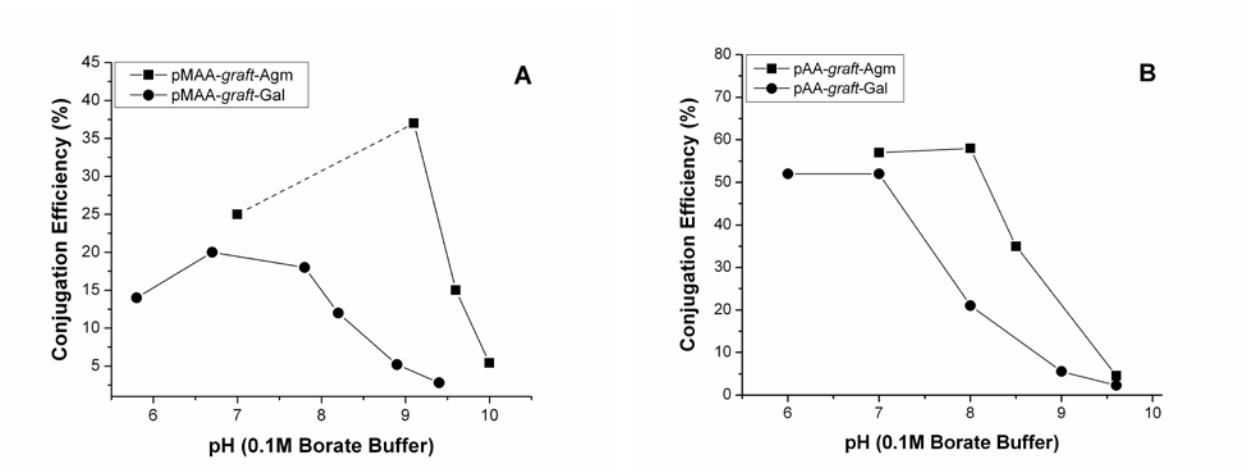

Figure 3.4: Relationship of conjugation efficiency with pH (adjusted at t = 0 h) in 0.1 M borate buffer using DMTMM as the condensing agent: (A) (■) pMAA-*graft*-Agm and (●) pMAA-*graft*-Gal. Dashed lines represents the pH range that was not analyzed due to precipitation of the polymer conjugates; (B) (■) pAA-*graft*-Agm and (●) pAA-*graft*-Gal. Reactions were conducted at room temperature for 24 h with $[\text{polymer}]_0$ = 3 mg/mL and $[\text{COOH}]_0$:$[\text{DMTMM}]_0$:$[\text{NH}_2]_0$ = 1:1:2. Data was generated from an average of two repetitions with standard error $\leq$ 6%. pMAA M_n = 8,100 (PDI = 1.24); pAA M_n = 10,400 (PDI = 1.20).

reaction to favor the deprotonation of the amine groups and enhance reactivity toward the ester intermediate did not have a positive impact on the conjugation efficiency leading to equal or lower Gal and Agm substitutions in both pMAA and pAA (data not shown). It is possible that the ester intermediate begins to hydrolyze before the amidation reaction completely takes place, as also suggested by the lower conjugation efficiencies for reactions carried out at higher pH values (Figure 3.4).

3.3.4 Single conjugation of Gal and Agm to pMAA or pAA. Table 3.1 includes the actual ligand substitutions of Gal and Agm in pMAA and conjugation efficiencies at various $[COOH]_0$:$[DMTMM]_0$ molar ratios. The conjugation efficiency was calculated from the molar ratio of actual ligand substitution to targeted substitution, which is determined from the $[DMTMM]_0$ to $[COOH]_0$ molar ratio. From this data, a noticeable trend is distinguished in which the conjugation efficiency decreases as the reactant ratios of $[DMTMM]_0$ and $[NH_2]_0$ relative to $[COOH]_0$ increases, likely due to steric hindrance. This behavior is observed for both Gal and Agm conjugations to pMAA. The highest conjugation efficiencies obtained with DMTMM were 30% for Gal and 53% for Agm; however, this was when only 40% of the carboxyl groups in pMAA were targeted.

For a direct comparison to other common conjugation reagents, an analogous chemical modification using EDC/NHS was performed. Similar results were obtained at comparable targeted substitutions further suggesting that the polymer and/or ligand structure might be in part responsible for this relatively low conjugation efficiency. Maximum total ligand substitutions (mol %) of 23% Gal and 53% Agm were achieved for pMAA. Decreasing the polymer concentration 3-fold had a negative impact on the conjugation efficiency particularly for Agm substitution which was reduced by half its value. Potential reasons for such conjugation

Table 3.1: Gal and Agm conjugation to pMAA[a]

Entry	Ligand	Condensing agent	$[pMAA]_0$ (mg/mL)	$[COOH]_0$: [condensing agent]$_0$ (mol L^{-1})	Actual substitution (AS)[b] (%)	Conjugation efficiency (CE)[c] (%)
1	Gal[d]	DMTMM	3	1:0.4	12	30
2	Gal[d]	DMTMM	3	1:0.7	18	26
3	Gal[d]	DMTMM	3	1:1	20	20
4	Gal[d]	DMTMM	3	1:2	23	12
5	Gal[d]	DMTMM	1	1:1	16	16
6	Agm[e]	DMTMM	3	1:0.4	21	53
7	Agm[e]	DMTMM	3	1:0.7	30	43
8	Agm[e]	DMTMM	3	1:1	37	37
9	Agm[e]	DMTMM	3	1:2	53	27
10	Agm[e]	DMTMM	1	1:1	17	17
11	Gal[f]	EDC	2	1:1	26	26
12	Gal[f]	EDC	2	1:2	30	15
13	Agm[f]	EDC	2	1:1	25	25
14	Agm[f]	EDC	2	1:2	28	14

[a]Reactions were conducted at room temperature for 24 h. pMAA M_n = 8,100 (PDI = 1.24). [b]As determined by ^{1}H NMR (400MHz) with D_2O as the solvent. [c]As calculated by CE = AS/([condensing agent]$_0$/[COOH]$_0$). [d]Reactions were conducted in 0.1 M borate buffer, pH 6.7 with $[NH_2]_0 = 2\cdot[DMTMM]_0$. [e]Reactions were conducted in 0.1 M borate buffer, pH 9.1 with $[NH_2]_0 = 2\cdot[DMTMM]_0$. [f]Reactions were conducted in a final concentration of 0.042M MES, 0.42M NaCl and 0.017M phosphate buffer, pH 7.5 with $[NH_2]_0 = 5\cdot[EDC]_0$ and $[NHS]_0 = 2.5\cdot[EDC]_0$.

deficiencies might be the chemical characteristics of the polymer and/or ligands, or the short distance between the side chain carboxyl groups and polymer backbone along with the α-methyl group in the polymer backbone which can generate steric hindrance. Previous work by Kazakov and collaborators[14,28] demonstrated that pMAA has a local compact conformation at pH < 5 in part due to the hydrophobic methyl groups attached to the polymer chain. This suggests that the α-methyl group in the polymer backbone has an important role in the conformation of this polymer in solution, and this may influence its ability to interact with other moieties.

In contrast to pMAA, pAA achieved much higher conjugation efficiencies leading to higher total ligand contents under equivalent conditions. The highest total ligand substitutions (mol %) obtained for pAA were 56% Gal and 78% Agm (Table 3.2). Compared to pMAA, a similar decreasing trend of conjugation efficiency with increasing targeted substitution was observed for both Gal and Agm conjugations to pAA, likely due to steric hindrance. It is evident that for both polymer precursors, Agm was more readily incorporated into the polymer side chains than Gal. The low Gal conjugation efficiency may be due to its relatively large, ring-like structure which may cause steric hindrance as compared to the more elongated structure of Agm.

The solubility in aqueous solution of both pMAA-Agm and pAA-Agm conjugates was found to be directly affected by degree of substitution of the ligand (Table 3.3). Agm substituted to less than half of the available carboxyl groups in the polymer will lead to solubility issues in more acidic environments. In contrast, Agm substituted to more than half of the available carboxyl groups in the polymer will experience solubility issues in more basic environments. For instance, by visual inspection, pMAA-25%Agm is insoluble at 3 < pH < 5.8 and pMAA-37%Agm is insoluble at 3 < pH < 6.8, while pMAA-53%Agm is insoluble at pH > 4.9. Similarly for pAA-Agm conjugates, pAA-30%Agm is insoluble at 3 < pH < 5.9, while pAA-

Table 3.2: Gal and Agm conjugation to pAA[a]

Entry	Ligand	$[pAA]_0$ (mg/mL)	$[COOH]_0:[DMTMM]_0:[NH_2]_0$ (mol L^{-1})	Actual substitution (AS)[b] (%)	Conjugation efficiency (CE)[c] (%)
1	Gal[d]	3	1:0.5:1	35	70
2	Gal[d]	3	1:0.7:1.4	41	59
3	Gal[d]	3	1:1:2	52	52
4	Gal[d]	3	1:2:4	56	28
5	Gal[d]	1	1:1:2	43	43
6	Agm[e]	3	1:0.5:1	30	60
7	Agm[e]	3	1:0.7:1.4	46	66
8	Agm[e]	3	1:1:2	57	57
9	Agm[e]	3	1:2:4	78	39
10	Agm[e]	1	1:1:2	32	32

[a]Reactions were conducted at room temperature for 24 h using DMTMM as the condensing agent with $[NH_2]_0 = 2 \cdot [DMTMM]_0$. pAA M_n = 10,400 (PDI = 1.20). [b]As determined by ^{1}H NMR (400MHz) with D_2O as the solvent. [c]As calculated by CE = AS/($[DMTMM]_0/[COOH]_0$). [d]Reactions were conducted in 0.1 M borate buffer, pH 7.0. [e]Reactions were conducted in 0.1 M borate buffer, pH 8.0.

Table 3.3: Solubility of pMAA and pAA conjugates (by visual inspection)

Entry	% Ligand	pH where samples are soluble
pMAA conjugates		
1	53% Agm	pH < 4.9
2	37% Agm	pH > 6.8, pH < 3
3	25% Agm	pH > 5.8, pH < 3
4	12% Gal	Soluble at all pH
5	18% Gal	Soluble at all pH
6	20% Gal	Slightly opaque at all pH
pAA conjugates		
7	78% Agm	Soluble at all pH
8	57% Agm	pH < 8
9	30% Agm	pH > 5.9, pH < 3
10	52% Gal	Soluble at all pH

57%Agm is insoluble at pH > 8. pAA-78%Agm remains soluble at all pHs. These overall pH behaviors are likely due to the presence of both positive and negative charges in the polymer, which at specific pHs cause electrostatic interactions between the charged polymers chains, leading to aggregation and altered solubility. Polymers with lower Agm substitution (< 50%) become soluble at higher pH values as the available carboxyl groups undergo ionization providing a net negative charge which reduces electrostatic interactions between the polymer chains. On the contrary, polymers with higher Agm substitution (> 50%), become soluble at lower pH values as the available carboxyl groups become protonated generating a net positive charge that reduces electrostatic interaction between the polymer chains. The higher the Agm substitution, the more soluble these conjugates become due to a net positive charge in the polymer regardless of the degree of ionization of the available carboxyl groups, as distinguished for pAA-78%Agm. Aggregation of polymer conjugates at certain pHs was confirmed through dynamic light scattering. Figure 3.5 shows the relationship of mean particle diameter (Z-average, nm) with pH for pMAA-37%Agm (A) and pAA-57%Agm (B). pMAA-37%Agm shows aggregation at pH 3-7 while pAA-57%Agm shows aggregation at pH > 8.

For pMAA-Gal conjugates, only relatively high Gal substitution (≥ 20%) produced solubility issues. However, these were on a much smaller scale and were accompanied by a light opaqueness of the polymer solution at all pH ranges. pAA-Gal conjugates did not show any solubility issues regarding the Gal total content, corroborating the role of the cationic charge produced by Agm in solubility issues and aggregation.

To evaluate the impact of the polymer molecular weight on the conjugation efficiency of the ligands, various Agm and Gal conjugations were carried out with pAA of higher M_n, specifically 33,100 Da and 55,200 Da. Solubility issues were more prominent with increasing

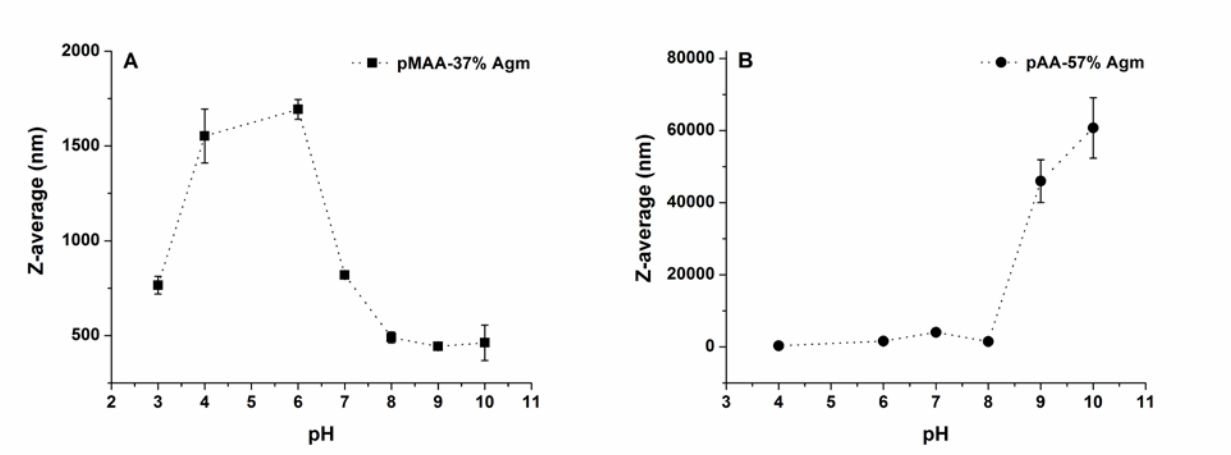

Figure 3.5: Relationship of mean particle diameter (Z-average, nm) with pH in 0.1 M borate buffer. Instruments: Malvern Zetasizer Nano-ZS. Data was generated from three measurements, each consisting of 10 runs of 10 s each. Error bars represents standard deviations from those three measurements. (A) pMAA-37%Agm; (B) pAA-57%Agm.

polymer M_n for pAA-Agm conjugates. As the reaction progressed, these polymer conjugates precipitated out of solution, in which case, they were acidified until fully dissolved prior to dialysis. Total ligand content and conjugation efficiencies were consistent with those values for lower M_n polymers (Table 3.4). To aid the solubility of these polymer conjugates, equivalent reactions were carried out at a lower initial pH (pH 6). However, conjugation efficiencies were ~ 40% lower than the reactions carried out at an initial pH of 8, and solubility issues were still present (data not shown).

In addition to the ease in preparation of single-step reactions and the mild reaction conditions, another significant advantage of post-polymerization modifications mediated by DMTMM is its reproducibility. For single conjugations of Gal or Agm to pMAA and pAA, 70% of the conditions were repeated at least twice and up to four times, all with standard errors $\leq$ 6%. This attribute provides a batch-to-batch consistency that is important to reduce variability of the final product.

3.3.5 Sequential conjugation of Gal and Agm to pMAA or pAA. Owing to their different optimal conjugation characteristics, simultaneous conjugation of both Gal and Agm to pMAA was not viable in a one-step reaction. Following a single-step conjugation containing both ligands, Agm was the only ligand efficiently conjugated, limiting Gal substitution in the polymer side chains (data not shown). Moreover, Gal was unable to be subsequently incorporated in high amounts into pMAA-*graft*-Agm, making a two-step reaction, where Gal was first introduced to the polymer followed by Agm, the most favorable route to having both groups present. The corresponding substitutions and conjugation efficiencies of the two-step approach are shown in Table 3.5. In contrast to pMAA, both Gal and Agm were able to conjugate to pAA sequentially. For both polymers, similar to single conjugations, the conjugation efficiency decreased as higher

Table 3.4: Gal and Agm conjugation to pAA of different molecular weights (M_n)[a]

Entry	pAA M_n (Da)	Ligand	$[COOH]_0$:$[DMTMM]_0$:$[NH_2]_0$ (mol L^{-1})	Actual substitution (AS)[b] (%)	Conjugation efficiency (CE)[c] (%)
1	33,200	Gal[d]	1:1:2	52	52
2	33,200	Gal[d]	1:2:4	60	30
3	33,200	Agm[e]	1:1:2	56	56
4	33,200	Agm[e]	1:2:4	77	39
5	55,100	Gal[d]	1:1:2	49	49
6	55,100	Gal[d]	1:2:4	60	30
7	55,100	Agm[e]	1:1:2	50	50
8	55,100	Agm[e]	1:2:4	75	38

[a]Reactions were conducted at room temperature for 24 h using DMTMM as the condensing agent. [b]As determined by ^{1}H NMR (400MHz) with D_2O as the solvent. [c]As calculated by CE = AS/($[DMTMM]_0$/$[COOH]_0$). [d]Reactions were conducted in 0.1 M borate buffer, pH 7.0. [e]Reactions were conducted in 0.1 M borate buffer, pH 8.0.

Table 3.5: Sequential conjugation of Agm to pMAA-*graft*-Gal and pAA-*graft*-Gal, and of Gal to pAA-*graft*-Agm[a]

Entry	Polymer	$[COOH]_0$:$[DMTMM]_0$:$[NH_2]_0$ (mol L^{-1})	Ligand	Actual substitution (AS)[b] (%)	Conjugation efficiency (CE)[c] (%)
1	pMAA-12%Gal[d]	1:0.5:1	Agm	13	30
2	pMAA-12%Gal[d]	1:0.8:1.6	Agm	21	30
3	pMAA-12%Gal[d]	1:1.1:2.2	Agm	24	25
4	pMAA-18%Gal[d]	1:0.5:1	Agm	15	37
5	pMAA-18%Gal[d]	1:0.8:1.6	Agm	20	30
6	pMAA-18%Gal[d]	1:1.2:2.4	Agm	24	24
7	pMAA-20%Gal[d]	1:0.5:1	Agm	16	40
8	pMAA-20%Gal[d]	1:0.8:1.6	Agm	20	31
9	pMAA-20%Gal[d]	1:1.2:2.4	Agm	24	25
10	pAA-35%Gal[e]	1:0.5:1	Agm	12	37
11	pAA-35%Gal[e]	1:1.1:2.2	Agm	24	34
12	pAA-35%Gal[e]	1:4.8:9.6	Agm	42	13
13	pAA-56%Gal[e]	1:0.5:1	Agm	6	27
14	pAA-56%Gal[e]	1:1.1:2.2	Agm	10	21
15	pAA-56%Gal[e]	1:5.7:11.4	Agm	33	13
16	pAA-30%Agm[f]	1:0.6:1.2	Gal	20	48
17	pAA-30%Agm[f]	1:1.3:2.6	Gal	26	29
18	pAA-30%Agm[f]	1:6.8:13.6	Gal	35	7
19	pAA-46%Agm[f]	1:2.7:5.4	Gal	14	10
20	pAA-46%Agm[f]	1:6.8:13.6	Gal	26	7
21	pAA-57%Agm[f]	1:1.1:2.2	Gal	4	8
22	pAA-57%Agm[f]	1:4.3:8.6	Gal	8	4
23	pAA-78%Agm[f]	1:5:10	Gal	3	3

[a]Reactions were conducted at room temperature for 24 h using DMTMM as the condensing agent with $[NH_2]_0 = 2 \cdot [DMTMM]_0$ and $[polymer]_0 = 3$ mg/mL. pMAA M_n = 8,100 (PDI = 1.24); pAA M_n = 10,400 (PDI = 1.20). [b]As determined by ^{1}H NMR (400MHz) with D_2O as the solvent. [c]As calculated by $CE = AS/(([DMTMM]_0/[COOH]_0) \cdot X_{COOH})$, where X_{COOH} is the fraction of available COOH groups in a polymer chain. [d]Reactions were conducted in 0.1 M borate buffer, pH 9.1. [e]Reactions were conducted in 0.1 M borate buffer, pH 8.0. [f]Reactions were conducted in 0.1 M borate buffer, pH 7.0.

substitutions were targeted, possibly due to an increase in steric hindrance produced by the neighboring pendant groups. Although lower conjugation efficiencies relative to single substitutions were obtained, the versatility of pAA to incorporate both moieties likely makes it a more suitable polymer for this type of conjugation, particularly when a high content of a positively charged moiety (i.e. Agm) is desired.

3.3.6 Simultaneous conjugation of Gal and Agm to pAA. In contrast to pMAA, Agm and Gal were able to conjugate simultaneously to pAA with comparable overall efficiency to single conjugations (Table 3.6). A pH of 7 was selected to accommodate both Gal and Agm conjugations to pAA resulting in the effective substitution of both groups. The flexibility of simultaneous conjugation to pAA offers vast possibilities for dual-functionalization and perhaps multiple simultaneous conjugations of other ligands to these polymer precursors.

3.4 Conclusions

Both pMAA and pAA were modified by the side chain substitution of Gal and Agm at various ratios. A nearly two-fold increase in conjugation efficiencies for both ligands to pAA was achieved as compared to pMAA under identical conditions reaching up to 56% and 80% of Gal and Agm of total content, respectively. The low side chain substitution of Agm, the cationic source, to pMAA caused these polymers to be unable to effectively interact with negatively charged siRNA. Therefore, due to the higher Agm/Gal substitutions relative to pMAA, pAA conjugates were selected for evaluation as siRNA delivery vectors. By varying the $[pAA]_0$ to $[DMTMM]_0$ molar ratio, various Agm/Gal binary combinations were achieved for each polymer precursor. A total of 22 polymer conjugates were evaluated for *in vitro* siRNA delivery.

Table 3.6: Simultaneous conjugation of Gal and Agm to pAA[a]

Entry	$[COOH]_0$:$[DMTMM]_0$:$[Gal]_0$:$[Agm]_0$ (mol L^{-1})	Gal:Agm AS (AS_{Gal}:AS_{Agm})[b] (%)	Gal:Agm CE (CE_{Gal}:CE_{Agm})[c] (%)	Overall CE ($CE_{overall}$)[d] (%)
1	1:1:0.25:0.75	13:39	52:52	52
2	1:1:0.5:0.5	27:28	54:56	55
3	1:1:0.75:0.25	36:17	48:68	53
4	1:1:1:1	30:30	30:30	60
5	1:2:1:1	38:32	38:32	35

[a]Reactions were conducted in 0.1 M borate buffer, pH 7.0 at room temperature for 24 h using DMTMM as the condensing agent with $[polymer]_0$ = 3 mg/mL. pAA M_n = 10,400 (PDI = 1.20). AS = actual substitution. CE = conjugation efficiency. [b]As determined by ^1H NMR (400MHz) with D_2O as the solvent. [c]As calculated by $CE_{Gal} = AS_{Gal}/([Gal]_0/[COOH]_0)$ and $CE_{Agm} = AS_{Agm}/([Agm]_0/[COOH]_0)$. [d]As calculated by $CE_{overall} = (AS_{Gal}+AS_{Agm})/([DMTMM]_0/[COOH]_0)$.

REFERENCES

1 Brocchini, S. Combinatorial chemistry and biomedical polymer development. *Adv. Drug Delivery Rev.* **53**, 123-130 (2001).

2 Anderson, D. G., Akinc, A., Hossain, N. & Langer, R. Structure/property studies of polymeric gene delivery using a library of poly(β-amino esters). *Mol. Ther.* **11**, 426-434 (2005).

3 Anderson, D. G., Lynn, D. M. & Langer, R. Semi-Automated Synthesis and Screening of a Large Library of Degradable Cationic Polymers for Gene Delivery. *Angew. Chem., Int. Ed.* **42**, 3153-3158 (2003).

4 Green, J. J., Langer, R. & Anderson, D. G. A Combinatorial Polymer Library Approach Yields Insight into Nonviral Gene Delivery. *Acc. Chem. Res.* **41**, 749-759 (2007).

5 Lynn, D. M., Anderson, D. G., Putnam, D. & Langer, R. Accelerated Discovery of Synthetic Transfection Vectors: Parallel Synthesis and Screening of a Degradable Polymer Library. *J. Am. Chem. Soc.* **123**, 8155-8156 (2001).

6 Wong, S. Y., Sood, N. & Putnam, D. Combinatorial Evaluation of Cations, pH-sensitive and Hydrophobic Moieties for Polymeric Vector Design. *Mol.Ther.* **17**, 480-490 (2009).

7 Wong, S. Y. & Putnam, D. Overcoming limiting side reactions associated with an NHS-activated precursor of polymethacrylamide-based polymers. *Bioconjugate Chem.* **18**, 970-982 (2007).

8 Thomas, M., Lu, J. J., Zhang, C., Chen, J. & Klibanov, A. M. Identification of Novel Superior Polycationic Vectors for Gene Delivery by High-throughput Synthesis and Screening of a Combinatorial Library. *Pharm. Res.* **24**, 1564-1571 (2007).

9 Brocchini, S., James, K., Tangpasuthadol, V. & Kohn, J. Structure-property correlation in a combinatorial library of degradable biomaterials. *J. Biomed. Mater. Res.* **42**, 66-75 (1998).

10 Jaffe, M., Pai, V., Ophir, Z., Wu, J. & Kohn, J. Relationships of Erodable Polymeric Biomaterials, I: Poly(desaminotyrosyl Arylates). *Polym. Adv. Technol.* **13**, 926-937 (2002).

11 Weber, N., Bolikal, D., Bourke, S. L. & Kohn, J. Small changes in the polymer structure influence the adsorption behavior of fibrinogen on polymer surfaces: Validation of a new rapid screening technique. *J. Biomed. Mater. Res.* **68A**, 496-503 (2004).

12 Montalbetti, C. A. G. N. & Falque, V. Amine bond formation and peptide coupling. *Tetrahedron* **61**, 10827-10852 (2005).

13 Hermanson, G. T. *Bioconjugate Techniques*. (Second ed. (Pierce Biotechnology, Thermo Fisher Scientific, Rockford, IL) pp 219-223, Part II, Academic Press, 2008).

14 Kazakov, S. V. *et al.* Light Scattering Study of the Antibody-Poly(methacrylic acid) and Antibody-Poly(acrylic acid) Conjugates in Aqueous Solutions. *Macromol. Biosci.* **1**, 157-163 (2001).

15 Giacomelli, G., Porcheddu, A. & Luca, L. d. [1,3,5]-Triazine: A Versatile Heterocycle in Current Applications of Organic Chemistry. *Curr. Org. Chem.* **8**, 1497-1519 (2004).

16 Kamiński, Z. J., Paneth, P. & Rudziński, J. A Study on the Activation of Carboxilic Acids by Means of 2-Chloro-4,6-dimethoxy-1,3,5-triazine and 2-Chloro-4,6-diphenoxy-1,3,5-triazine *J. Org. Chem.* **63**, 4248-4255 (1998).

17 Kunishima, M., Kawachi, C., Iwasaki, F., Terao, K. & Tani, S. Synthesis and Characterization of 4-(4,6-Dimethoxy-1,3,5-triazin-2-yl)-4-methylmorpholininum Chloride. *Tetrahedron* **40**, 5327-5330 (1999).

18 Kunishima, M., Kawachi, C., Hioki, K., Terao, K. & Tani, S. Formation of carboxamides by direct condensation of carboxilic acids and amines in alcohols using a new alcohol- and water- soluble condensing agent: DMT-MM. *Tetrahedron* **57**, 1551-1558 (2001).

19 Kunishima, M. *et al.* 4-(4,6-Dimethoxy-1,3,5-triazin-2-yl)-4-methyl-morpholinium Chloride: An efficient Condensing Agent Leading to the Formation of Amides and Esters. *Tetrahedron* **55**, 13159-13170 (1999).

20 Thompson, K. & Michielsen, S. Novel Synthesis of N-Substituted Polyaxrylamides: Derivatization of Poly(acrylic acid) with Amines Using a Triazine-Based Condensing Reagent. *J. Polym. Sci., Part A: Polym. Chem.* **44**, 126-136 (2006).

21 Farkaš, P. & Bystrický, S. Efficient activation of carboxyl polysaccharides for the preparation of conjugates. *Carbohydr. Polym.* **68**, 187-190 (2007).

22 Shlottmann, S. A., Jain, N., Chirmule, N. & Esser, M. T. A novel chemistry for conjugating pneumococcal polysaccharides to Luminex microsperes. *J. Immunol. Methods* **309**, 75-85 (2006).

23 Joyce, J. *et al.* Immunogenicity and Protective Efficacy of Bacillus anthracis Poly-γ-D-glutamic Acid Capsule Covalently Coupled to a Protein Carrier Using a Novel Triazine-based Conjugation Strategy. *J. Biol. Chem.* **281**, 4831-4843 (2006).

24 Shieh, W.-C. *et al.* Synthesis of sterically-hindered peptidomimetics using 4-(4,6-dimethoxy-1,3,4-triazine-2-yl)-4-methyl-morpholinium chloride. *Tetrahedron Lett.* **49**, 5359-5362 (2008).

25 Pelet, J. M. & Putnam, D. High Molecular Weight Poly(methacrylic acid) with Narrow Polydispersity by RAFT Polymerization. *Macromolecules* **42**, 1494-1499 (2009).

26 Blaskó, A., Bunton, C. A., Bunel, S., Ibarra, C. & Moraga, E. Determination of acid dissociation constants of anomers of amino sugars by ^{1}H NMR spectroscopy. *Carbohydr. Res.* **298**, 163-172 (1997).

27 Gründemann, D., Hahne, C., Berkels, R. & Schomig, E. Agmatine Is Efficiently Transported by Non-Neuronal Monoamine Transporters Extraneuronal Monoamine Transporter (EMT) and Organic Cation Transporter 2 (OCT2). *J. Pharmacol. Exp. Ther.* **304**, 810-817 (2003).

28 Kazakov, S. V., Galaev, I. Y. & Mattiasson, B. Characterization of Macromolecular Solutions by a Combined Static and Dynamic Light Scattering Technique. *International Journal of Thermophysics* **23**, 161-173 (2002).

CHAPTER 4

COMBINATORIAL LIBRARY OF BI-FUNCTIONAL POLYMERIC VECTORS FOR siRNA DELIVERY *IN VITRO*

4.1 Introduction

The discovery of RNA interference[1] (RNAi) has led to a revolution in molecular biology and disease treatment. RNAi is a highly regulated post-transcriptional mechanism that modulates protein expression within cells, and has become extremely attractive for studies involving protein regulation both *in vitro* and *in vivo*[2-4]. By taking advantage of this endogenous mechanism, gene silencing can be induced by sequence-specific cleavage of a messenger RNA, thus reducing or eliminating undesired protein expression. Inducing protein knockdown in mammalian systems can be achieved through different effectors, including synthetic small interfering RNA (siRNA), short hairpin RNA (shRNA) which are rapidly converted to siRNA in the cell cytoplasm and DNA encoding for shRNA[5]. Particularly, synthetic siRNA, a 21-23 base pair long oligonucleotide, offers numerous advantages such as a wide range of mRNA targets with high specificity and localized cytoplasmic targeting without chromosomal DNA interference.

Introducing siRNA into cells is limited by numerous challenges, predominantly the lack of effective delivery systems that can safely transport these macromolecules to their site of action while overcoming a manifold of barriers hindering the delivery pathway[6]. In contrast to viral vectors, non-viral delivery systems have become promising therapeutic alternatives due to their low cytotoxicity profiles, low immune response and ease in chemical modifications. Among non-viral delivery systems, polymer-based vectors have increasingly gained attention primarily

due to the ability to tailor their architectures and consequently their physicochemical properties[7-9]. Although several drawbacks exist, such as limited cargo and impermeability through the cell membrane, polymeric vectors can be designed to integrate specific functionalities that provide beneficial properties including cell targeting, pH-responsiveness, and stability in the extracellular medium. Multifunctional polymers are adaptable to address multiple design criteria for bioactive materials[10]; however, identifying optimal structural characteristics from a wide structure-parameter space can be challenging.

Combinatorial libraries of polymers have become a valuable avenue for the design of functional biomaterials, particularly for gene delivery[11-17]. Through combinatorial libraries, the structure-function relationship of biomaterials can be correlated to identify the most favorable structural parameters for optimal outcomes - these being high transfection efficiencies with minimal cytotoxicity. Therefore, this combinatorial approach can be remarkably favorable for the development of bioactive polymers as siRNA delivery systems.

In this study, a combinatorial chemistry approach was employed for a rational design of polymeric vectors for enhanced siRNA delivery through a mechanistic understanding of their structure-function relationships. Toward this goal, poly(acrylic acid) (pAA) of different molecular weights (M_n) was synthesized by reversible addition-fragmentation chain transfer (RAFT). Based on these precursors, a library of polymers was generated by the side chain substitutions of two distinct moieties, D-(+)-galactosamine (Gal) and agmatine (Agm), at different ratios. Agm provides a cationic source to facilitate interactions with the siRNA and enhance cell membrane permeability, while Gal can serve as a tissue-specific targeting ligand. The structural parameters examined include: (1) molecular weight (M_n) of the polymer, (2) Agm content, and (3) Gal content. The biophysical and cellular characterization of these polymeric

vectors was carried out and herein reported. This includes binding affinity of polymers with siRNA, polyplex stability in the presence of competitive ionic species (sodium heparin), polyplex stability in serum, polyplex effective diameter and zeta potential, cytotoxicity and transfection efficiency using MDA-MB-231-luc+ cells as a model cell line.

4.2 Materials and methods

4.2.1 Materials. 25 kDa branched polyethylenimine (PEIb), sodium heparin from porcine intestinal mucosa, fluoresceinamine (FA) and ethidium bromide (EtBr) were purchased from Sigma-Aldrich. Tris(2-carboxyethyl) phosphine hydrochloride (TCEP·HCl) was purchased from Fisher Scientific. HEPES buffer (10mM, pH 7.2) was prepared with ultrapure water and filtered through a 0.2 μm PES membrane. TBE buffer (0.089 M Tris base, 0.089 M boric acid, and 2 mM sodium EDTA) and SYBR green II RNA gel stain were purchased from Invitrogen. MDA-MB-231-luc+ cells were maintained in Dulbecco's Modified Eagle Medium (DMEM, Cellgro, Mediatech Inc., Manassas VA) with 10% v/v Fetal Bovine Serum (FBS, HyClone, Thermo Scientific) at 37°C and 5% CO_2. GL3 siRNA duplex (sense sequence 5'- CUU ACG CUG AGU ACU UCG A dTdT -3') and nonspecific control siRNA duplex (sense sequence 5'-AUG UAU UGG CCU GUA UUA G UU -3'), were purchased from Dharmacon, Thermo Scientific.

4.2.2 Polymer conjugates. pAA of various M_n and polymer conjugates were synthesized as previously reported by our group[18]. M_n and PDI values for pAA were obtained using a Waters Gel Permeation Chromatography (GPC) system and were calculated based on poly(methacrylic acrylic) standards. A library of polymers was synthesized by conjugating D-(+)-galactosamine (Gal) and agmatine (Agm), at different ratios, to the side chains of pAA. The conjugation of these groups was mediated via a condensation reaction using 4-(4,6-dimethoxy-1,3,5-triazin-2-

yl)-4-methylmorpholinium chloride (DMTMM) as the condensing agent. Reactions were carried out in 0.1 M borate buffer, pH 7 and pH 8 for Gal and Agm conjugations, respectively, at room temperature for 48 h. To obtain different ligand content, the $[COOH]_0$ to $[DMTMM]_0$ molar ratio was varied with $[NH_2]_0 = 2 \cdot [DMTMM]_0$. The degree of side chain substitution of each ligand (percent conjugation) in pAA was determined by ^1H NMR (Inova 400MHz) spectroscopy with deuterium oxide (D_2O) as the solvent.

4.2.3. Fluoresceinamine conjugation to polymer conjugates. A representative example for 10% targeted FA conjugation to available carboxyl groups in 10kDa pAA-78%Agm-3%Gal (10-P2) which corresponds to $[COOH]_0$:$[DMTMM]_0$:$[FA]_0$ = 1:0.1:0.2 is as follows: In a 5 mL pear-shaped flask equipped with a magnetic stir bar, 10-P2 (10 mg, 0.012 mmol COOH) and FA (0.83 mg, 0.0024 mmol in 34 µl of DMSO) were dissolved with 2 mL of 0.1M borate buffer, pH = 8.5. After 10 min under stirring, a DMTMM solution (0.33 mg, 0.0012 mmol; in 1.3 ml of 0.1M borate buffer, pH = 8.5) was transferred dropwise, and the pH was adjusted to 7.5 with additions of 1N sodium hydroxide (NaOH). The reaction flask was capped with a rubber septum and continuously stirred (600 rpm) for 24 h at room temperature. The product was purified by dialysis using Spectra/Por regenerated cellulose dialysis tubing (3.5 kDa MWCO) against deionized-water for 3 days and lyophilized for 24 h.

4.2.4 Preparation of polyplexes. A 0.5 mg/mL stock solution of polymer conjugates was prepared with 10 mM HEPES buffer, pH 7.2. Immediately prior to formation of the polyplex, the polymer conjugate stock solution was sonicated for 60 s. A specified volume of 20 µM or 2 µM siRNA was mixed with aliquots of polymer conjugates stock solution to form the designated polymer:siRNA ratio (w:w). The final volume was adjusted with 10 mM HEPES buffer, pH 7.2. After vortexing for 5 s, the polyplex solution was incubated at room temperature for 20 min.

4.2.5 Relative binding affinity and heparin competitive displacement. The relative strength of electrostatic binding between siRNA and polymer conjugates and the displacement of siRNA from the polyplex by heparin (competitive anionic species) were measured by EtBr fluorescence quenching. Stock solutions of siRNA, polymer conjugates, sodium heparin, and EtBr were prepared with 10 mM HEPES buffer, pH 7.2. Polyplexes were formed as previously described. siRNA (20 µL of 2 µM stock solution) was combined with a specific volume of the polymer conjugate stock solution to achieve the designated polymer:siRNA ratio (w:w), and the final volume was adjusted to 120 µL. The polyplex solution (100 µL) was transferred to a black 96-well plate.

For the relative binding affinity assay, 50 µL of 14 µM EtBr solution was added to each well, and plates were incubated at room temperature for 20 min. For the competitive heparin displacement assay, 10 µL of sodium heparin solution of varying concentrations were transferred to each corresponding well, and plates were incubated at 37°C for 20 min. EtBr solution (40 µL of 17.5 µM stock solution) was added to each well, and plates were incubated at room temperature for an additional 20 min.

The final concentration of EtBr was 4.67 µM and the siRNA phosphate group to EtBr ratio was 2:1. Fluorescence was read using a Molecular Devices SpectraMax GeminiEM at λ_{exc} = 535 and λ_{emi} = 595 nm. Each condition was performed in triplicate.

4.2.6 Polyplex stability in serum. The stability of polyplexes in the presence of serum proteins was evaluated as previously described[19]. Briefly, polyplexes were formed as previously described. siRNA (18.8 µL of 20 µM stock solution) was combined with a specific volume of the polymer conjugate stock solution to achieve the designated polymer:siRNA ratio (w:w), and the final volume was adjusted to 200 µL. Polyplexes were incubated at 37 °C with equal volume

of DMEM with 20% v/v FBS. The FBS final concentration was 10% v/v. At the designated times (0, 1, 2, 4, 8, 16, 24 and 48 h), an aliquot of the polyplex solution (40 µL) was removed, frozen with liquid nitrogen and stored at -80 °C. To terminate serum activity and dissociate the siRNA from the complex, samples were incubated at 80 °C for 5 min and sodium heparin (5 µL of 1 mg/mL stock solution) was added, respectively. The integrity of the siRNA was assessed by electrophoresis using a 15% TBE-urea polyacrylamide gel (Invitrogen) at a constant voltage of 200 V for 1 h in 1x TBE buffer. Gels were incubated for 40 min in SYBR green II RNA gel stain (1:10,000 dilution in filtered water), and siRNA bands were visualized under a UV transilluminator (λ = 302 nm).

4.2.7 Effective diameter and zeta potential. Polyplexes were formed as previously described. siRNA (19.8 µL of 20 µM stock solution) was combined with a specific volume of the polymer conjugate stock solution to achieve the designated polymer:siRNA ratio (w:w), and the final volume was adjusted to 1.05 mL. The siRNA final concentration was 5 µg/mL. Effective diameter and zeta potential of polyplexes were determined by dynamic light scattering (DLS) using a Malvern Zetasizer Nano-ZS. For the effective diameter, three measurements consisting of 10 runs of 10 s each were performed on each sample at room temperature. For the zeta potential, three measurements consisting of 15 runs each were performed on each sample at room temperature. The Smoluchowski model was applied to calculate the zeta potential.

4.2.8 Confocal microscopy. MDA-MB-231-luc+ cells (1 x 10^6 cells/plate) were seeded in 2 mL of growth medium (DMEM with 10% v/v FBS) in plates (60 mm x 15 mm) with 3 glass coverslips (12 mm diameter) 24 h prior to transfection and incubated at 37°C and 5% CO_2. Immediately prior to transfection, polyplexes were formed as previously described. siRNA (11.3 µL of 20 µM stock solution) was combined with a specific volume of the polymer conjugates

stock solution to achieve the designated polymer:siRNA ratio (w:w), and the final volume adjusted to 310 µL. After formation of the polyplex, 4.19 mL of serum-free medium was added to the polyplex solution. The growth medium was removed from the plates, and cells were rinsed with 2 mL of 1x Dulbecco's phosphate buffered saline (DPBS, Cellgro, Mediatech Inc., Manassas VA). The glass coverslips were transferred to new plates with 2 mL of serum-free medium (3 coverslips/plate), corresponding to 120,000 cells/plate. The serum-free medium from the plates was replaced with 2.25 mL of the polyplex solution. The siRNA concentration per plate was 0.67 µg/mL (1.5 µg siRNA per plate). Plates were incubated at 37°C and 5% CO_2 for 4 h. Cells were rinsed 3 times with DPBS, fixed with 3.7% formaldehyde in DPBS for 10 min followed by quenching with 10 mg/mL BSA in DPBS. Coverslips were mounted in microscopy slides using Vectashield mounting medium (Vector Laboratories, Burlingame CA), and cells were immediately imaged using a Leica TCS SP2 laser scanning confocal system with a HCX PL APO 63x/1.32-0.6 oil immersion CS objective. FA-containing polymer conjugates were detected by excitation at 488 nm with a 4-line argon laser, and fluorescence emission was collected at 500-550 nm.

4.2.9 Cytotoxicity. MDA-MB-231-luc+ (8,000 cells/well) were seeded in 100 µL of growth medium (DMEM with 10% v/v FBS) in clear 96-well plates 24 h prior to transfection and incubated at 37°C and 5% CO_2. A 0.5 mg/mL polymer stock solution was prepared with 10 mM HEPES buffer, pH 7.2 and sonicated for 60 s. From this stock solution, polymer conjugates were diluted with 10mM HEPES buffer, pH 7.2 to various concentrations at a final volume of 120 µL and vortexed for 5 s. The growth medium was removed from the wells, and cells were rinsed with 150 µL of DPBS. Serum-free medium (no phenol red, 120 µL) was added to the wells, followed by aliquots of polymer dilutions (30 µL). The final polymer concentrations per well

were 0, 1, 2.5, 5, 7.5, 10, 15, 20, 30, 40, 60, 100 and 150 µg/mL. Plates were incubated at 37°C and 5% CO_2 for 4 h, after which the medium in each well was replaced with 150 µL of fresh growth medium (DMEM with 10% v/v FBS). Plates were incubated at 37°C and 5% CO_2 for an additional 44 h. Cytotoxicity was assessed by the MTS Assay using CellTiter 96® AQueous One Solution Cell Proliferation Assay (Promega, Madison WI) according to the manufacturer's instructions. Following incubation of the plates at 37°C and 5% CO_2 for 2 h, the absorbance was obtained using a Molecular Devices SpectraMax Plus^{384} UV/Vis spectrophotometer at λ_{abs} = 490 nm. Data was fitted to sigmoidal (dose-response) curve using OriginPro 8, and IC_{50} values were calculated as the polymer concentration (in µg/mL) corresponding to 50% cell survival or half the absorbance measured at a polymer concentration of 0 µg/mL. Each condition was performed in triplicate.

4.2.10 siRNA transfection. MDA-MB-231-luc+ (8,000 cells/well) were seeded in 100 µL of growth medium (DMEM with 10% v/v FBS) in both white and clear 96-well plates 24 h prior to transfection and incubated at 37°C and 5% CO_2. Immediately prior to transfection, polyplexes were formed as previously described. The growth medium was removed from the wells, and cells were rinsed with 150 µL of DPBS. Serum-free medium (no phenol red, 120 µL) was added to the wells, followed by aliquots of the polyplex solution (30 µL). The siRNA concentration per well was varied from 0.33 µg/ml (50 ng of siRNA/well) to 3 µg/ml (450 ng of siRNA/well). Plates were incubated at 37°C and 5% CO_2 for 4 h, after which the medium in each well was replaced with 150 µl of fresh growth medium (DMEM with 10% v/v FBS). Plates were incubated at 37°C and 5% CO_2 for an additional 44 h.

As a positive control, cells were transfected with PEIb, RNAiFECT (Qiagen) and TransIT-siQuest (Mirus Bio, Madison WI). PEIb followed the same procedure as previously

described for polymer conjugates. Transfections with RNAiFECT were performed according to the manufacturer's instructions with a siRNA:RNAiFECT (µg:µL) = 1:6 in Buffer EC-R supplied. Transfections with TransIT-siQuest were performed according to the manufacturer's instructions with a siRNA:RNAiFECT (µg:µL) = 1:5 in Opti-MEM. Aliquots of the polyplex solution (30 µl) were added to the cells in 120 µL of serum-free medium. Plates were incubated at 37°C and 5% CO_2 for 4 h, after which the medium in each well was replaced with 150 µL of fresh growth medium (DMEM with 10% v/v FBS). Plates were incubated at 37°C and 5% CO_2 for an additional 44 h.

White 96-well plates were assayed for luciferase activity using Bright-Glo Luciferase Assay (Promega, Madison WI) according to the manufacturer's instructions. Clear 96-well plates were assayed for either total protein content using BCA Protein Quantification Assay (Thermo Scientific Pierce) according to the manufacturer's instructions or relative cell viability by MTS assay as previously described. Each polyplex/control condition was performed in triplicate for luciferase activity, total protein quantification and cell viability.

4.2.11 Bright-glo luciferase assay. Prior to luciferase activity quantification, growth medium was removed from the wells of the white 96-well plate, and cells were rinsed with 150 µl of DPBS. Serum-free medium (no phenol red, 100 µL) was added to each well. Bright-Glo working solution (Promega, Madison WI) (100 µL) was added to each well followed by 2 min incubation at room temperature. Luminescence (in RLU units) was obtained with a Veritas Microplate Luminometer (Turner Biosystems).

4.2.12 BCA protein quantification assay. Prior to total protein quantification, growth medium was removed from the wells of the clear 96-well plate, and cells were rinsed with 150 µL of DPBS. Glo-lysis buffer (Promega, Madison WI) (10 µL) was added to each well, and plates was

gently shaken at room temperature on a microplate shaker for 10 min. BCA working solution (Thermo Scientific) (200 µL) was added to each well and incubated at 37°C and 5% CO_2 for 1 h. Absorbance was obtained using a Molecular Devices SpectraMax Plus^{384} UV/Vis spectrophotometer at λ_{abs} = 562 nm. The total protein (in µg per well) was calculated from a calibration curve generated from a BSA protein standard with concentrations varying from 0 to 2000 µg/mL performed simultaneously with each experiment.

4.2.13 Statistical analysis. All data included are presented as the mean $\pm$ standard deviation. Statistical analysis between samples was performed via a two-tailed unpaired t-test. Difference between samples were considered significant if $p \leq 0.05$.

4.3 Results

4.3.1 Polymer conjugates. pAA was synthesized via RAFT polymerization using 4,4-azobis(cyanopentanoic acid) (A-CPA) and 4-cyanopentanoic acid dithiobenzoate (CPA-DB) as the radical initiator and chain transfer agent (CTA), respectively. By varying the monomer to CTA molar ratio, pAA of four different M_n, specifically 2,900 kDa, 4,800 kDa, 10,400 kDa and 20,900 kDa, were synthesized with PDIs ranging from 1.36 to 1.19 depending on the M_n. The M_n range for pAA was selected based on the limited solubility of the polymer conjugates at physiological pH.

A library of polymers was synthesized by conjugating two distinct moieties, Gal and Agm, at different ratios to the side chains of pAA. The conjugation of both moieties was mediated via an amidation reaction between the side chain carboxyl groups in pAA and the amino groups in these ligands using DMTMM as the condensing agent. The conjugation of both ligands to pAA was achieved in a two-step reaction, where Agm was first introduced followed

by Gal (Figure 4.1). Simultaneous conjugation of both ligands is possible; however, in order to achieve high Agm content (> 39%), a two-step conjugation reaction is more effective. The degree of side chain substitution of each ligand was determined by ^{1}H NMR (400MHz) spectroscopy with D_2O as the solvent and is referred to as a percentage value. The percentage reported (mol %) corresponds to the total ligand content relative to the total side chains (or repeating units) in each polymer. To obtain different ligand content, the $[COOH]_0$ to $[DMTMM]_0$ molar ratio was varied while keeping $[NH_2]_0 = 2 \cdot [DMTMM]_0$ and $[pAA]_0 = 3.0$ mg/mL.

Table 4.1 includes the polymer conjugates comprising the library with their corresponding M_n, PDI, Gal content and Agm content. A total of 22 polymers were evaluated; four M_n pAA, and six polymer conjugates (except for 21kDa-P polymers) per M_n pAA, each with a unique combination of Gal and Agm content. 21kDa-P polymers only have four Gal/Agm combinations (21-P1 to 21-P4) due to solubility issues at physiological conditions for 21-P5 and 21-P6.

4.3.2 Relative binding affinity. Figure 4.2(A-D) shows the relative binding affinity for all polymer conjugates with siRNA at various polymer:siRNA ratios (w:w); (A) 3kDa-P, (B) 5kDa-P, (C) 10kDa-P and (D) 21kDa-P. The relative strength of electrostatic interactions between the polymer and siRNA can be measured by EtBr fluorescence quenching. EtBr intercalates between the strands of nucleic acids generating a strong fluorescence. Maintaining the siRNA concentration constant, as the polymer concentration in solution increases, its binding with siRNA excludes EtBr from interacting with the siRNA, thus generating a reduction in the detectable fluorescence. This effect provides a quantitative analysis of the relative binding strength of the polymer conjugates with siRNA.

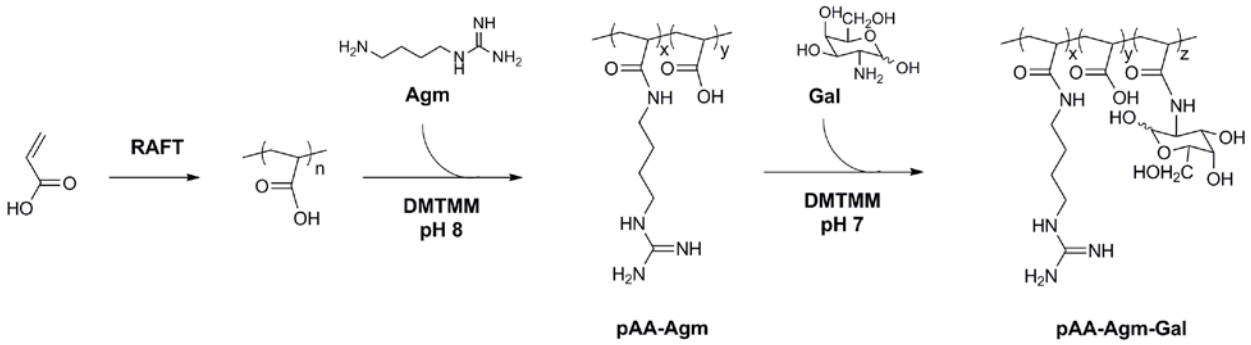

Figure 4.1: Synthesis schematic of polymer conjugates. Polymers precursor (pAA) were synthesized by RAFT polymerization with different molecular weights, followed by a two-step conjugation of Agm and Gal at different mol percent (%) substitutions.

Table 4.1: Polymer precursor (pAA) M_n and PDI, Agm content and Gal content for polymer conjugates

Entry	Name		pAA M_n[a]	PDI[a]	Agm Content (%)[b]	Gal Content (%)[b]
1	3kDa-P	3-P1	2 900	1.36	76	0
2		3-P2			76	3
3		3-P3			56	17
4		3-P4			56	8
5		3-P5			45	22
6		3-P6			45	13
7	5kDa-P	5-P1	4 800	1.32	76	0
8		5-P2			76	2
9		5-P3			55	17
10		5-P4			55	10
11		5-P5			46	28
12		5-P6			46	14
13	10kDa-P	10-P1	10 400	1.19	78	0
14		10-P2			78	3
15		10-P3			56	18
16		10-P4			56	10
17		10-P5			46	26
18		10-P6			46	14
19	21kDa-P	21-P1	20 900	1.19	72	0
20		21-P2			72	3
21		21-P3			55	12
22		21-P4			55	4

[a]As determined by size exclusion chromatography. [b]As determined by ^{1}H NMR (400MHz, D_2O).

From Figure 4.2(A-D) a trend directly correlated to the Agm and Gal contents can be distinguished for all polymers. The higher the Agm content, the higher the cationic density in the polymer and the stronger the electrostatic interactions with the negatively charged siRNA. The Gal content in the polymer influences the total cationic density as well by blocking some of the free carboxyl groups in pAA which could have become ionized in solution imparting a negative charge to the polymer. Therefore, keeping Agm content constant, the higher the Gal content the more effective the binding of the polymer with siRNA.

For all M_n polymers, P1 and P2 were shown to be the most effective in condensing siRNA to at least 80% at a polymer:siRNA (w:w) = 5:1 or higher. As the Agm content decreases, the ability to fully condense the siRNA lessens. For instance, P3 and P4 are able to condense ~70% of the siRNA at a polymer:siRNA (w:w) $\geq$ 20:1 for 3kDa-P and 5kDa-P, and at a polymer:siRNA (w:w) = 10:1 for 10kDa-P and 21kDa-P. P5 is able to condense ~60% of the siRNA; however, to achieve this a polymer:siRNA (w:w) ratio of 40:1 or higher are required. P6 can also condense ~60% of the siRNA at a polymer:siRNA (w:w) = 40:1 for 10kDa-P, and ~40% of the siRNA at a polymer:siRNA (w:w) = 20:1 for 3kDa-P and 5kDa-P.

4.3.3 Heparin competitive displacement. To evaluate the stability of the polyplex in the presence of other anionic compounds, a heparin competitive displacement assay was carried out. In this assay, the polyplex is exposed to different amounts of heparin, a highly anionic polysaccharide. The heparin will compete with the siRNA for interactions with the polymer conjugate, thus displacing the siRNA from the polyplex. This dissociation can be evaluated by quantifying the displaced siRNA in the solution by means of EtBr fluorescence. A relative polyplex stability (RPS) is calculated from equation 4.1:

$$\text{RPS} = \frac{F_{siRNA} - F_{hep}}{F_{siRNA} - F_{polyplex}} \qquad (4.1)$$

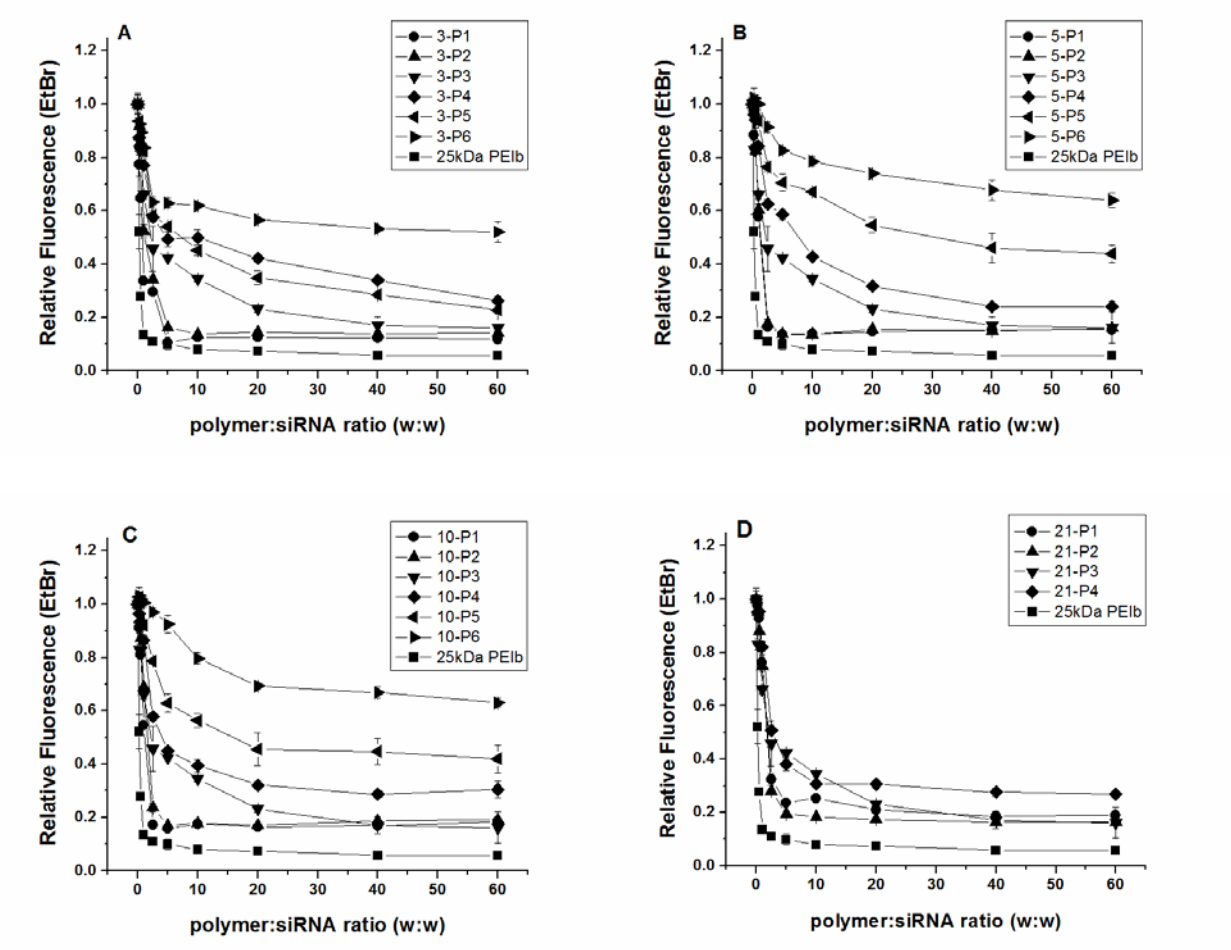

Figure 4.2: Relative binding affinity of polymer conjugates with siRNA as measured by ethidium bromide fluorescence quenching. [siRNA] = 3 µg/mL. N = 3. Error bars represents standard deviation. 25kDa PEIb was included for comparison. (A) 3kDa-P; (B) 5kDa-P; (C) 10kDa-P; (D) 21kDa-P.

where F_{siRNA} is the corrected fluorescence siRNA in the absence of the polymer vector, $F_{polyplex}$ is the corrected fluorescence of siRNA in the presence of the polymer vector and F_{hep} is the corrected fluorescence of siRNA in the presence of the polymer vector and heparin. Figure 4.3(A-C) shows relative fluorescence of EtBr after exposing the polyplex to varying amounts of sodium heparin. For the 10kDa-P library as a representative example (Figure 4.3(A)), polymers with higher Agm content, particularly 10-P1 and 10-P2, provide a stronger resistance to interactions with competitive anionic species, as correlated to the stronger binding affinity with siRNA. Taking 10-P2 as a representative example, as the polymer:siRNA (w:w) ratio increases, the strength of electrostatic binding between siRNA and the polymer is higher, thus higher amounts of heparin are needed to disrupt the siRNA-polymer complex (Figure 4.3(B)). For instance heparin:siRNA (w:w) = 2.5:1 is required to disrupt a polymer:siRNA (w:w) = 5:1, while a heparin:siRNA (w:w) = 10:1 is required to disrupt a polymer:siRNA (w:w) = 10:1 and polymer:siRNA (w:w) = 20:1. The polymer precursor M_n also has an impact on the competitive binding of heparin with cationic polymers. It is evident from Figure 4.3(C) that lower M_n polymer conjugates provide higher polyplex stability in solution as it shows less siRNA displacement by competitive anionic species as compared to their higher M_n counterparts.

4.3.4 Polyplex stability in serum. The stability of the polyplexes in serum and the ability of the polymer conjugates to protect the siRNA from nuclease degradation was evaluated. In this assay, polyplexes were incubated in 10% FBS for various times, following which the siRNA was dissociated from the polyplex, and its integrity was examined via gel electrophoresis. Figure 4.4 shows images of RNA polyacrylamide gels where each lane correspond to a different incubation time. Naked siRNA was degraded within 2 h of incubation in 10% FBS (Figure 4.4A), while siRNA recovered from polyplexes formed with 10-P2 and 10-P3 remained almost intact at 48 h

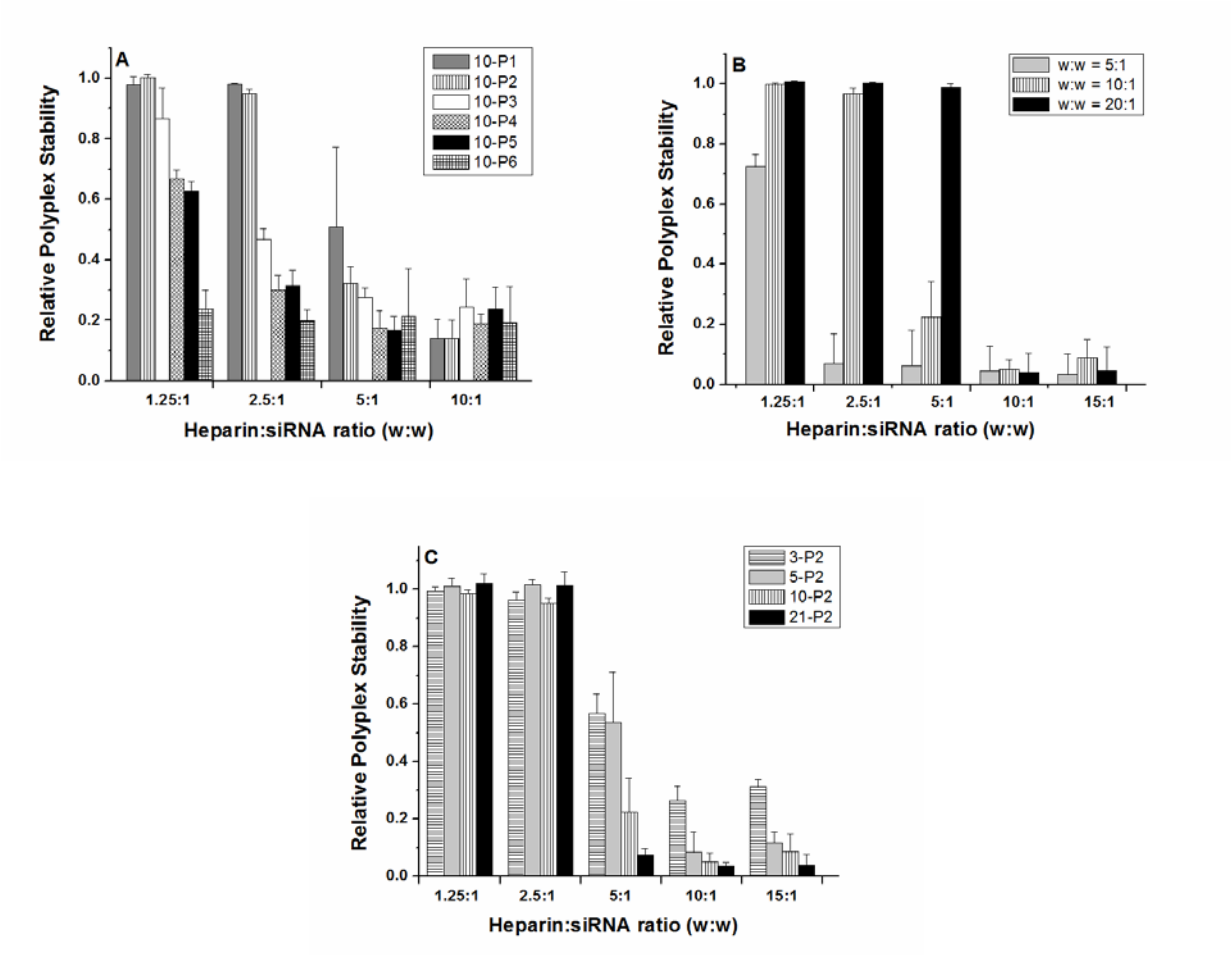

Figure 4.3: Relative polyplex stability. Displacement of siRNA from polyplex by the competitive interaction of heparin with polymer conjugates was measured by ethidium bromide fluorescence quenching. [siRNA] = 3 µg/mL. N = 3. Error bars represent standard deviation. (A) 10kDa-P library at polymer:siRNA (w:w) = 10:1: 10-P1 (dark gray), 10-P2 (vertical lines), 10-P3 (white), 10-P4 (diamond), 10-P5 (black), 10-P6 (squares). (B)10-P2 at various polymer:siRNA ratios (w:w): w:w = 5:1 (light gray), w:w = 10:1 (vertical lines) and w:w = 20:1 (black). (C) P2 polymers at polymer:siRNA (w:w) = 10:1: 3-P2 (horizontal lines), 5-P2 (light gray), 10-P2 (vertical lines), 21-P2 (black).

and 16 h of incubation in 10% FBS, respectively (Figure 4.4(B-C)). This suggests that the polymer conjugates are able to protect the siRNA from serum nuclease degradation.

4.3.5 Effective diameter and zeta potential. Figure 4.5A shows the effective diameter of polyplexes formed from the polymer conjugates and siRNA at a polymer:siRNA (w:w) = 10:1. For all M_n, a trend was distinguished where particle size increases as Agm content decreases. For 10kDa-P at a polymer:siRNA (w:w) = 10:1, the particle size ranges from 125 nm to 180 nm. Decreasing, as well as increasing, the M_n of the precursor showed a decrease in effective diameter reaching polyplex sizes of ~80 nm. In addition, for 10-P2, increasing the polymer:siRNA (w:w) ratio to 20:1 decreases the particle size to ~90 nm (Figure 4.5B). Similar trend is observed for other M_n polymers.

Figure 4.6A shows the zeta potential of polyplexes formed from the polymer conjugates and siRNA at a polymer:siRNA (w:w) = 10:1. All polymers conjugates, except P6, exhibit positive zeta potentials ranging from 20-40 mV. All P6 polymer conjugates showed a net negative zeta potential. Taking 10-P2 as a representative example at varying polymer:siRNA (w:w) of 1:1, 2.5:1. 5:1, 10:1 and 20:1 (Figure 4.6B), polyplexes exhibit a net positive zeta potentials of similar values for all polymer:siRNA (w:w) ratios except for polymer:siRNA (w:w) = 1:1, which showed a negative zeta potential.

4.3.6. Confocal microscopy Confocal microscopy imaging was performed to visualize the internalization of polyplexes into cells. Two FA-labeled polymer conjugates, 10-P2-FA and 10-P3-FA, were selected as representative examples for this analysis. For both conditions, polyplex internalization was achieved as distinguished by the strong fluorescence emitted from the interior of the cell 4 h post-transfection (Figure 4.7). Punctuated as well as diffused fluorescence was perceived in both samples.

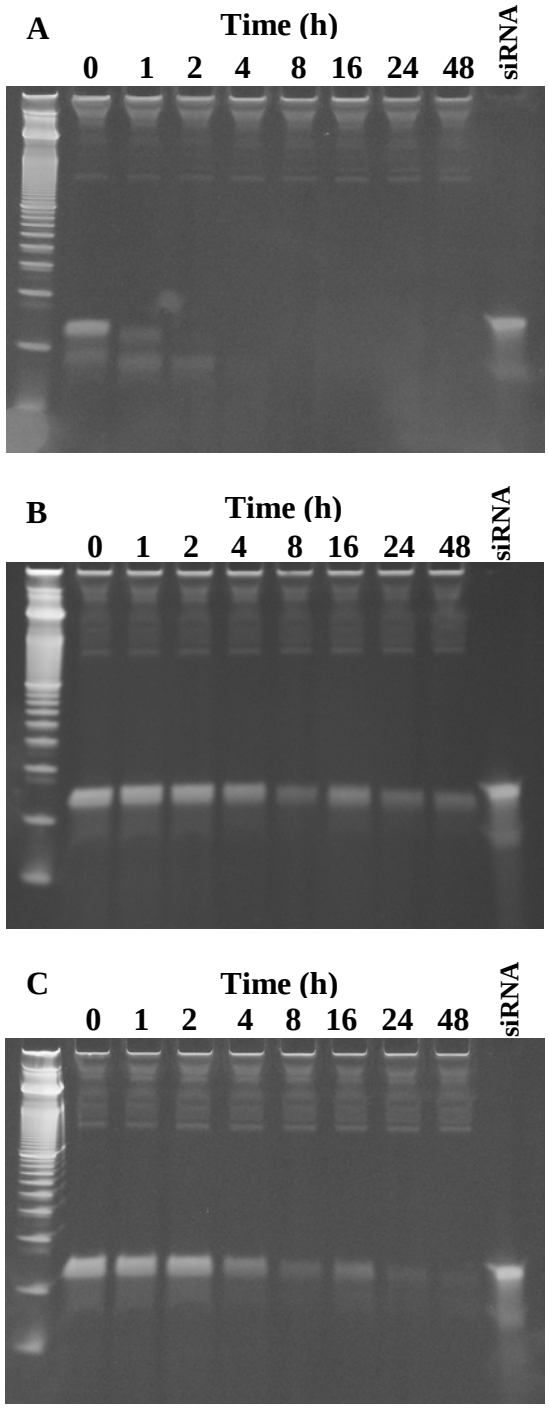

Figure 4.4: Polyplex stability in serum. siRNA integrity was evaluated by gel electrophoresis after incubation of polyplexes at 37 °C in 10% v/v FBS at various times. siRNA bands were stained with SYBR green II RNA gel stain and visualized under a UV transilluminator. Lane 1 corresponds to a 10bp DNA ladder. (A) naked siRNA; (B) polyplexes formed with 10-P2 and siRNA (w:w = 10:1); (C) polyplexes formed with 10-P3 and siRNA (w:w = 20:1).

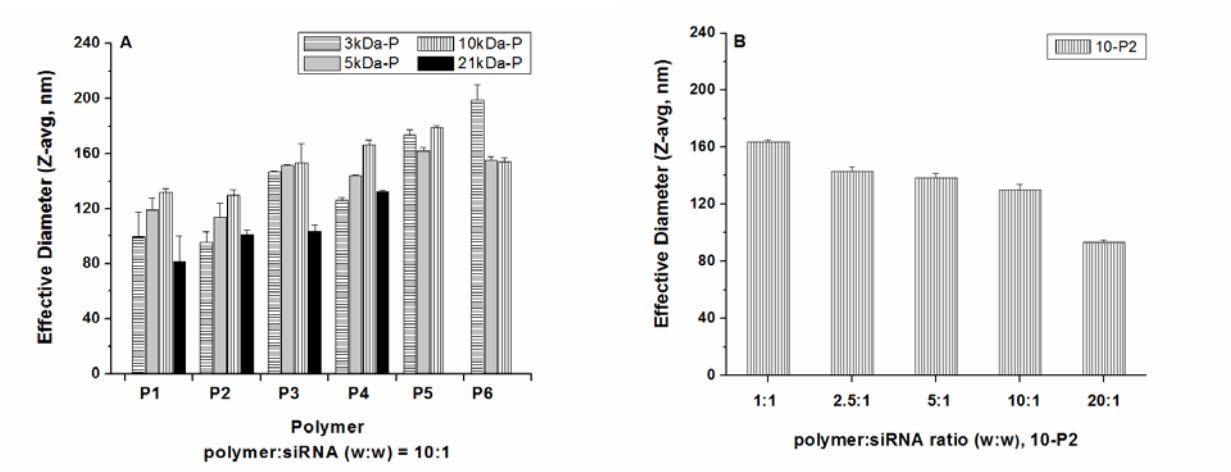

Figure 4.5: Effective diameter (Z-ave, nm) of polyplexes formed from polymer conjugates and siRNA. [siRNA] = 5 µg/ml. Three measurements were performed on each sample. Error bars represents standard deviation. (A) All polymer conjugates at a polymer:siRNA (w:w) = 10:1: 3kDa-P (horizantal lines), 5kDa-P (dark gray), 10kDa-P (vertical lines), 21kDa-P (black). (B)10-P2 at various polymer:siRNA ratios (w:w).

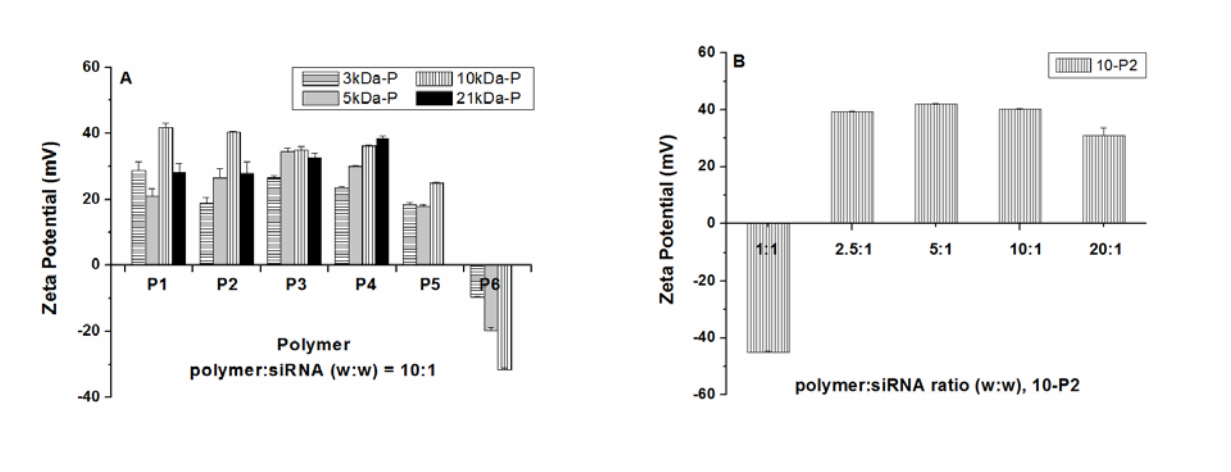

Figure 4.6: Zeta potential (mV) of polyplexes formed from polymer conjugates and siRNA. [siRNA] = 5 µg/mL. Three measurements were performed on each sample. Error bars represents standard deviation. (A) All polymer conjugates at a polymer:siRNA (w:w) = 10:1: 3kDa-P (horizantal lines), 5kDa-P (dark gray), 10kDa-P (vertical lines), 21kDa-P (black). (B)10-P2 at various polymer:siRNA ratios (w:w).

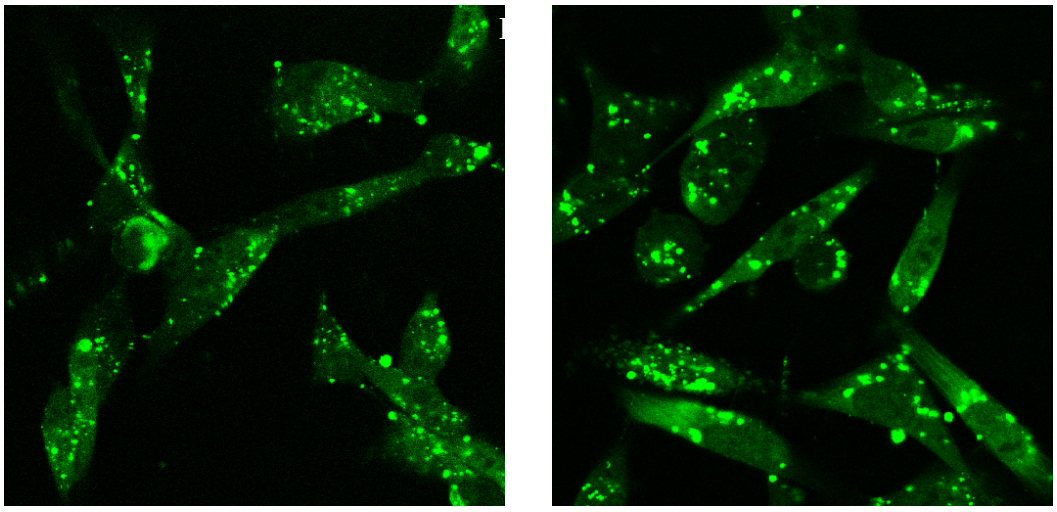

Figure 4.7: Confocal microscopy images of polyplexes internalized by MDA-MB-231-luc+ cells 4 h post-transfection. Cell were transfected with polyplexes formed from FA-labeled polymer conjugates and siRNA. [siRNA] = 0.67 μg/mL (1.5 μg siRNA per plate). (A) 10-P2-FA, polymer:siRNA (w:w) = 10:1; (B) 10-P3-FA, polymer:siRNA (w:w) = 20:1.

4.3.7 Cytotoxicity. The cytotoxicity of free polymers conjugates was assessed by calculating the IC_{50} values or half maximal inhibitory concentration that refers to the polymer concentration needed to kill 50% of the cell population. A sigmoidal fit was applied to the plot of $\log_{10}$(polymer concentration) vs. relative absorbance at 490 nm (MTS assay), and the polymer concentration was calculated at 50% cell survival.

Table 4.2 includes the IC_{50} values for all polymer conjugates. Two trends are distinguished for these polymer conjugates: (1) the cytotoxicity decreases as Agm content decreases; (2) the cytotoxicity decreases as pAA M_n decreases. Cytotoxicity was more prominent for P1 and P2 which had conserved IC_{50} values of ~5-6 µg/mL for all M_n polymers. Still, for all polymer conjugates, the cytotoxicity obtained was lower than for 25 kDa PEIb, which had an IC_{50} value of 2.9 µg/mL at the same conditions.

4.3.8 siRNA transfection. MDA-MB-231-luc+ cells (human breast carcinoma cell line) were transfected with siRNA targeting the luciferase protein. Figure 4.8(A-D) shows the relative cell viability and relative luciferase expression 48 h after siRNA transfection mediated by the polymer conjugates. Polyplexes were formed at various polymer:siRNA (w:w) ratios with a constant siRNA concentration of 0.33 µg/mL (50 ng/well). Luciferase expression (RLU) was normalized with the total protein content as determined by the BCA total protein assay. The relative cell viability after treating the cells with polyplexes was performed simultaneously.

A wide range of polymer:siRNA (w:w) ratios for each polymer conjugate was assessed to identify the optimal parameter that would achieve the highest transfection efficiency. The w:w ratio was varied for each polymer according to their relative binding affinities with siRNA and IC_{50} values. For all M_n, polymers with the highest Agm content, particularly P1, P2 and P3, achieved improved transfection efficiency than those with low Agm content, leading to a lower

Table 4.2: IC_{50} values for polymer conjugates and 25kDa PEIb after 48 h incubation with MDA-MB-231-luc cells+ (MTS assay). N = 3.

Entry		Polymer	$IC_{50,\ free\ polymer}$
1	3-P1	3kDapAA-76%A	6.5 ± 0.2
2	3-P2	3kDapAA-76%A-3%G	7.5 ± 0.7
3	3-P3	3kDapAA-56%A-17%G	55.7 ±1.9
4	3-P4	3kDapAA-56%A-8%G	121.9 ± 2.5
5	3-P5	3kDapAA-45%A-22%G	> 150
6	3-P6	3kDapAA-45%A-13%G	> 150
7	5-P1	5kDapAA-76%A	5.0 ± 0.5
8	5-P2	5kDapAA-76%A-2%G	5.2 ± 0.7
9	5-P3	5kDapAA-55%A-17%G	54.9 ± 1.1
10	5-P4	5kDapAA-55%A-10%G	48.8 ± 1.2
11	5-P5	5kDapAA-46%A-28%G	> 150
12	5-P6	5kDapAA-46%A-14%G	> 150
13	10-P1	10kDapAA-78%A	4.7 ± 0.4
14	10-P2	10kDapAA-78%A-3%G	5.9 ± 0.4
15	10-P3	10kDapAA-56%A-18%G	13.1 ± 0.9
16	10-P4	10kDapAA-56%A-10%G	20.2 ± 1.0
17	10-P5	10kDapAA-46%A-26%G	> 150
18	10-P6	10kDapAA-46%A-14%G	> 150
19	21-P1	10kDapAA-72%A	6.5 ± 0.6
20	21-P2	10kDapAA-72%A-3%G	5.4 ± 0.5
21	21-P3	10kDapAA-55%A-12%G	10.0 ± 0.9
22	21-P4	10kDapAA-55%A-4%G	15.3 ± 0.6
23	PEIb	25kDa	2.9 ± 0.3

Figure 4.8: Relative cell viability and relative luciferase expression of MDA-MB-231-luc+ cells 48 h post-transfection for all polymer conjugates at [siRNA] = 0.33 μg/mL (50 ng siRNA/well). N = 3. Error bars represent standard deviation. Conditions showing statistically significant protein knockdown ($p < 0.05$) as compared to nonspecific siRNA transfection carried out under the same conditions are indicated by an asterisks (*). (A) 3kDa-P; (B) 5kDa-P; (C) 10kDa-P; and (D) 21kDa-P.

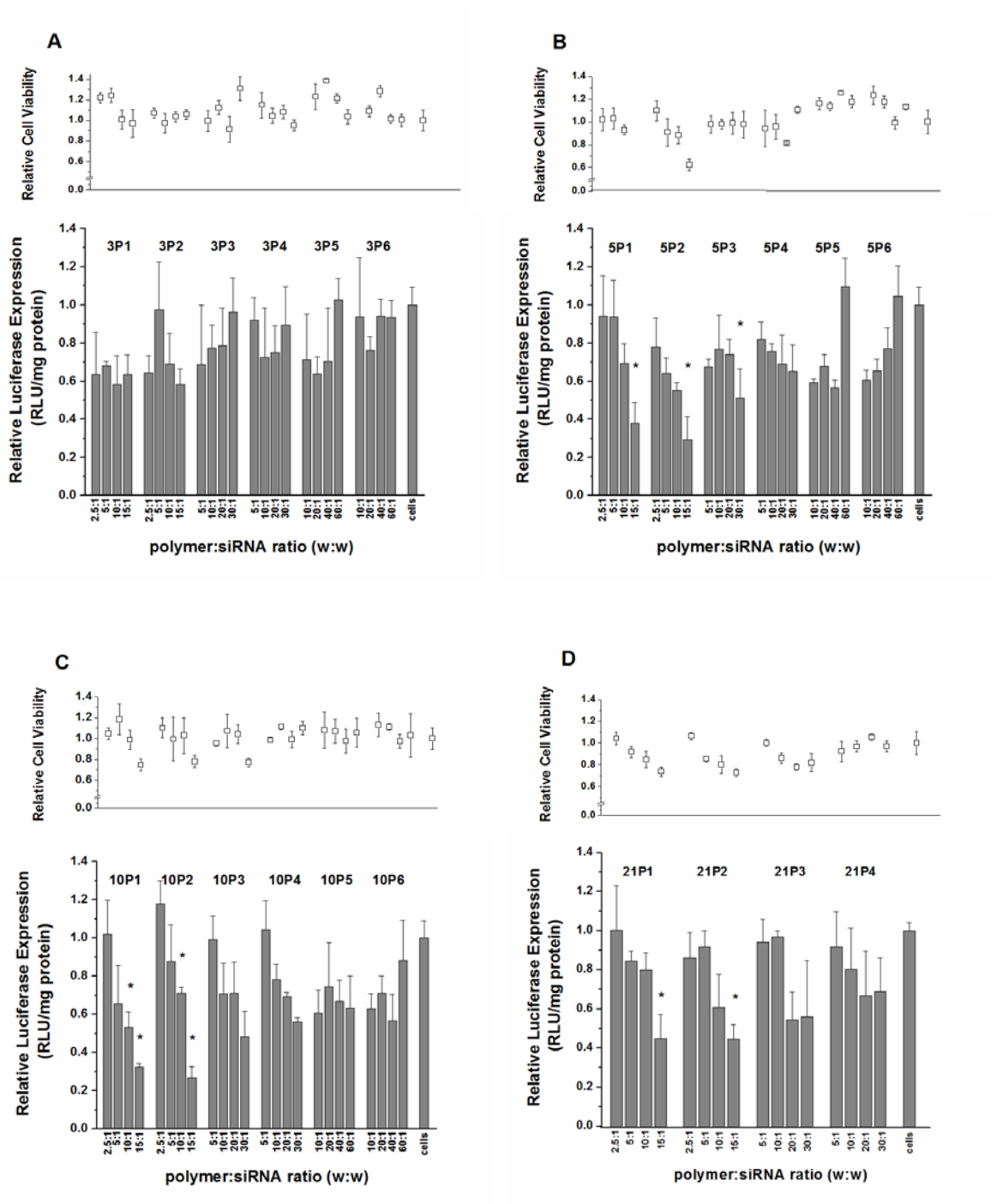
A
Relative Cell Viability
Relative Luciferase Expression (RLU/mg protein)
3P1
3P2
3P3
3P4
3P5
3P6
polymer:siRNA ratio (w:w)
B
Relative Cell Viability
Relative Luciferase Expression (RLU/mg protein)
5P1
5P2
5P3
5P4
5P5
5P6
polymer:siRNA ratio (w:w)
C
Relative Cell Viability
Relative Luciferase Expression (RLU/mg protein)
10P1
10P2
10P3
10P4
10P5
10P6
polymer:siRNA ratio (w:w)
D
Relative Cell Viability
Relative Luciferase Expression (RLU/mg protein)
21P1
21P2
21P3
21P4
polymer:siRNA ratio (w:w)

protein expression 48 h after treatment.

Although no detectable cytotoxicity was perceived for the 3kDa-P library at a constant siRNA concentration of 0.33 µg/mL, only a modest protein knockdown of ~40% was achieved with 3-P1 and 3-P2 at various polymer:siRNA (w:w) ratios. However, these values are not considered statistically significant as compared to nonspecific siRNA transfection carried out under the same conditions. In contrast, 5kDa-P and 10kDa-P libraries were both more successful at siRNA transfection and protein knockdown as compared to the 3kDa-P library, particularly for P1 and P2 polymers. 5-P1 and 5-P2 (w:w = 15:1) achieved ~60% knockdown while 10-P1 and 10-P2 (w:w = 15:1) achieved ~70% knockdown, all being statistically significant as compared to nonspecific siRNA transfection carried out under the same conditions ($p < 0.05$). In addition, for both libraries, P3 polymers (w:w = 30:1) achieve ~50% protein knockdown. As the Agm content decreases, less significant varied results were obtained (~0-40% protein knockdown). In the case of the 21kDa-P library, only 21-P1 and 21-P2 at w:w = 15:1 showed protein knockdown that was statistically significant as compared to nonspecific siRNA transfection carried out under the same conditions ($p < 0.05$). Under these conditions, protein knockdown of ~ 56% was achieved with a relative cell viability > 70%.

Polymers that exhibited negligible cytotoxicity, though modest transfection efficiencies at siRNA concentration of 0.33 µg/mL, were further evaluated for protein knockdown at higher siRNA concentrations up to 3.0 µg/mL (Figure 4.9(A-D)). These polymer conjugates include P3 at w:w = 10:1 and w:w = 20:1, and P5 at w:w = 60:1. For all conditions, increasing the siRNA concentration lead to a significant increase in protein knockdown. P3 polymers at a w:w = 20:1 were shown to be the most effective transfection reagents as revealed by the marked decrease in relative luciferase expression. Particularly, 5-P3 at w:w = 20:1 achieved up to 84% protein

Figure 4.9: Relative cell viability and relative luciferase expression of MDA-MB-231-luc+ cells 48 h post-transfection with varying siRNA concentration. Polymers evaluated were P3 (w:w = 10:1 and w:w = 20:1) and P5 (w:w = 60:1) polymers. N = 3. Error bars represent standard deviation. Conditions showing statistically significant protein knockdown ($p < 0.05$) as compared to nonspecific siRNA transfection carried out under the same conditions are indicated by an asterisks (*). (A) 3kDa-P; (B) 5kDa-P; (C) 10kDa-P; and (D) 21kDa-P.

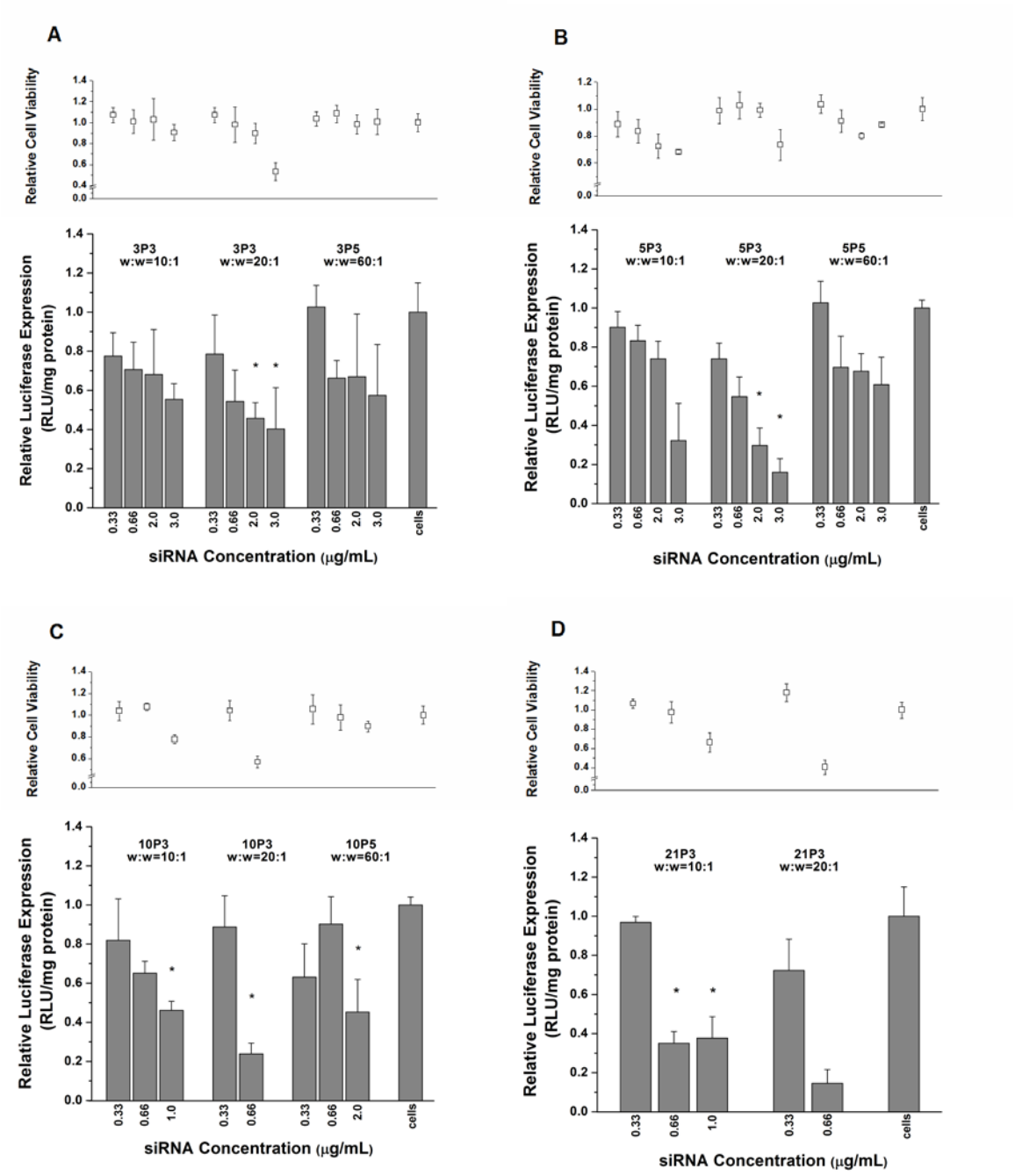
A
Relative Cell Viability
Relative Luciferase Expression (RLU/mg protein)
3P3 w:w=10:1
3P3 w:w=20:1
3P5 w:w=60:1
0.33
0.66
2.0
3.0
cells
siRNA Concentration (μg/mL)
B
Relative Cell Viability
Relative Luciferase Expression (RLU/mg protein)
5P3 w:w=10:1
5P3 w:w=20:1
5P5 w:w=60:1
siRNA Concentration (μg/mL)
C
Relative Cell Viability
Relative Luciferase Expression (RLU/mg protein)
10P3 w:w=10:1
10P3 w:w=20:1
10P5 w:w=60:1
1.0
siRNA Concentration (μg/mL)
D
Relative Cell Viability
Relative Luciferase Expression (RLU/mg protein)
21P3 w:w=10:1
21P3 w:w=20:1
siRNA Concentration (μg/mL)

knockdown with > 70% cell viability.

Transfection of siRNA with 25kDa PEIb, one of the most effective polymeric delivery vectors, and two commercially-available transfection reagents (RNAiFECT and TransIT-siQuest) were included for comparison (Figure 4.10A). Some of the conditions evaluated for our polymer conjugates achieved better outcomes than PEIb which could generate up to ~55% protein knockdown at [siRNA] = 0.33 μg/mL (w:w = 5:1) or [siRNA] = 0.66 μg/mL (w:w = 2.5:1). Higher siRNA concentrations or PEIb:siRNA (w:w) ratios to enhance protein knockdown is not viable due to the high cytotoxicity accompanied by PEIb. For the commercially-available transfection reagents, at analogous conditions, protein knockdown of ~60% and ~80% was achieved for RNAiFECT and TransIT-siQuest, respectively. Nonspecific siRNA transfection carried out under the same conditions (for those considered statistically significant) are shown in Figure 4.10B.

4.4 Discussion

The favorable transfection of siRNA into culture cells is reliant on multiple factors including the structural components of the polymeric vector and the polymer:siRNA weight ratio. These features will alter both the biophysical and biochemical properties which will have a great influence on siRNA delivery efficiency. Herein we have analyzed a library of polymers with a variety of structural elements including M_n of the polymer, side chain composition and side chain density.

One of the side chain functional groups incorporated into the design is Agm, which imparts a cationic density essential for electrostatic interactions between polymer chains and siRNA, and cellular membrane. The guanidium groups from the Agm moieties are protonated at

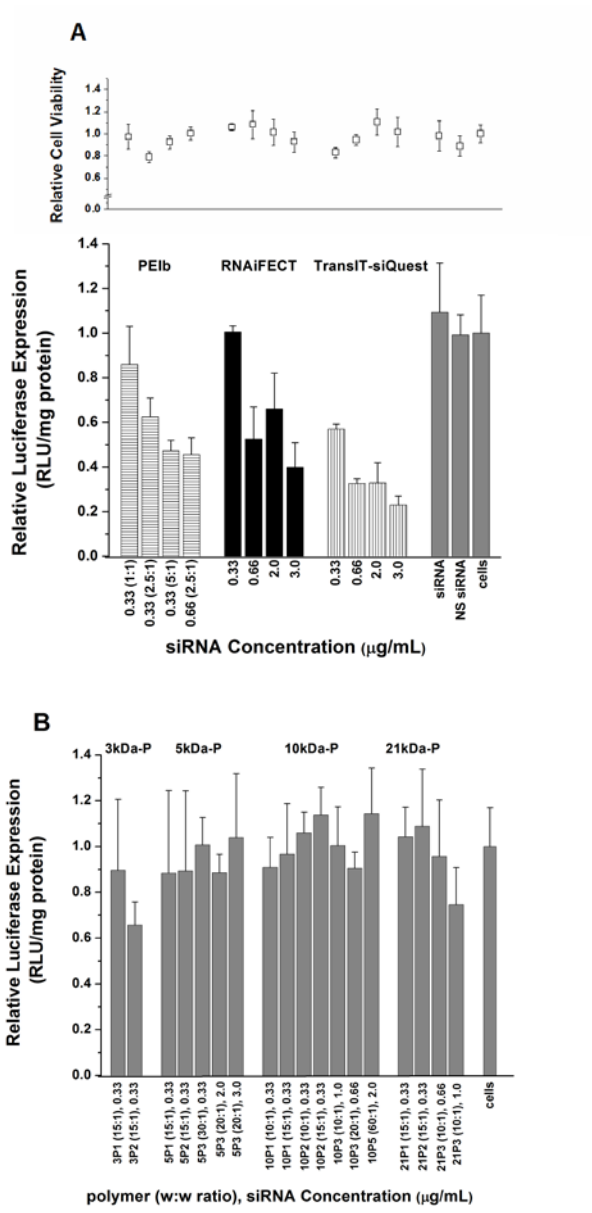

Figure 4.10: Relative cell viability and relative luciferase expression of MDA-MB-231-luc+ cells 48 h post-transfection. N = 3. Error bars represent standard deviations. (A) Commercially-available transfection reagents; 25kDa PEIb (horizontal lines), RNAiFECT (black), TransIT-siQuest (vertical lines), siRNA (3.0 μg/mL), nonspecific (NS) siRNA (3.0 μg/mL) and cells only (dark gray); (B) nonspecific siRNA transfection carried out with polymer conjugates under the same conditions.

physiological conditions providing a strong electrostatic interaction with negatively charged phosphate groups along the siRNA backbone. Moreover, Agm has been shown to promote cellular internalization due to interactions between the guanidium groups and the sulfate groups of the cell surface glycosaminoglycan[20]. The number of guanidium groups in arginine-rich peptides have been found to significantly influence the translocation[21,22]. Thus controlling the Agm content is critical for efficient interactions with the cell membrane while avoiding non-specific targeting. The second component incorporated into the design is Gal. Carbohydrates can enhance transfection efficiencies and promote cell-specific targeting through lectins (sugar-binding proteins) localized on cell membranes. For instance, lactosylated and galactosylated polymers have been shown to enhance nucleic acid delivery to hepatocytes both *in vitro* and *in vivo*[23-28]. However, the degree of substitution of Gal into polymer vectors can have an impact on the polyplex size and transfection efficiency[24]. Therefore, careful identification of optimal number of Gal residues in the polymer is crucial for effective siRNA delivery.

The library comprises of a total of 22 polymers; four M_n polymer precursors (3kDa, 5kDa, 10kDa to 21kDa), each with varying combinations of Agm and Gal content. The higher the Agm content in the polymer, the stronger electrostatic binding with siRNA and the higher polyplex stability in the presence of other anionic species; in addition to smaller effective particle diameters and higher net zeta potentials. However, polymer conjugates with high Agm content generate higher cytotoxicity as identified by the low IC_{50} values (~5 μg/mL). In contrast, polymers with the lowest amount of Agm (45%-46%) exhibited minimal cytotoxicity (IC_{50} > 150 μg/mL); however these are not able to fully condense siRNA. This may be due to the low amount of guanidium groups and the presence of both positive and negative charges in the polymer chain which may hinder the siRNA from effective interaction with the available positive

charges. The M_n of the polymer precursor influences the biophysical properties of these vectors, particularly the stability in the presence of anionic species. Lower M_n polymers appeared more stable in the presence of heparin than their higher M_n counterparts, possibly due to their more comparable chain length with siRNA. Polycations and polyanions with charged segments of matched chain length have been found to undergo molecular recognition in solution forming assemblies of higher stability[29].

The internalization of polyplexes was examination via confocal microscopy as this is effective technique to analyze siRNA delivery in cell culture[30]. For 10-P2 and 10-P3 polymers, confocal images showed both punctuated and diffused fluorescence in the interior of the cell 4 h post-transfection. The punctuated fluorescence corresponds to polyplexes localized in the endosome, while the diffused fluorescence corresponds to polyplexes in the cytosol. This suggests that the polyplexes were able to successfully escape the endosomal compartment after cellular internalization by receptor-mediated endocytosis, one of the major intracellular barriers of siRNA delivery.

Although the lower M_n (3kDa-P) is inclined to be less cytotoxic and more stable in the presence of anionic species, these polymers are shown to be less efficient mediating siRNA transfection. On the other hand, although high transfection efficiencies at some conditions, the higher M_n (21kDa-P) causes more prominent cytotoxicity effects. Therefore, 5kDa-P and 10kDa-P libraries are considered the most promising candidates for siRNA delivery, particularly P2 and P3 polymers. Our most favorable condition was 5-P3 at a polymer:siRNA (w:w) = 20:1 which showed a good balance between high transfection efficiency and low cytotoxicity. The results for this polymer were superior to PEIb and comparable to TransIT-siQuest; however, a direct comparison with PEIb is more relevant since it is a polymer-based vector.

REFERENCES

1 Fire, A. *et al.* Potent and specific genetic interference by double-stranded RNA in Caenorhabditis elegans. *Nature* **391**, 806-811 (1998).

2 Dillon, C. P. *et al.* "RNAi as an experimental and therapeutic tool to study and regulate physiological and disease processes". *Annu. Rev. Physiol.* **67**, 147-173 (2005).

3 Dykxhoorn, D. M. & Lieberman, J. The silent revolution: RNA interference as basic biology, research tool, and therapeutic. *Annu. Rev. Med.* **56**, 401-423 (2005).

4 Shan, G. RNA interference as a gene knockdown technique. *Int. J. Biochem. Cell Biol.* **42**, 1243-1251 (2010).

5 Doody, A. & Putnam, D. RNA-interference effectors and their delivery. *Crit. Rev. Ther. Drug Carrier Syst.* **23**, 134-160 (2006).

6 Wiethoff, C. M. & Middaugh, C. R. Barriers to nonviral gene delivery. *J. Pharm. Sci.* **92**, 203-217 (2003).

7 Wong, S. Y., Pelet, J. M. & Putnam, D. Polymer systems for gene delivery - Past, present and future. *Prog. Polym. Sci.* **32**, 799-837 (2007).

8 Pack, D. W., Hoffman, A. S., Pun, S. & Stayton, P. S. Design and development of polymers for gene delivery. *Nat. Rev. Drug Disc.* **4**, 581-593 (2005).

9 Putnam, D. Polymers for gene delivery across length scales. *Nat. Mater.* **5**, 439-451 (2006).

10 Demeneix, B., Hassani, Z. & Behr, J. P. Towards multifunctional synthetic vectors. *Curr. Gene Ther.* **4**, 445-455 (2004).

11 Green, J. J., Langer, R. & Anderson, D. G. A combinatorial polymer library approach yields insight into nonviral gene delivery. *Acc. Chem. Res.* **41**, 749-759 (2007).

12 Lynn, D. M., Anderson, D. G., Putnam, D. & Langer, R. Accelerated discovery of synthetic transfection vectors: parallel synthesis and screening of a degradable polymer library. *J. Am. Chem. Soc.* **123**, 8155-8156 (2001).

13 Anderson, D. G., Akinc, A., Hossain, N. & Langer, R. Structure/property studies of polymeric gene delivery using a library of poly(β-amino esters). *Mol. Ther.* **11**, 426-434 (2005).

14 Anderson, D. G., Lynn, D. M. & Langer, R. Semi-Automated Synthesis and Screening of a Large Library of Degradable Cationic Polymers for Gene Delivery. *Angew. Chem., Int. Ed.* **42**, 3153-3158 (2003).

15 Wong, S. Y., Sood, N. & Putnam, D. Combinatorial evaluation of cations, pH-sensitive and hydrophobic moieties for polymeric vector design. *Mol.Ther.* **17**, 480-490 (2009).

16 Thomas, M., Lu, J. J., Zhang, C., Chen, J. & Klibanov, A. M. Identification of novel superior polycationic vectors for gene delivery by high-throughput synthesis and screening of a combinatorial library. *Pharm. Res.* **24**, 1564-1571 (2007).

17 Chen, D. J., Majors, B. S., Zelikin, A. & Putnam, D. Structure-function relationships of gene delivery vectors in a limited polycation library. *J. Control. Release* **103**, 273-283 (2005).

18 Pelet, J. M. & Putnam, D. An In-Depth Analysis od Polymer Analogous Conjugation using DMTMM. *Bioconjugate Chem.* **In Press.** (2011).

19 Katas, H. & Alpar, H. O. Development and characterisation of chitosan nanoparticles for siRNA delivery. *Journal of Controlled Release* **115**, 216-225 (2006).

20 Kolonko, E. M. & Kiessling, L. L. A polymeric domain that promotes cellular internalization. *J. Am. Chem. Soc.* **130**, 5626-5627 (2008).

21 Nakase, I. *et al.* Cellular uptake of arginine-rich peptides: Roles for macropinocytosis and actin rearrangement. *Mol Ther* **10**, 1011-1022 (2004).

22 Futaki, S. *et al.* Arginine-rich peptides. An abundant source of membrane-permeable peptides having potentials as carriers for intracellular protein delivery. *J. Biol. Chem.* **276**, 5836-5840 (2001).

23 Oishi, M., Nagasaki, Y., Itaka, K., Nishiyama, N. & Kataoka, K. Lactosylated poly(ethylene glycol)-siRNA conjugate through acid-labile beta-thiopropionate linkage to construct pH-sensitive polyion complex micelles achieving enhanced gene silencing in hepatoma cells. *J. Am. Chem. Soc.* **127**, 1624-1625 (2005).

24 Kunath, K., Harpe, A. v., Fischer, D. & Kissel, T. Galactose-PEI-DNA complexes for targeted gene delivery: degree of substitution affects complex size and transfection efficiencies. *J. Control. Release* **88**, 159-172 (2003).

25 Zhang, X.-Q. *et al.* Galactosylated ternary DNA/polyphosphoramidate nanoparticles mediate high gene transfection efficiency in hepatocytes. *J. Control. Release* **102**, 749-763 (2005).

26 Sagara, K. & Kim, S. W. A new synthesis of galactose-poly(ethylene glycol)-polyethylenimine for gene delivery to hepatocytes. *J. Control. Release* **79**, 271-281 (2002).

27 Hashida, M., Takemura, S., Nishikawa, M. & Takakura, Y. Targeted delivery of plasmid DNA complexed with galactosylated poly(L-lysine). *J. Control. Release* **53**, 301-310 (1998).

28 Nishikawa, M., Takemura, S., Takakura, Y. & Hashida, M. Targeted delivery of plasmid DNA to hepatocytes in vivo: Optimization of the pharmacokinetics of plasmid DNA/Galactosylated poly(L-lysine) complexes by controlling their physicochemical properties. *J. Pharmacol. Exp. Ther.* **287**, 408-415 (1998).

29 Harada, A. & Kataoka, K. Chain length recognition: Core-shell supramolecular assembly from oppositely charged block copolymers. *Science* **283**, 65-67 (1999).

30 Portis, A. M., Carballo, G., Baker, G. L., Chan, C. & Walton, S. P. Confocal microscopy for the analysis of siRNA delivery by polymeric nanoparticles. *Microsc. Res. Tech.* **73**, 878-885 (2010).

CHAPTER 5

CLIMB GK-12: SUMMER PROGRAM AND INQUIRY-BASED CURRICULUM DEVELOPMENT

5.1 Introduction

The Cornell Learning Initiative in Medicine and Bioengineering (CLIMB) GK-12 program is a bridge between graduate students in the biomedical engineering field and high/middle school science teachers. Through this program, science teachers were integrated in a six-week long summer research project with a graduate student. In addition, an inquiry-based lesson plan was developed and implemented during the following academic year. Through this program, I had the pleasure of working with Carolyn Wilczynski, a Biology Teacher at Binghamton High School (Binghamton NY).

The summer research was a collaborative effort between the partner teacher and the graduate fellow. The research project focused on the internalization of bioactive materials into cells, an important process in gene delivery. Through fluorescently-labeling polymeric vectors, the uptake of polyplexes by culture cells was visualized via confocal laser scanning microscopy. Understanding these interactions and cellular internalization processes of biomaterials are of great relevance for gene therapy application, an important topic in biomedical engineering.

As part of the curriculum development, a more fundamental biology topic, specifically enzymes and chemical reactions, was approached as a need to bring novel activities into this substantial area. This topic, covered in "The Living Environment Core Curriculum", is relevant to the New York State Learning Standards - Living Environment, particularly Standard 1 (Analysis, Inquiry and design) and Standard 4 (physical setting and living environment)

(http://www.emsc.nysed.gov/ciai/). The activity developed presented a simple inquiry-based exercise in which students learned about chemical reactions, enzyme activity and how different environmental factors can affect enzymatic reactions in biology. The lesson plan, entitled "Enzymes and Their Functions", consisted of three main parts. Part 1 was an introductory activity in which students correlated real locks and keys with enzymes and substrates to understand what enzymes are and how they work. For Part 2, a standard experiment was carried out where enzyme action was investigated by quantifying the production of glucose by α-amylase activity over starch using a spectrophotometer. Part 3 was an inquiry-based lesson in which the students designed their own experiment based on enzyme activity. The lesson plan developed was administered to high school students (9^{th} grade) in the Bridges Program at Binghamton High School during 11 class periods of 45 min each. Part 2 and Part 3 of the lesson plan are herein described.

5.2 Summer research

Elucidating the internalization and intracellular trafficking pathways of polyplexes within cells will aid in the understanding of the mechanisms by which nucleic acids are delivered and utilized. In our case, internalization of polyplexes into cells is facilitated by receptor-mediated endocytosis. Once internalized, the polyplex is localized in the endosome compartment until escape into the cytosol is achieved. An alternative to visualize and/or identify the intracellular destination of polyplexes in fixed or living cells is through fluorescent-labeling and confocal microscopy. The goal of the summer research was to visualize the internalization of polyplexes formed from three distinct polymer conjugates and siRNA at various times post-transfection. The polymer conjugates were composed of poly(acrylic acid) (pAA) with various side chain

substitutions of two ligands, agmatine (Agm) and D-(+)-galactosamine (Gal). The ligands and polymer structures, and ligands percent (%) substitution are shown in Figure 5.1. The information collected was intended to aid in the design of polymeric vectors for siRNA delivery.

Polymer conjugates were fluorescently labeled with fluoresceinamine. From these polymer conjugates, polyplex were formed with siRNA at a polymer:siRNA (w:w) ratio of 5:1. 24 h prior to transfection, HepG2/C3A cells were seeded in three glass disks (12 mm diameter) in microscopy plates (60 mm diameter) at a cell density of 1 x 10^6 cells/mL and incubated at 37°C with 5% CO_2. Cells were treated with the fluorescently-labeled polyplexes and Alexa546 transferrin (endosome marker) and incubated at 37°C with 5% CO_2. Cells were fixed with 3.7% formaldehyde at the designated times (2 h, 3 h and 4 h) and imaged using a Leica TCS SP2 laser scanning confocal system with a HCX PL APO 63x/1.32-0.6 oil immersion CS objective. A sequential imaging procedure was applied.

Figure 5.2(A-L) showed the confocal images for Polymer 1 (Figure 5.2(A-D)), Polymer 2 (Figure 5.2(E-H)) and Polymer 3 (Figure 5.2(I-L)) at times 2 h, 3 h and 4 h post-transfection. Both Polymer 1 (pAA-78%Agm) and Polymer 2 (pAA-78%Agm-3%Gal) were readily internalized by cells at 2 h post-transfection, independently of the presence or absence of Gal in the polymer. However, Polymer 3 (pAA-32%Agm-55%Gal), corresponding to low Agm and high Gal contents, did not show any significant uptake even at 4 h post-transfection as perceived by the low fluorescence emitted inside the cell. These results indicate that Agm, a highly cationic species, has a greater influence on cellular uptake than Gal. Gal, although expected to enhance cellular internalization through interactions with the asialoglycoprotein receptors in the cell surface of hepatocytes, did not show any significant contribution for internalization into HepG2/C3A cells.

A

		Polymer 1	Polymer 2	Polymer 3
Name	Structure	Substitution (%)		
Agmatine (Agm)	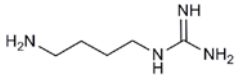	78	78	32
D-(+)-Galactosamine (Gal)	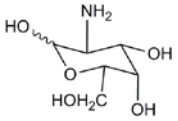	0	3	55

B

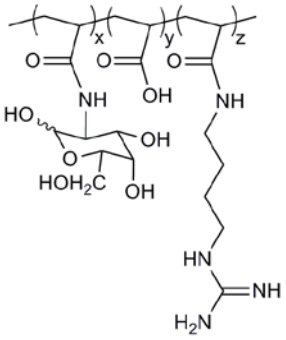

Figure 5.1: (A) Agm and Gal structures, and degree of side chain substitution (%) in pAA. (B) Polymer conjugates structure.

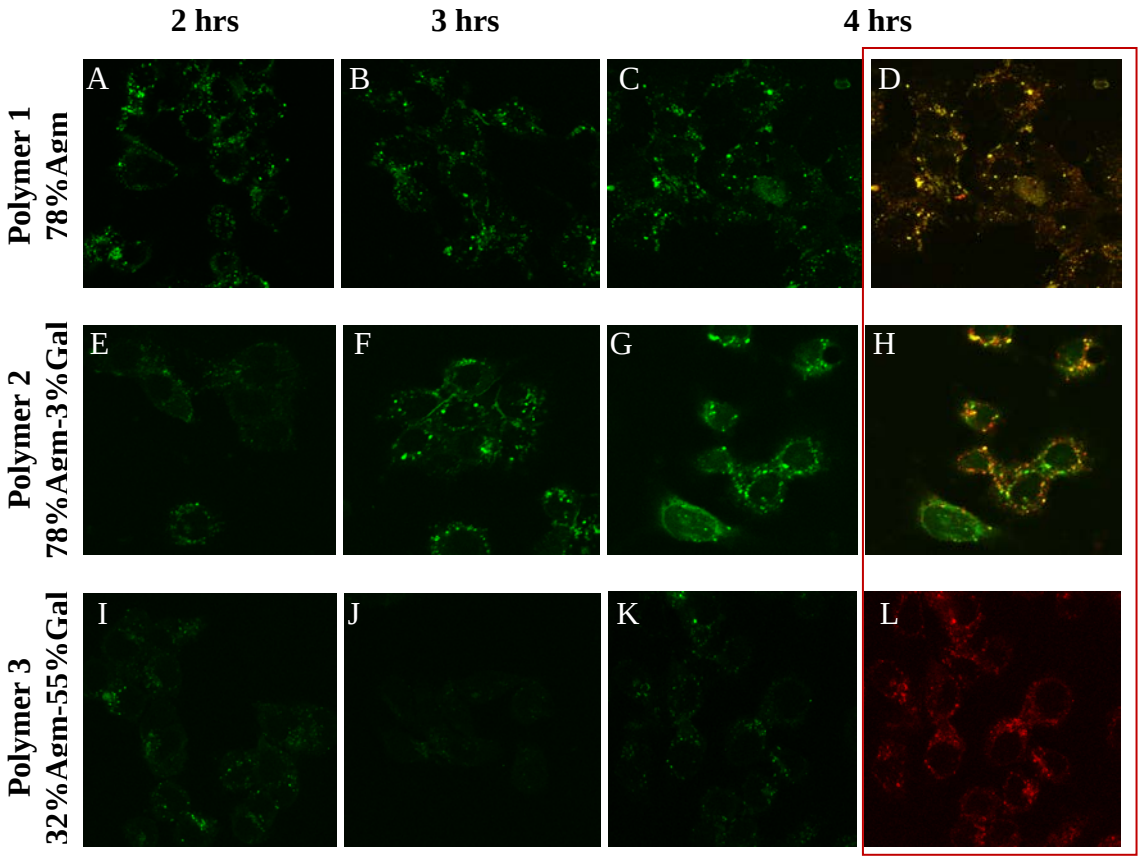

Figure 5.2. Confocal microscopy images. Polymer were labeled with fluoresceinamine (green) and endosomes were stained with Alexa546-transferrin (red). Yellow areas (images D, H and L) show colocalization of polyplexes with endosomes. Polymer 1 (pAA-78%Agm) at 2 h (A), 3 h (B) and 4 h (C-D) post-transfection. Polymer 2 (pAA-78%Agm-3%Gal) at 2 h (E), 3 h (F) and 4 h (G-H) post-transfection. Polymer 3 (pAA-32%Agm-55%Gal) at 2 h (I), 3 h (J) and 4 h (K-L) post-transfection.

5.3 Inquiry-based curriculum development: Enzyme action in biology - breaking starch down into glucose.

5.3.1 Introduction. Enzymes are biological catalysts that are essential components in many biochemical processes. In biological systems, enzymes assist the breakdown and synthesis of multiple compounds by affecting the rate of a chemical reaction with a particular substrate. Enzymes are needed to digest food, produce energy, remove toxins from the bloodstream, to name a few processes, and are ubiquitous in every biological function. Therefore, it is important for students to understand the concept of enzymes and how they function, as well as how enzyme activity can be affected by different environmental factors (e.g. temperature, pH and enzyme/substrate concentration). Enzymes and chemical reactions involved in cell function are important topics in Biology curricula, as acknowledged by The National Science Education Standards, Science Content Standard - The Cell.[1]

In this inquiry-based lesson, students design an experiment that will allow them to visualize the effect of environmental factors on enzyme activity. This sort of inquiry-based learning encourages students to develop a deep understanding of a scientific topic by challenging them to generate their own questions and propose a means by which to find a solution[2-4]. Particularly in this laboratory activity, students study how the enzyme α-amylase acts upon its starch substrate. Amylase converts polysaccharides (long chains of sugars) into monosaccharides (single sugar molecules). In the case of starch, α-amylase will break down starch into glucose as illustrated in Figure 5.3. This important reaction takes place in the human digestive system where starch, which is a significant part of our diet, is broken down in smaller, assimilable sugars.

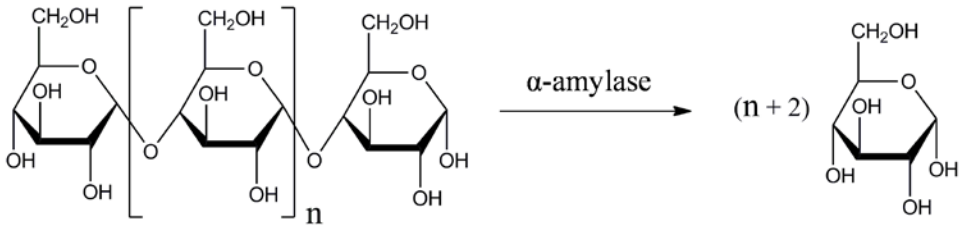

Figure 5.3: Breakdown of starch into glucose by α-amylase.

When α-amylase and starch are mixed, the α-amylase begins to breakdown the starch into glucose. If this reaction takes place inside a dialysis tube, a semi-permeable membrane, the glucose produced from the α-amylase/starch reaction will diffuse out of the dialysis tube since it is small enough to pass through the pores of the membrane. However, the α-amylase and the starch will remain inside the dialysis tube because these molecules are too large to diffuse out (Figure 5.4). Students can quantify the amount of glucose present outside the dialysis tube over a period of time, to learn about the rate of enzyme activity. Moreover, once a standard experiment is established, they can investigate how real biological processes can be regulated by specific environmental factors (e.g. temperature, pH, and enzyme/substrate concentration) and how these factors affect the enzyme activity and the resulting rate of its action.

The presence of glucose can be qualitatively observed by the formation of a red precipitate following the addition of Benedicts solution[5]. Furthermore, quantitative measurements of the glucose concentration using Benedict's solution can be achieved using spectrophotometry. This technique is a simple and practical way to determine the amount of glucose produced from the α-amylase/starch reaction.

In this lab, students will: (1) understand the concept of enzymes, substrates, and chemical reactions; (2) quantify the amount of glucose produced from an α-amylase/starch reaction over time; (3) develop an experiment based on an environmental factor that affects enzyme activity (inquiry-based lesson). This laboratory activity is suited for high school biology students, including students with special needs, general education students, as well as those in advanced courses. Further information on this lesson and additional materials, including student's activity sheets, can be found through the Cornell's Learning Initiative in Medicine and Bioengineering (CLIMB) website (http://climb.bme.cornell.edu/).

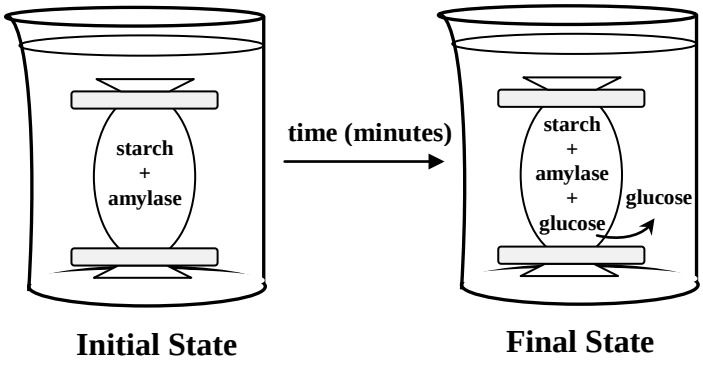

Figure 5.4: Schematic representation of glucose diffusion through a dialysis tube.

5.3.2 Materials and methods. Reagents and equipment can be obtained from Carolina (Burlington NC) or Fisher Scientific. List of materials can be found in Figure 5.5.

5.3.2.1 Pre-laboratory: glucose calibration curve. A calibration curve of glucose concentration with absorbance is needed to quantify the amount of glucose produced by the α-amylase/starch reaction. In the laboratory activity, students will measure the absorbance of a glucose/Benedict's solution with an unknown amount of glucose. The value obtained will be correlated with one from the calibration curve to determine the amount of glucose in the unknown sample.

The calibration curve is prepared by utilizing several different solutions of known concentrations of glucose with a fixed amount of Benedict's solution. The absorbance of each sample is detected using a spectrophotometer, and a plot of absorbance (y-axis) vs. glucose concentration (x-axis) is generated (Figure 5.6). A linear regression of this data will provide a slope (*m*) and a y-intercept (*b*) value according to equation 5.1:

$$y = (m \cdot x) + b \qquad (5.1)$$

A general calibration curve should be generated by the teacher/instructor prior to the experiment. If time is a constraint, our generated values of m = 1 and b = 0.6 can be used; however, it is highly recommended that a unique calibration curve is prepared, since the results can vary depending on the Benedict's solution used. This procedure for generating the calibration curve is based on ones used in undergraduate Cell Biology laboratories[6].

1. Place 500 mL of water in a 600 mL beaker (hot water bath), stir and heat to ~80 °C using a heating/stir plate and magnetic stir bar. Do not allow water to boil.
2. Prepare a 1 mg/mL glucose solution by dissolving 10 mg of glucose with 10 mL of water.
3. Label 7 Eppendorf tubes (2 mL) with numbers from 1 to 7. To each tube add the specified

Figure 5.5: List of equipments and materials for pre-lab (glucose calibration curve) and lab.

Equipment:

- Spectrophotometer
- Small centrifuge
- vortexer

Materials for Pre-lab (Glucose Calibration Curve):

- Benedict's solution
- Tap water
- Glucose or dextrose (2 mg)
- 600 ml Beaker
- Micropipettor (P1000)
- Micropipette tips, 1 ml
- Eppendorf tubes, 2 ml (7)
- Floating Eppendorf tube holder
- Tube holder
- Plastic cuvettes (7)
- Cuvette holder
- Waste container
- Timer
- Stir/heating plate
- Safety goggles
- Gloves

Materials for Lab (per group of students):

- Benedict's solution
- Tap water
- Starch (3 g, pre-weighed)
- α-amylase (1 g, pre-weighed)
- 600 ml Beaker (2)
- Dialysis tubing, 15 cm (~ 3cm width, molecular weight cutoff of 12,000 to 14,000 MW)
- Micropipettor (P1000)
- Micropipette tips, 1 ml
- Transfer pipettes (2)
- Eppendorf tubes, 2 ml (7)
- Floating Eppendorf tube holder
- Tube holder
- Plastic cuvettes (7)
- Cuvette holder
- Waste container
- Magnetic stir bar, 3.5-5 cm
- Dialysis clips (2)
- Timer
- Stir plate
- Stir/heating plate
- Safety goggles
- Gloves

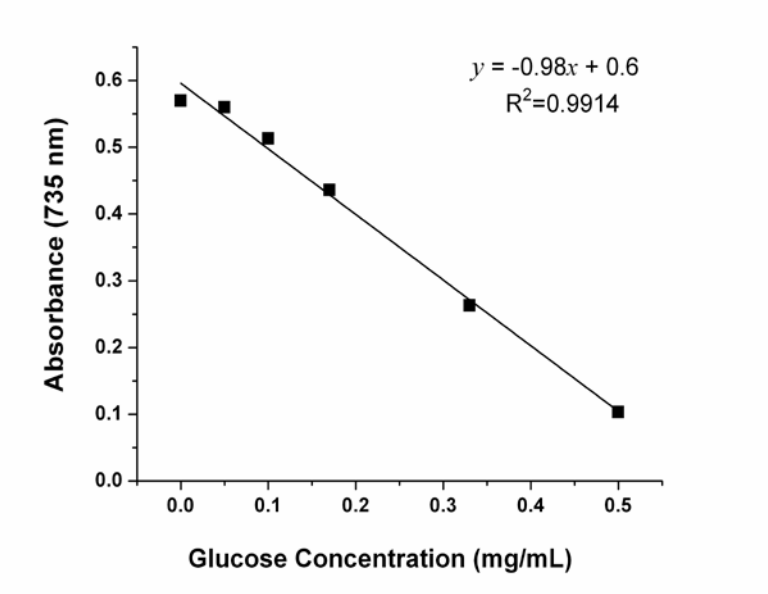

Figure 5.6: Representative plot of glucose concentration with absorbance (calibration curve).

amounts of the solutions listed in Table 5.1. Mix each solution for 5 s.

4. Insert all the tubes in a floating Eppendorf tube holder, and place the tube holder in the hot water for 10 min.
5. Remove the tubes from the hot water and allow them to cool down to room temperature (~3 min). Centrifuge the tubes at ~6,600 rpm for 3 min.
6. Without disturbing the precipitate in the sample tube, use a micropipettor to remove 1 mL of the liquid and place it in a plastic cuvette labeled with the same number.
7. Set the spectrophotometer wavelength to 735 nm. Use cuvette 7 (only water) to set a reference for the spectrophotometer. Obtain the absorbance of each sample (cuvettes 1 to 6).
8. Plot glucose concentration (x-axis) vs. absorbance (y-axis). Perform a linear regression and obtain a slope (*m*) and a y-intercept (*b*) value according to Equation 5.1.

5.3.2.2 Standard enzyme reaction. The following procedure includes directions on how to collect and analyze data for the standard α-amylase/starch experiment. The standard experiment is carried out at room temperature in water (pH ~ 7) with fixed amounts of starch (3 g) and α-amlylase (1 g). Each group of students should prepare their own standard experiment for comparison with the subsequent inquiry-based lesson, where the effect of environmental factors on enzyme activity is examined.

Collecting Data

1. Select the times at which samples will be collected. Recommended times are 0, 5, 10, 15, 20 and 30 min. Label 7 Eppendorf tubes with numbers from 1 to 7, each corresponding to a time point plus a control.
2. Place 500 mL of water in a 600 mL beaker. From this beaker, remove 1.5 mL of water and transfer to Tube 1 (time = 0 min).

Table 5.1: Volumes (mL) to be added in each tube for calibration curve of glucose concentration with absorbance.

Tube #	Glucose stock solution, 1 mg/mL (mL)	Water (mL)	Benedict's solution (mL)	Final glucose concentration (mg/mL)
1	0	1.50	0.3	0.00
2	0.075	1.425	0.3	0.05
3	0.15	1.35	0.3	0.10
4	0.25	1.25	0.3	0.17
5	0.5	1.0	0.3	0.33
6	0.75	0.75	0.3	0.50
7	0	1.80	0	0.00

3. Prepare the starch and amylase solutions:
    a. Dissolve 3 g of starch with 5 mL of water. Mix the starch solution.
    b. Dissolve 1 g of amylase with 5 mL of water. Mix the amylase solution.
4. Seal the bottom of the dialysis tubing by wrapping one of the ends around a stir bar and clipping this end with a dialysis clip.
5. Use a transfer pipette to add all of the starch solution into the dialysis tubing. Use another transfer pipette to add all of the amylase solution into the dialysis tubing. Clip the other end (top part) of the dialysis tubing with a dialysis clip.
6. Insert the sealed dialysis tubing in the beaker with water and start the timer. Set the stir dial in the stir plate to the lowest setting.
7. Remove 1.5 mL of the water from the beaker and place it in a 2 mL labeled Eppendorf tube at each specified time (Tubes 2 through 6).

Analyzing the Data

The concentration of glucose is determined in the manner previously described to generate the glucose calibration curve (Pre-Laboratory). Add 0.3 mL of Benedict's solution to each Eppendorf tube labeled 1 through 6. Do not add Benedict's solution to Tube 7, the control. Tube 7 will contain only water. Thoroughly mix all tubes (1-7) and then place them in a hot water bath for 10 min. Afterwards, the tubes should be centrifuged for 3 min. Place 1 mL of the supernatant from each sample in plastic cuvettes that are numbered similarly to the Eppendorf tubes, and measure the absorbance at 735 nm. Calculate the glucose concentration for each time point sample using the '*m*' and '*b*' values from the glucose calibration curve (Pre-laboratory). Use Equation 2 to calculate the glucose concentration, and plot glucose concentration (y-axis) vs. time (x-axis).

$$\text{Glucose Concentration} = \frac{y - b}{m} \qquad (5.2)$$

Glucose will diffuse out the membrane as α-amylase breaks down starch inside the dialysis tube. The glucose concentration will increase over time until all of the starch is converted to glucose. Thus, for the plot of glucose concentration vs. time, an increasing linear trend is expected (Figure 5.7). A small inaccuracy is expected due to the time it takes glucose diffuse out the dialysis tubing; however, constant low-stirring of the dialysis tubing should minimize this error due to an increase in diffusion rate.

5.3.2.3 Inquiry-based activity. Students can design their own experiment to explore and understand how different factors affect enzyme activity after they have performed the standard experiment and are comfortable with measuring glucose concentration and working with the equipment/reagents. This experimental design should include: a statement of the problem, a hypothesis and an experimental procedure. Following the experimental design, students should be allowed to: set up the experiment, record data, analyze results and draw a conclusion.

Examples of factors to be evaluated can be: temperature (higher or lower), pH (acidic or basic), or varying enzyme/substrate concentration. The materials provided to students will depend on their specific experimental design. Common materials are those used in the standard experiment. Additional materials that may be needed could include pH meter, hydrogen chloride (HCl) solution, sodium hydroxide (NaOH) solution, and ice. A representative example for an experiment conducted at a higher temperature (48 °C) is illustrated in Figure 5.8.

After the inquiry exercise, students and teachers can discuss what happens in biological systems when environmental factors change, such as what happens to digestive enzymes when acid reflux occurs, or muscle enzymes as we exercise, and enzyme deficiency problems such as lactase (lactose intolerance).

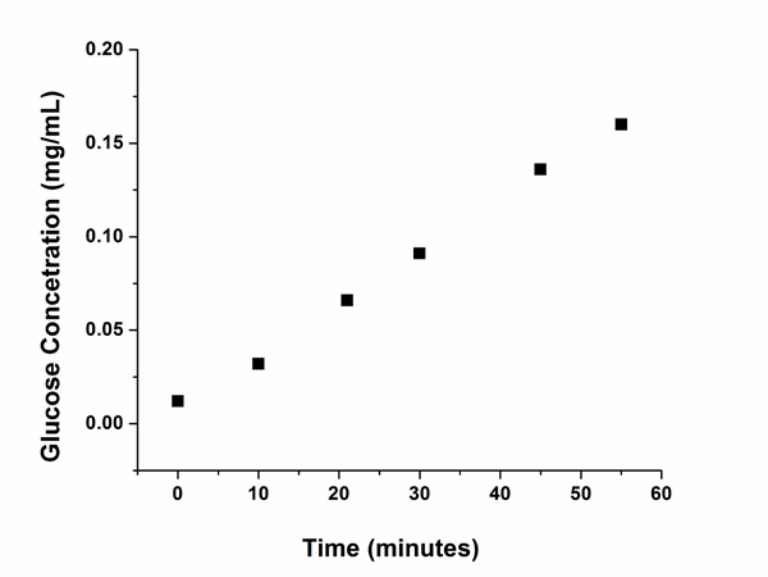

Figure 5.7: Representative plot of glucose concentration vs. time.

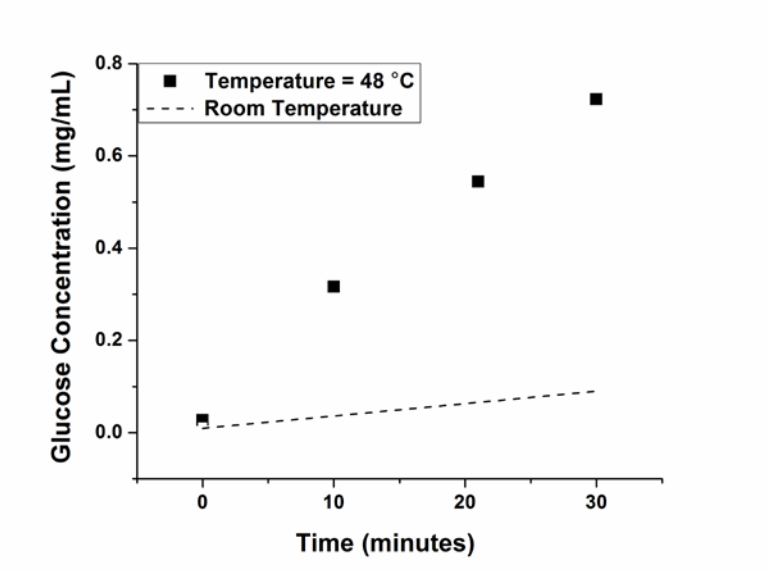

Figure 5.8: Representative plot of glucose concentration vs. time at a higher temperature (48°C).

5.3.3 Additional information

Suggested question for students

1. What trend for glucose concentration with the independent variable was observed in your data?
2. Compared to the standard experiment, what effect did the experimental factor selected have on enzyme activity (i.e. higher or lower reaction rate)?
3. Write a conclusion for this experiment (include whether your results support or refute your hypothesis).
4. What are some possible sources of error?
5. Ideas for future experiments?

Additional Notes to Teachers

Note 1: The α-amylase will form a light brown layer on the top of the dialysis tube, while the starch will form a white layer on the bottom. The brown layer (α-amylase) will become larger over the course of the experiment, while the white layer (starch) will become smaller. This can be pointed out as a qualitative observation of the α-amylase/starch reaction, and can be used as a demonstration of enzyme action for younger children who are not able to carry out the entire experiment.

Note 2: A negative control experiment can be performed in which only starch and Benedict's solution are placed in the dialysis tube (no α-amylase). Students should predict that glucose will not be found in the outer side of the membrane after 30 min.

5.3.4 Content assessment. A content assessment was performed through a pre- and post-test to evaluate the gain in knowledge of the material. A pre-test was administered before the lab to provide a measure of current knowledge and a post-test (identical to the pre-test) given after the

lab experience. Results between the two sets were compared.

Pre-test was given three days before conducting the lab. 14 students completed the pre and post-test. Pre and post-test were identical and consisted of 10 questions (8 multiple choice and 2 open questions). Figure 5.9 includes the individual scores for the pre- and post-test (Figures 5.9A) and the relative score increase for the post-test (Figure 5.9B). The overall score for the pre- and post-test were 27.9% and 40.4%, respectively, corresponding to a 12.5 score increase (44.8% of the pre-test score).

5.3.5 Attitude assessment. The questionnaire in Table 5.2 was given to the students as part of the post-test. Pre-test included Question 8 – 11 but did not reveal any change in attitude. A total of 11 students completed the questionnaire. The score is an average of answers based on: 5=strongly agree, 4=agree, 3=neutral, 2=disagree and 1=strongly disagree. Open questions were also included as part of the questionnaire. Some of the answers for the open questions section are included in Table 5.3.

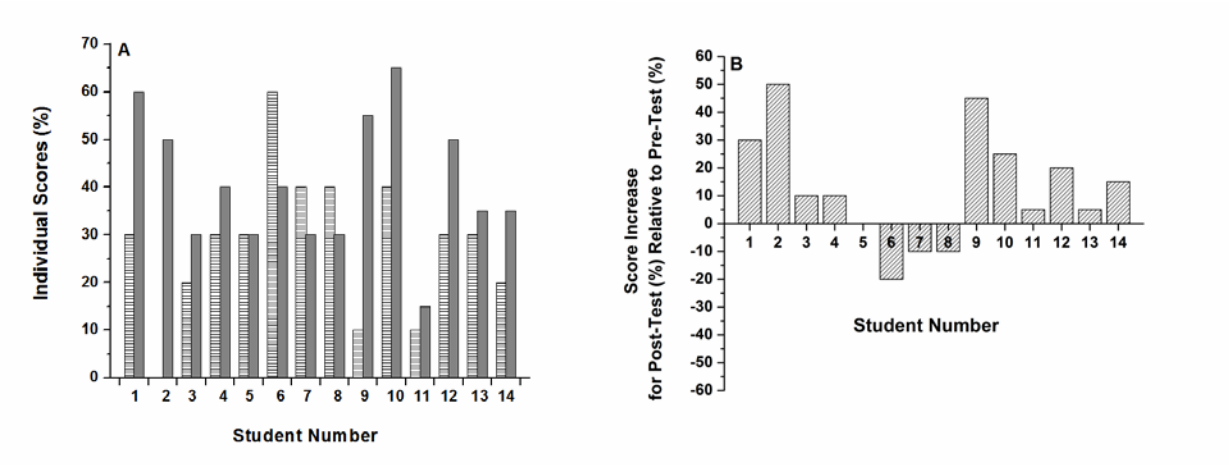

Figure 5.9: (A) Individual scores for pre-test (horizontal lines) and post-test (gray bars). (B) Score increase for post-test relative to pre-test.

Table 5.2: Attitude assessment questionnaire and overall scores

Attitude assessment questionnaire	Overall score
1. I enjoyed the enzyme lab.	4.0 ± 1.0
2. The enzyme lab was more difficult than most science labs.	2.6 ± 1.1
3. The lock-and-key activity helped me understand better what enzymes are.	3.6 ± 0.9
4. I enjoyed designing my own experiment about enzymes.	4.1 ± 1.0
5. I worked well with my teammate.	4.2 ± 1.1
6. I feel more comfortable designing research experiments than before.	3.6 ± 1.0
7. I enjoyed the enzyme lab more than most science labs.	3.1 ± 1.2
8. I enjoy science lessons.	3.5 ± 1.1
9. I enjoy science more than other school subjects.	2.7 ± 0.6
10. I prefer to understand something by doing an experiment rather than just reading about it.	3.9 ± 1.2
11. Science is more difficult than other school subject.	3.2 ± 1.0

Table 5.3: Selected answers from students from open questions in attitude assessment questionnaire

What I liked most about this lab:	**What I did not like about this lab was:**
▪ *Being able to do my own lab* (4 students)	▪ *All the writing and the test*
▪ *Making my own lab was cool*	▪ *It wasn't the best subject*
▪ *Making my own lab and using the pipettors*	▪ *All the writing was boring*
▪ *The key and lock* (2 students)	▪ *The lock and key part*
▪ *Not being rushed to do the experiments*	

REFERENCES

1 Assessment, N. C. o. S. E. S. a. & Council, N. R. *National Science Education Standards*. (The National Academies Press, 1996).

2 Chiappetta, E. L. Inquiry-based Science. *The Science Teacher* **64**, 22-26 (1997).

3 Rehorek, S. J. Inquiry-based Teaching: An Example of Descriptive Science in Action. *The American Biology Teacher* **66**, 493-499 (2004).

4 Colborn, A. An Inquiry Primer. *Science Scope* **23**, 42-44 (2000).

5 Sreeranjit, C. V. K. & Lal, J. J. in *Encyclopedia of Food Sciences and Nutrition* (ed Caballero Benjamin) 2898-2903 (Academic Press, 2003).

6 Sutherland, M. Hendrix College, Biology Department. Cell biology technique manual: Benedict's test.

CHAPTER 6

CONCLUSIONS AND RECOMMENDATIONS

Combinatorial chemistry can be an useful tool for the development of polymers as non-viral delivery systems, as it offers great flexibility and the advantage of simultaneous analyses of a wide chemical and structural parameter range. Mapping the structure-function parameter space through polymer libraries is valuable to understand the mechanisms of siRNA delivery potentially leading to safer and more efficient delivery systems. In this work, we developed polymer libraries for the rational design of non-viral delivery systems. Characterization of these vectors allows the identification of optimal structural properties for efficient transport and delivery of siRNA into cells.

The development of siRNA delivery systems entails an iterative process for the design optimization of these vectors. A series of steps were carried out for the development of these vectors, which includes: (1) synthesis of polymer precursors, (2) synthesis of polymer libraries, (3) *in vitro* biophysical and cellular characterization of polymer/siRNA complexes, and (4) correlation of polymer structure to siRNA delivery. Depending on the outcome, either *in vivo* characterization is completed or re-optimization of the original design is performed (Figure 6.1).

We employed RAFT polymerization to synthesize poly(methacrylic acid) (pMAA) and poly(acrylic acid) (pAA) with different molecular weights (M_n) up to 113,900 and 55,200 respectively. The selected I/CTA system, resulted in an effective method that, for these particular monomers, produced well controlled polymerizations under specific conditions. Various synthesis conditions including solvent, initial monomer concentration and pH were evaluated, and a kinetic analysis was performed with several variations on the initial reactant

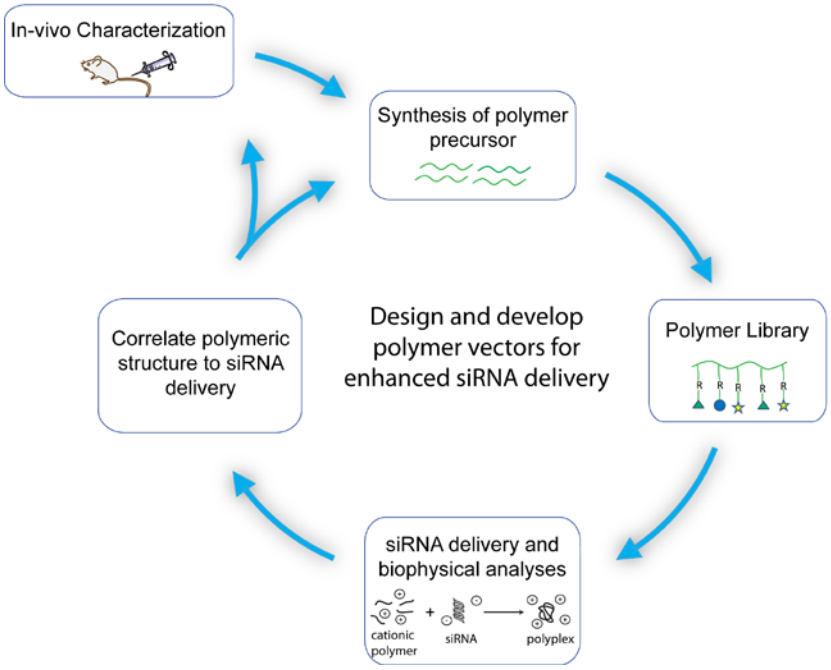

Figure 6.1: Iterative process for the design and development of polymer vectors for siRNA delivery.

ratios for MAA RAFT polymerizations. It was determined that methanol is a more suitable solvent for the polymerization due to higher stability of the reactants and good control throughout the polymerization under the conditions analyzed. Based on the results obtained for pMAA, pAA was synthesized in an analogous fashion using methanol as a solvent of choice. Both of these polymers were evaluated as precursors for the development of polymer libraries.

Combinatorial libraries are a practical approach to investigate the structure-function relationships of polymeric biomaterials. In particular, branched polymers with reactive side chain groups are an alternative for polymer precursors due to multiple sites available for modifications with different functional groups. With this in mind, our goal was to fully evaluate the single and binary substitution of two distinct amine-containing ligands, D-(+)-galactosamine (Gal) and agmatine (Agm), to the side chains of pMAA and pAA by using DMTMM as a condensing agent. The conjugation efficiency of these moieties was found to be influenced by the media pH, polymer concentration and ligands/polymer structures. Under comparable conditions, the substitution of both ligands in pAA was significantly higher than in pMAA, reaching close to a two-fold increase in conjugation efficiencies, presumably due to the absence of a hydrophobic α-methyl group that generated solution conformation issues in the pMAA reactions. In addition, Agm surpassed Gal total content in both polymers. Nevertheless, total Gal and Agm content in pMAA reached 23% and 53%, while total Gal and Agm content in pAA reached 56% and 78%, respectively.

Due to the anionic density at physiological conditions from the carboxyl groups in the polymer, a minimum amount of Agm moieties are required to impart a net positive charge to the polymer chains, this being more than half of the available carboxyl groups present. A net cationic charge is required to allow electrostatic interactions with negatively charged siRNA.

The low degree of substitution of Agm in pMAA, proved that these polymer conjugates were not suitable as transfection reagents due to the poor binding affinity to siRNA (data not shown). Therefore, pAA was selected as a precursor to generate polymer libraries that were evaluated as non-viral delivery vectors. pAA with four distinct M_n, 3 kDa (PDI = 1.36), 5 kDa (PDI = 1.32), 10 kDa (PDI = 1.19) and 21 kDa (PDI = 1.19), were synthesized. To the side chains of these polymer precursors, various combinations of Agm and Gal were substituted. A total of 22 polymers were evaluated with Agm varying from 78% to 46% and Gal contents as high as 26%. (For abbreviations and compositions of polymer conjugates refer to Table 4.1).

The biophysical and cellular characterization of these polymeric vectors revealed interesting correlations pertaining to their efficacy as siRNA delivery systems. In general for these polymers conjugates, the higher the Agm content, the more compact and stable polyplexes were formed and the higher transfection efficiency, but also the higher cytotoxicity. As for the effect of molecular weight, the lower the polymer M_n, the more compact and stable polyplexes were formed and the lower cytotoxicity, but also the lower transfection efficiency. Therefore, a critical balance between the polymer M_n and ligands substitution must be attained to optimize the transfection efficiency while maintaining high cell viability in culture. Based on these criteria, the most favorable M_n identified were 5 kDa and 10 kDa. From these libraries, P2 and P3 polymers were the most effective, particularly 5-P3 which corresponds to a 5 kDa pAA with a side chain composition of 55% Agm and 17% Gal.

In future work, the efficacy of the selected vectors will be evaluated for siRNA delivery *in vivo*, specifically targeting Factor VII protein in mice. Factor VII is a glycoprotein involved in coagulation cascades that is synthesized in the liver but circulates in an inactive form in the bloodstream. Therefore, *in vivo* delivery targeted to the liver will be carried out, and the

transfection efficiency of the polymer conjugates will be evaluated by quantifying the expression of Factor VII protein at various times after intravenous injection (i.v.) of polyplexes. In addition, to increase the stability of the polymer vector and avoid non-specific interactions with serum proteins, polyethylene glycol (PEG, 5,000 Da) will be incorporated through a maleimide-thiol linkage at the polymer conjugate end-group (Appendix II). PEGylated polymer conjugates will also be evaluated for siRNA delivery *in vivo*. Preliminary data on *in vivo* siRNA delivery is included in Appendix III.

From the initial library generated, specific structural parameters that achieved favorable outcomes (high transfection efficiency with low cytotoxicity) were identified. To further optimize the design of these vectors for enhanced siRNA delivery, additional structural modifications can be considered. For instance, higher polyplex stability may be accomplished by introducing a reversible disulfide linkage between the siRNA and polymer conjugate. Cytotoxicity might be reduced by generating degradable copolymers from two low M_n polymer conjugates, since these have shown to be less cytotoxic than their higher M_n counterparts. It is possible that some of these polymer conjugates are not able to efficiently escape the endosomal compartment, which can lead to lower transfection efficiencies. Therefore, additional pH-responsive moieties could be incorporated to overcome this intracellular barrier.

In summary, we developed polymer libraries that consist of structurally different but related cationic polymeric vectors, examined their biophysical properties and evaluated their ability to deliver siRNA to cells *in vitro*. A tight control over their molecular structure is vital in order to achieve favorable outcomes. The approach developed allowed the identification of potential candidates that could serve as siRNA delivery systems and provided a foundation upon which larger polymer libraries and more effective delivery vectors can be generated.

APPENDIX I

ACRYLIC ACID UNDERGOES PARTIAL METHYLATION DURING RAFT POLYMERIZATION IN METHANOL

AI.1 Introduction

RAFT polymerizations[1,2] have proven to be extremely successful for the direct polymerization of many acidic monomers including acrylic acid (AA). RAFT polymerization of AA has been carried out in many solvents including dimethylformamide, ethanol, 2-propanol, dioxane, methanol and water[1,3,4,5]. However, the solvent employed for such polymerizations can ultimately affect the end product.

Upon characterization of poly(acrylic acid) (pAA) synthesized by RAFT polymerization in methanol, we identified partial methylation (~6%) of the carboxyl side chains in pAA. Hydrolysis of the esters to obtain AA homopolymers was achieved by post-polymerization treatment with sodium hydroxide (NaOH).

AI.2 Materials and methods

AI.2.1 Materials. Acrylic acid (99%), 4,4'-azobis(4-cyanopentanoic acid) (98.0%, Fluka) and 1,4-dioxane, anhydrous (99.8%) were purchased from Sigma-Aldrich. N-ethylmaleimide (99+%) was purchased from Alfa Aesar. Tris(2-carboxyethyl) phosphine hydrochloride (TCEP·HCl) was purchased from Fisher Scientific. HEPES buffer saline (HBS, 10 mM HEPES, 150 mM NaCl, pH 7.2) was prepared with ultrapure water and filtered through a 0.2 μm PES membrane. All other chemicals were purchased from Fisher Scientific at the highest

purity available. CPA-DB was synthesized as previously described[6]. Prior to the experiment, all solvents were purged under nitrogen for at least 10 min.

AI.2.2 AA RAFT polymerization in methanol. In a 5 mL glass ampule equipped with a magnetic stirbar, AA (0.6 mL, 8.8 mmol) and CPA-DB (16.5 mg, 0.059 mmol; in 1.6 mL methanol) were transferred and purged under nitrogen for 5 min. A-CPA (4.2 mg, 0.015 mmol; in 0.73 mL methanol) was added, and the solution was purged under nitrogen for 2 additional min. The ampule was flame-sealed and inserted in a 60 °C oil bath under continuous stirring. The reaction was stopped at the designated time by inserting the ampule in an ice bath and exposing the solution to air. The product was either directly purified or treated with NaOH for hydrolysis of side chains. To purify the product, the solution was placed under vacuum for 10 min to remove ~50% of the methanol, diluted with deionized-water and dialyzed using Spectra/Por regenerated cellulose dialysis tubing (3.5 kDa or 1kDa MWCO) against deionized-water for 3 days. The product was recovered by lyophilization for 24 h.

AI.2.3 Post-polymerization hydrolysis of side chains. Immediately after the polymerization, a 0.1 mL aliquot of the polymer solution was mixed with 0.2 mL of NaOH (3N, 5N or 10N; NaOH:methanol (v/v) = 2:1). The reaction was stirred at room temperature under nitrogen for 2.5 h. The solution was neutralized with formic acid, 88% and purified by dialysis using Spectra/Por regenerated cellulose dialysis tubing (3.5 kDa MWCO) against deionized-water for 3 days and lyophilized for 24 h.

AI.2.4 Disulfide reduction by TCEP. Reduction of disulfide bonds between polymer end-groups was modified from previously established protocols[7]. Briefly, pAA (30 mg, 0.0021 mmol, M_n = 14,300) was dissolved in 4 mL of HBS, pH 7.2 and purged with nitrogen for 10 min. TCEP·HCl (6.0 mg, 0.021 mmol; in 1 mL HBS) was added, and the reaction was stirred

for 1 h at room temperature under nitrogen. N-ethyl maleimide (5.3 mg, 0.042 mmol; in 1 mL HBS) was transferred, and the reaction was allowed to stir overnight at room temperature. The product was purified by dialysis using Spectra/Por regenerated cellulose dialysis tubing (3.5 kDa MWCO) against deionized-water for 3 days and lyophilized for 24 h.

AI.2.5 Characterization. M_n and PDI for polymers were obtained using a Waters Gel Permeation Chromatography (GPC) system equipped with two Ultrahydrogel^{TM} columns (Waters) in series (500 Å and 250 Å), a 1515 isocratic HPLC pump and a 2414 refractive index detector. Temperature throughout the system was controlled at 30 °C. The mobile phase employed was phosphate buffer saline (pH=7.4) at a rate of 0.8 mL min^{-1} calibrated with poly(methacrylic acid), sodium salt standards. ^{1}H NMR was performed using a Inova 400MHz spectrometer with deuterium oxide (D_2O) as the solvent.

AI.3 Results and discussion

pAA was synthesized via RAFT polymerization using A-CPA as the radical initiator and CPA-DB as the chain transfer agent (Figure AI.1). Figure AI.2(A-B) shows the H^1 NMR (400 MHz, D_2O) spectra of pAA synthesized by RAFT polymerization in (A) methanol and (B) water/1,4-dioxane (4:1 v/v). The chemical shifts for the protons in the pAA backbone are distinguished at 1.2-2.0 ppm (methylene, -CH_2) and 2.0-2.8 ppm (methyne, -CH). For pAA synthesis in methanol (Figure AI.2A), the H^1 NMR spectra revealed a peak at 3.7 ppm corresponding to the protons in the pendant methyl group (-CH_3) produced from the esterification of side chain carboxyl groups with methanol. The degree of methylation corresponds to approximately 6% of the total initial available carboxyl groups in pAA. For comparison, an analogous polymerization was conducted in water/1,4-dioxane (4:1 v/v).

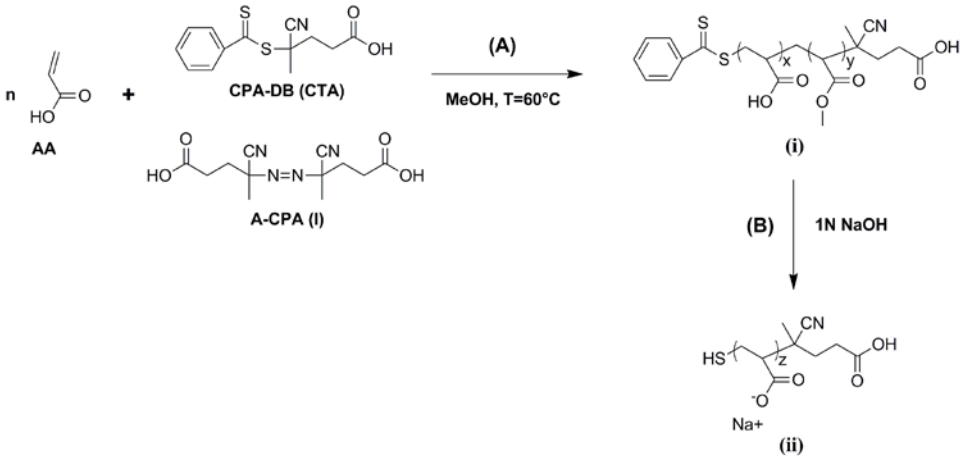

Figure AI.1: Synthesis schematic of pAA by RAFT polymerization in methanol

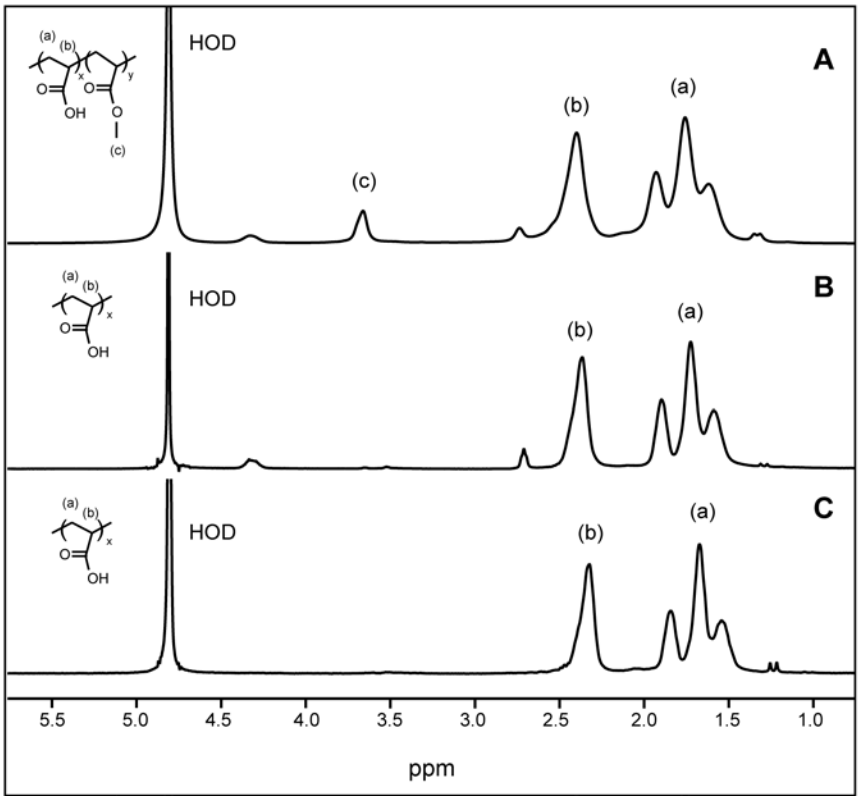

Figure AI.2: ^{1}H NMR spectra (400MHz, D_2O) of pAA synthesized by RAFT polymerization in (A) methanol; (B) water/1,4-dioxane (4:1 v/v); (C) methanol followed by NaOH treatment.

Polymerizations conducted in water/1,4-dioxane (Figure AI.2B) did not produce any side chain modification. Interestingly, partial methylation is not observed in methacrylic acid RAFT polymerization under equivalent conditions[8].

Under alkaline conditions, esters undergo hydrolysis by the nucleophilic attack of hydroxides. Poly(acrylic acid)-*co*-poly(methyl acrylate) (pAA-*co*-pMA) (Structure i in Figure AI.1) successfully undergoes hydrolysis of the ester bonds in the methyl acrylate units by treatment with 3N sodium hydroxide (NaOH) or higher NaOH concentrations. The final product is the sodium salt of pAA (Structure ii in Figure AI.1), as confirmed by the complete elimination of the $-CH_3$ peak at 3.7 ppm in the ^1H NMR spectrum (Figure AI.2C). Treatment of pAA-*co*-pMA with lower NaOH concentration hydrolyzes only a percentage of the esters. Strong protic acids, such as hydrochloric acid (HCl) or trifluoroacetic acid (TFA) can also promote ester hydrolysis. However, treatment of pAA-*co*-pMA with either 1 N HCl or TFA/water = 4:1 (v/v) had minimal effect on ester hydrolysis of the MA units. For our purposes, treatment with 3N NaOH was an effective route to achieve pAA; however, strong basic environments can also lead to hydrolysis of the thiocarbonylthio end-groups that result from the RAFT CTA.

In some circumstances where the RAFT CTA end-group functionality is not desired, hydroxides, as well as other reagents including borohydrides and amines, are used to cleave the thiocarbonylthio end-group[3,4,9,10]. This post-polymerization modification generates a thiol end-group (-SH). Strong oxidizing environments, as well as the presence of oxygen, can promote coupling of thiol groups to form disulfide bonds between polymer chains. As seen in the GPC trace in Figure AI.3A, a bimodal molecular weight distribution was obtained after 3N, 5N and 10N NaOH treatments corresponding to a two-fold increase in the peak-average molecular

weight (M_p). Molecular weight distribution (i) corresponds to a pAA of M_p = 17,800, M_n = 14,300 and PDI = 1.23. After NaOH treatment, the molecular weight distributions (ii)-(v) show a second peak of M_p = 34,500, close to two-fold the M_p of peak (i). The overall M_n and PDI increased to 18,600 and 1.31, respectively. As the NaOH concentration increases, the higher M_p peak becomes smaller relative to the lower M_p peak. It was previously shown that excess 10N NaOH to neutralize pAA post-polymerization (with trithiocarbonates as CTA), produces a substantial reduction in the sulfur content by the polymer end-group, as determined from elemental analysis[4]. This phenomenon was considered a result of decomposition of the thiol group in base. Therefore, using excess of 10N NaOH may be a potential route to avoid bridging between polymer chains if having a thiol end-group is not needed for further post-polymerization modifications.

Alternatively, disulfide bonds can be cleaved by reducing agents such as TCEP. As seen in Figure AI.3B, after treatment with TCEP/N-ethyl maleimide, the molecular weight distribution corresponding to the higher M_p was diminished, and only one molecular weight distribution peak was observed corresponding to the lower M_p pAA (vi).

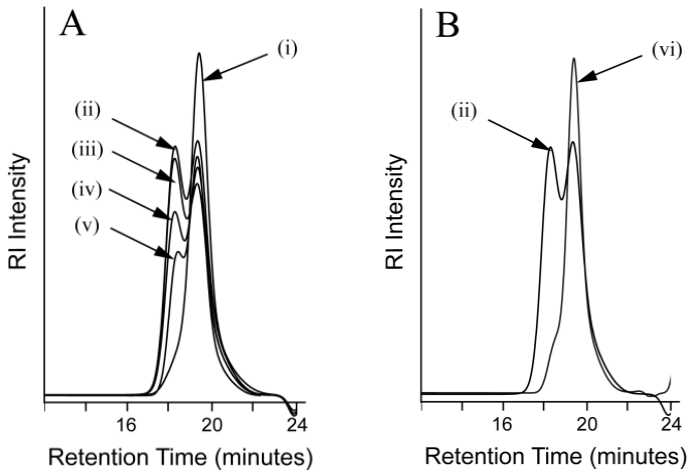

Figure AI.3: Molecular weight distribution for AA RAFT polymerization conducted in methanol. A(i) no NaOH treatment; A(ii) 3N NaOH, NaOH:methanol (v/v) = 2:1; A(iii) 5N NaOH, NaOH:methanol (v/v) = 2:1 A(iv); 10N NaOH, NaOH:methanol (v/v) = 2:1; A(v) 10N NaOH, NaOH:methanol (v/v) = 5:1; B(ii) 3N NaOH, NaOH:methanol (v/v) = 2:1; and B(vi) TCEP/maleimide treatment.

REFERENCES

1 Chiefari, J. *et al.* Living free-radical polymerization by reversible addition-fragmentation chain transfer: The RAFT process. *Macromolecules* **31**, 5559-5562 (1998).

2 Moad, G. *et al.* Living free radical polymerization with reversible addition - fragmentation chain transfer (the life of RAFT). *Polym. Int.* **49**, 993-1001 (2000).

3 Ladavière, C., Dörr, N. & Claverie, J. P. Controlled radical polymerization of acrylic acid in protic media. *Macromolecules* **34**, 5370-5372 (2001).

4 Loiseau, J. *et al.* Synthesis and characterization of poly(acrylic acid) produced by RAFT polymerization. Application as a very efficient dispersant of $CaCO_3$, kaolin, and TiO_2. *Macromolecules* **36**, 3066-3077 (2003).

5 Ji, J., Jia, L., Yan, L. & Bangal, P. R. Efficient synthesis of poly(acrylic acid) in aqueous solution via a RAFT process. *J. Macromol. Sci., Part A* **47**, 445 - 451 (2010).

6 Mitsukami, Y., Donovan, M. S., Lowe, A. B. & McCormick, C. L. Water-soluble polymers. 81. Direct synthesis of hydrophilic styrenic-based homopolymers and block copolomers in aqueous solutions via RAFT. *Macromolecules* **34**, 2248-2256 (2001).

7 Hermanson, G. T. *Bioconjugate Techniques*. (Second ed. (Pierce Biotechnology, Thermo Fisher Scientific, Rockford, IL) pp 219-223, Part II, Academic Press, 2008).

8 Pelet, J. M. & Putnam, D. High molecular weight poly(methacrylic acid) with narrow polydispersity by RAFT polymerization. *Macromolecules* **42**, 1494-1499 (2009).

9 Moad, G., Chong, Y. K., Postma, A., Rizzardo, E. & Thang, S. H. Advances in RAFT polymerization: the synthesis of polymers with defined end-groups. *Polymer* **46**, 8458-8468 (2005).

10 Sumerlin, B. S. *et al.* Modification of gold surfaces with water-soluble (co)polymers prepared via aqueous reversible addition−fragmentation chain transfer (RAFT) polymerization. *Langmuir* **19**, 5559-5562 (2003).

APPENDIX II

SYNTHESIS AND CHARACTERIZATION OF PEGYLATED POLYMER CONJUGATES

AII.1 Introduction

Incorporating polyethylene glycol (PEG) into polymer vectors is an alternative method to enhance polyplex stability in the presence of serum proteins. Copolymer of polymer conjugates and PEG were synthesized for a selected number of polymers, specifically 5-P2, 5-P3, 10-P2 and 10-P3. These polymers were selected for the evaluation of *in vivo* siRNA delivery to the liver (Appendix III).

AII.2 Materials and methods

AII.2.1 Materials. Tris(2-carboxyethyl) phosphine hydrochloride (TCEP·HCl) was purchased from Fisher Scientific. Methoxypolyethylene glycol 5,000 maleimide (PEG-mal) was purchased from Fluka. HEPES buffer saline (HBS, 10 mM HEPES, 150 mM NaCl, pH 7.2) was prepared with ultrapure water and filtered through a 0.2 μm PES membrane.

AII.2.2. Synthesis of PEG-*co*-pAA conjugates. A representative example for PEG conjugation to polymer conjugates end-group in 5kDapAA-78%Agm-3%Gal (5-P2) is as follows: In a 25 mL pear-shaped flask equipped with a magnetic stir bar, 5-P2 (30 mg, 0.0029 mmol) was dissolved with 13 mL of HBS, pH 7.2 and purged with nitrogen for 10 min. TCEP·HCl (4.2 mg, 0.015 mmol in 1 mL HBS) was transferred, and the reaction was stirred for 1 h at room temperature under nitrogen. PEG-mal (29 mg, 0.0058 mmol in 1 mL HBS) was transferred and the reaction was allowed to stir overnight at room temperature under nitrogen.

The product was purified by 8 times centrifugal filtration using Millipore Amicon Ultra filter units (regenerated cellulose, 10kDa MWCO), filtrated through a 0.2 μm PES membrane (sterile Acrodisc filter, Pall Corporation) and lyophilized for 24 h.

AII.2.2 Biophysical and cellular characterization. Biophysical and cellular characterization of PEGylated polymer conjugates were performed as previously described in Chapter 4. These include binding affinity of polymers with siRNA, polyplex effective diameter, polyplex zeta potential and cytotoxicity.

AII.3 Results and discussion

The conjugation of PEG into the polymer conjugates was mediated via a maleimide-thiol coupling reaction as shown in Figure AII.1. PEGylated polymer conjugates showed binding affinities to siRNA similar to non-PEGylated polymer conjugates (Chapter 4). P2 polymers are able to condense ~80% of the siRNA at a polymer:siRNA (w:w) $\geq$ 5:1, while P3 polymers are able to condense ~60% - 70% of the siRNA at a polymer:siRNA (w:w) $\geq$ 10:1 (Figure AII.1). At polymer:siRNA (w:w) corresponding to their non-PEGylated counterparts both effective diameters and zeta potentials were reduced, particularly for 10-P2-PEG and 10-P3-PEG polymers (Table AII.1). Moreover, the cytotoxicity of these polymers on MDA-MB-231-luc+ cells was significantly reduced by the incorporation of PEG chains into the polymer conjugates. IC_{50} values for PEGylated polymer conjugates were close to two-fold higher than for their non-PEGylated counterparts (Table AII.2).

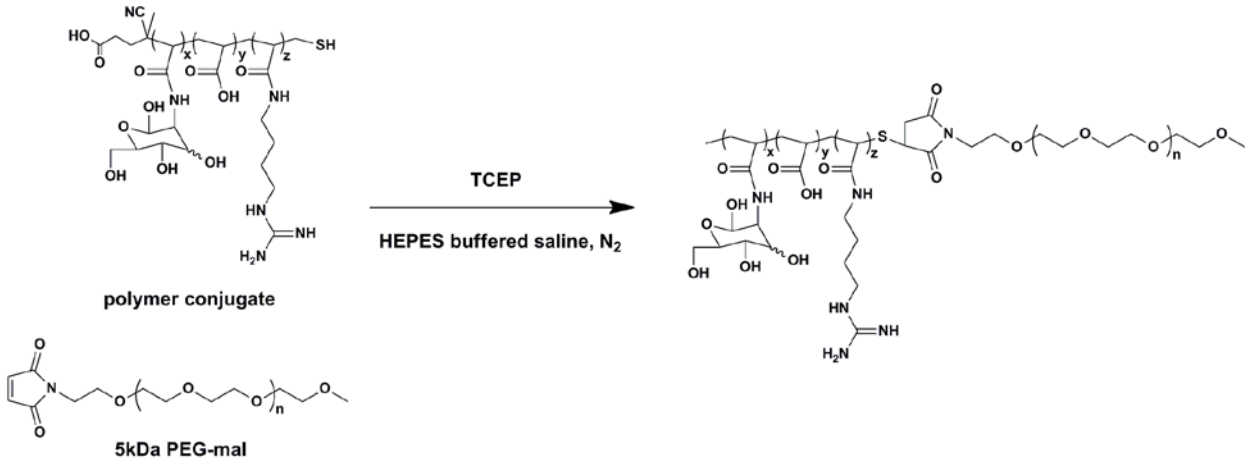

Figure AII.1: Synthesis schematic for PEGylation of polymer conjugates.

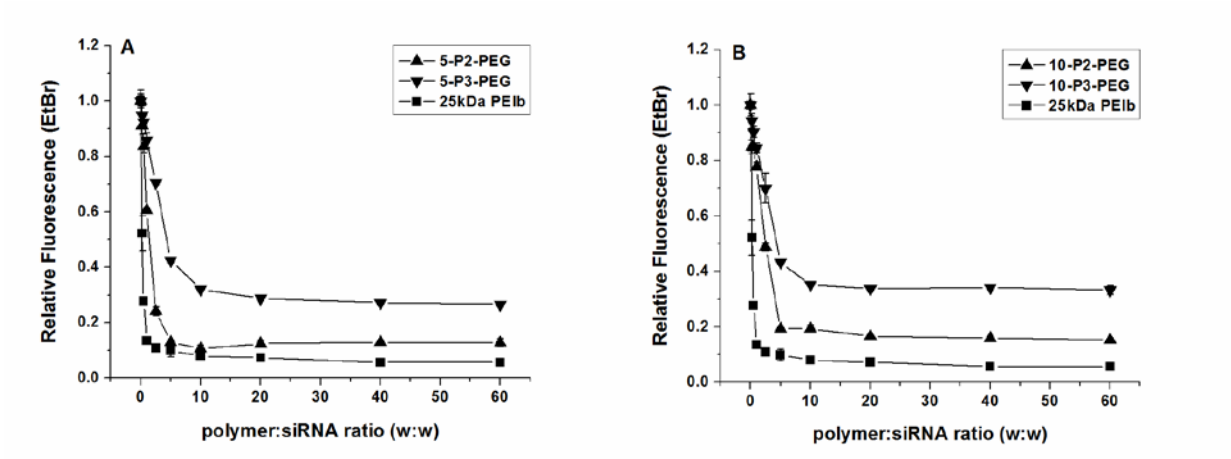

Figure AII.2: Relative binding affinity of polymer conjugates with siRNA as measured by ethidium bromide fluorescence quenching. N=3. Error bars represents standard deviation. 25kDa PEIb was included for comparison. (A) 5kDa-P-PEG; (B) 10kDa-P-PEG.

Table AII.1: Biophysical characteristics (size and zeta potential) of PEGylated polymer conjugates.[a]

Entry	Polymer	w:w ratio	Effective diamter (nm)	Zeta potential (mV)
1	5-P2-PEG	15:1[b]	94.1 ± 6.6	14.6 ± 1.1
2	5-P3-PEG	30:1[c]	105.2 ± 30.4	11.1 ± 0.8
3	10-P2-PEG	12:1[d]	39.9 ± 19.9	16.4 ± 1.5
4	10-P3-PEG	25:1[e]	38.3 ± 14.1	16.2 ± 1.3

[a]Effective diameter and zeta potential of polyplexes as determined by dynamic light scattering (DLS) using a Malvern Zetasizer Nano-ZS. [b]w:w = 15:1 (5-P2-PEG) corresponds to w:w = 10:1 of 5-P2. [c]w:w = 30:1 (5-P3-PEG) corresponds to w:w = 20:1 of 5-P3. [d]w:w = 12:1 (10-P2-PEG) corresponds to w:w = 10:1 of 10-P2. [e]w:w = 25:1 (10-P3-PEG) corresponds to w:w = 20:1 of 10-P3.

Table AII.2: IC_{50} values for PEGylated polymer conjugates after 48 h incubation with MDA-MB-231-luc+ cells (MTS assay). N=3.

Entry	Polymer	$IC_{50,\ free\ polymer}$
1	5-P2-PEG	12.7 ± 0.3
2	5-P3-PEG	97.6 ± 1.2
3	10-P2-PEG	16.6 ± 1.2
4	10-P3-PEG	27.4 ± 1.9

APPENDIX III

PRELIMINARY DATA ON *IN VIVO* siRNA DELIVERY

All animal experiments were performed according to federal and state regulations, and approved by the Institutional Animal Care and Use Committee (IACUC) at Cornell University. For transfection experiments, female 8-week old (~20 g) Balb/c mice (Charles Rivers Laboratory) were intravenously injected via the tail vein with a single dose (200 μL) of siRNA/polymer complex, Invivofectamine 2.0 reagent (Invitrogen), naked siRNA or buffer. Polyplexes were formed at the designated polymer:siRNA (w:w) ratio in 10mM HEPES buffer, 5% glucose, pH 7.2 with [siRNA] = 2.5 mg/kg body weight. Complexes from Invivofectamine 2.0 reagent were formed according to the manufacturer's instruction in PBS with [siRNA] = 2.5 mg/kg body weight. At designated times post-transfection (48 h and 96 h), blood was collected via submandibular bleed. Factor VII protein levels in serum were determined using a Biophen FVII assay (Aniara Corporation) according to the manufacturer's instructions.

All conditions analyzed are shown in Table AIII.1. Preliminary data for *in vivo* siRNA delivery revealed that 5-P3, 10-P3 and 10-P3-PEG were well tolerated by mice at the specified conditions. However, no significant Factor VII protein knockdown was achieved as compared to Invivofectamine 2.0 reagent, the positive control, which achieved > 95% protein knockdown (Figure AIII.1). Perhaps the conditions analyzed were not optimal or tissues other than the liver were targeted by these polymeric vectors. In the case of 5-P2, 5-P2-PEG, 5P3-PEG, 10-P2 and 10-P2-PEG, toxicity was generated as perceived by weight loss or death of mice. Further analyses are needed to fully evaluate the efficacy of these polymeric vectors for siRNA delivery *in vivo*.

Table AIII.1: Polymer conjugates analyzed for *in vivo* siRNA delivery.[a]

Entry		Polymer	w:w ratio
1	5-P2	5kDapAA-76%A-2%G	15:1
2	5-P2-PEG	PEG-*co*-5kDapAA-76%A-2%G	22.5:1[b]
3	5-P3	5kDapAA-55%A-17%G	20:1
4	5-P3-PEG	PEG-*co*-5kDapAA-55%A-17%G	30:1[c]
5	10-P2	10kDapAA-78%A-3%G	15:1
6	10-P2-PEG	PEG-*co*-10kDapAA-78%A-3%G	18.8:1[d]
7	10-P3	10kDapAA-56%A-18%G	20:1
8	10-P3-PEG	PEG-*co*-10kDapAA-56%A-18%G	25:1[e]

[a]Polyplexes were intravenously injected into mice through the tail vein at the designated polymer:siRNA (w:w) ratio in 200 µL of 10mM HEPES buffer, 5% glucose, pH 7.2 with [siRNA] = 2.5 mg/kg body weight. [b]w:w = 22.5:1 (5-P2-PEG) corresponds to w:w = 15:1 of 5-P2. [c]w:w = 30:1 (5-P3-PEG) corresponds to w:w = 20:1 of 5-P3. [d]w:w = 18.8:1 (10-P2-PEG) corresponds to w:w = 15:1 of 10-P2. [e]w:w = 25:1 (10-P3-PEG) corresponds to w:w = 20:1 of 10-P3.

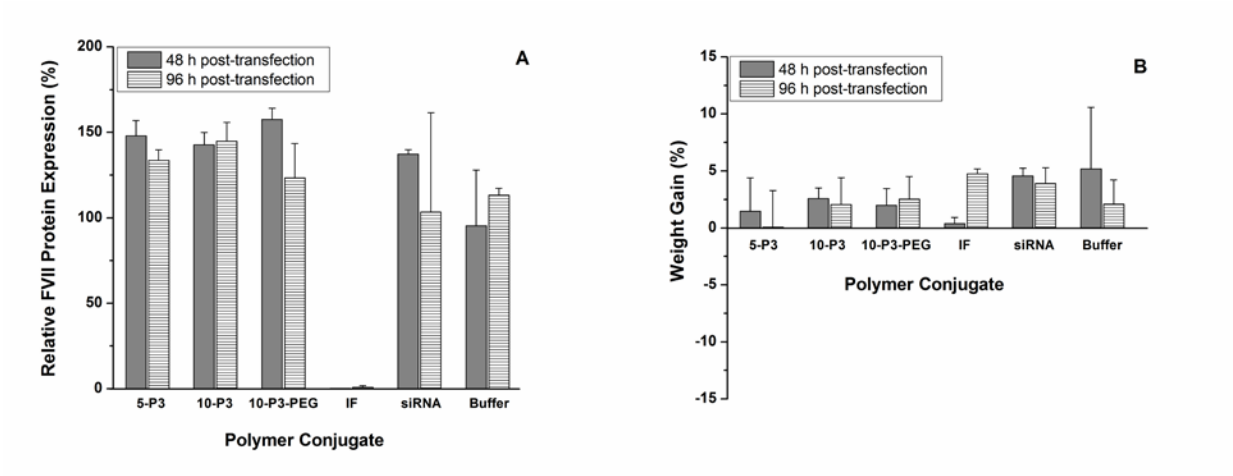

Figure AIII.1: (A) Relative FVII protein expression (%) 48 h and 96 h post-transfection. (B) Weight gains (%) 48 h and 96 h post-transfection. Conditions evaluated: 5-P3 (w:w = 20:1), 10-P3 (w:w = 20:1), 10-P3-PEG (w:w = 25:1), Invivofectamine 2.0 reagent (IF), naked siRNA and buffer (10mM HEPES, 5% glucose, pH 7.2). [siRNA] = 2.5 mg/kg body weight; total injection volume = 0.01 mL/g body weight. N = 4 for all conditions except IF (N = 3). Error bars represent standard deviation.